This project has received funding from the European Union's Horizon 2020 research and innovation programme under grant agreement No 101016608.

BEYOND 5G – OPTICAL NETWORK CONTINUUM
(H2020 – Grant Agreement № 101016663)

Deliverable D3.3

Final B5G-OPEN data plane infrastructure

Editor Lutz Rapp (Adtran)

Contributors TIM, BT, Adtran, NOKIA, CNIT, CTTC, INF-P, INF-D, HHI, OLC-E, TUE, PLF, ELIG

Version 2.0

Date July 31, 2024

Distribution PUBLIC (PU)

DISCLAIMER

REVISION HISTORY

Revision	*Date*	*Responsible*	*Comment*
1.0	*May,13, 2024*	*L. Rapp*	*First draft*
1.1	*July, 29, 2024*	*E. Riccardi*	*Document Revision*
2.0	*July, 31, 2024*	*L. Rapp*	*Submitted Version*

LIST OF AUTHORS

Partner ACRONYM	*Partner FULL NAME*	*Name & Surname*
Adtran	*Adtran Networks SE*	*Lutz Rapp, Dominic Schneider, Ukiwo Anya*
BT	*BT Group*	*Albert Rafel*
NNF	*Nokia Networks France*	*P. Layec, F. Boitier, A. May, P. Ramantanis*
TIM	*Telcom Italia*	*Emilio Riccardi, Anna Chiadò Piat, Marco Quagliotti*
ELIG	*E-lighthouse Network Solution*	*Pablo Pavón Mariño*
INF-P	*Infinera Unipessoal, Lda*	*João Pedro, Nelson Costa*
INF-G	*Coriant R&D GmbH*	*Antonio Napoli, Carlos Castro*
CNIT	*Consorzio Nazionale Interuniversitario per le Telecomuncazioni*	*Filippo Cugini, Andrea Sgambelluri,*
TUE	*Technische Universiteit Eindhoven*	*Nicola Calabretta, Shiyi Xia*
HHI	*Fraunhofer Gesellschaft*	*Johannes Fischer, Behnam Shariati, Abdelrahmane Moawad*
OLC-E	*OpenLightComm Europe s.r.o.*	*Chris Matrakidis*
PLF	*pureLiFi Ltd.*	*Rui Bian*

GLOSSARY

Abbreviations/Acronym	*Description*
ADC	*Analog to Digital Converter*
API	*Application Programming Interface*
ASE	*Amplified Spontaneous Emission*
ASIC	*Application Specific Integrated Circuit*
AWG	*Arrayed Waveguide Grating*
AWS	*Amazon Web Services*
BER	*Bit Error Ratio*
BDFA	*Bismuth-Doped Fiber Amplifier*
BPF	*Band-Pass Filter*
BVT	*Bandwidth Variable Transponder*
CAPEX	*CAPital EXpenditure*
CD	*Chromatic Dispersion*
CL	*Control Loop*
CM	*Correlation Method*
CMIS	*Common Management Interface Specification*
CO	*Central Office*
COV	*Control One Vehicle*
CP	*Cyclic Prefix*
CPU	*Central Processing Unit*
CUT	*Channel Under Test*
CW	*Continuous Wave*
DAC	*Digital to Analog Converter*
DC	*Data Center*
DCI	*Data Center Interconnection*
DD	*Direct Detection*
DNN	*Deep Neural Network*
DSCM	*Digital Sub-Carrier Modulation*
DS	*Downstream*
DSP	*Digital Signal Processing*
DWDM	*Dense Wavelength Division Multiplexing*
EDF	*Erbium-Doped Fiber*
EDFA	*Erbium-Doped Fiber Amplifier*
EOM	*Electro-Optical Modulator*
ER	*Extinction Ratio*
ERM	*Edge Resource Monitoring*
FaaS	*Function as a Service*
FEC	*Forward Error Correction*
FWM	*Four-Wave Mixing*
GFF	*Gain-Flattening Filter*
GPU	*Graphical Programming Unit*

IM	*Intensity Modulation*
IP	*Internet Protocol*
IPoWDM	*IP over WDM*
IQ	*In Phase/Quadrature*
LAN	*Local Area Network*
LiFi	*LightFidelity*
LL	*Least Loaded*
LP	*LightPath*
LRPS	*Layout Resource and Placement Specificatios*
LUT	*Look Up Table*
MAN	*Metro Area Network*
MB	*Multiband*
ML	*Machine Learning*
MBoSDM	*MB over SDM*
MCF	*Multi-Core Fiber*
MCS	*MultiCast Switch*
MMI	*Multi Mode Interference*
MMSE	*Minimum Mean Square Error*
MZM	*Mach Zehnder Modulator*
NE	*Next Edge*
NTF	*Node Telemetry Function*
OADM	*Optical Add Drop Multiplexer*
OFDM	*Optical Frequency Division Multiplexing*
OFE	*Optical Front-End*
OIF	*Optical Internetworking Forum*
OLS	*Optical Line System*
OMP	*Optimized Monitoring Placement*
OMS	*Optical Multiplex Section*
OOK-NRZ	*On-Off Keying – Non Return to Zero*
OSA	*Optical Spectrum Analizer*
OSC	*Optical Supervisory Channel*
OSFP	*Octal Small* Format *Pluggable*
OSNIR	*Optical Signal to Noise plus Interference Ratio*
OSNR	*Optical Signal to Noise Ratio*
OTDR	*Optical Time Domain Reflectometer*
P4	*Protocol-independent Packet Processors*
p2mp-SC	*Point-to-multi-point subcarrier-channel*
P4LB	*P4 Load Balancer*
PC	*Polarization Controller*
PDG	*Polarization Dependent Gain*
PDL	*Polarization Dependent Loss*
PDM	*Polarization Dual Multiplexing*
PIC	*Photonic Integrated Circuit*
PON	*Passive Optical Network*

POP	*Point Of Presence*
PPM	*Power Profile Monitoring*
PRBS	*Pseudo-Random Binary Sequence*
PSD	*Power Spectral Density*
PtMP	*Point to Multipoint*
PtP	*Point to Point*
QAM	*Quadrature Amplitude Modulation*
QSFP-DD	*Quad Small Form Pluggable Double Density*
R&D	*Research And Development*
R&S	*Route and Select*
RF	*Radio Frequency*
RMSE	*Root Mean Square Error*
ROADM	*Reconfigurable Optical Add Drop Multiplexer*
RR	*Round Robin*
RSSI	*Received Signal Strength IndicatorML*
RTO	*Real Time Oscilloscope*
RTT	*Round Trip Time*
RU	*Rack Unit*
RVCA	*Remote Vehicle Control Application*
S-BVT	*Sliceable-BVT*
S-OXC	*Spatial-Optical Cross Connect*
SC	*Sub-Carrier*
SDE	*Serverless Deployment Engine*
SDM	*Space-Division Multiplexer*
SDN	*Software Defined Network*
SE	*Spectral Efficiency*
SOA	*Semiconductor Optical Amplifier*
SOP	*State Of Polarization*
SPM	*Self-Phase Modulation*
SRN	*Signal to Noise Ratio*
SRS	*Stimulated Raman Scattering*
SSB	*Single Side Band*
SSM	*Single-Mode Fiber*
TDFA	*Thulium-D*oped Fiber *Amplifier*
TF	*Tunable Filter*
TLS	*Tunable Laser Source*
TS	*Training Symbol*
UDP	*User Datagram Protocol*
US	*Upstream*
VCSEL	*Vertical Cavity Surface Emitting Laser*
VOA	*Variable Optical Attenuator*
WB/WBL	*Wavelength Blocker*
WDM	*Wavelength Division Multiplexing*
WSS	*Wavelength Selective Switching or Switch*

XPM	*Cross-Phase Modulation*

EXECUTIVE SUMMARY

This structure of this deliverable is divided into two parts with the first two chapters dedicated to data plane architecture and technical proposal from B5G-OPEN, and the rest of the document describing the activities of WP3 during the third year of the project.

High-level architecture as discussed by WP2 concerns both the network level (i.e., central offices and geographical connectivity between them) and the Central Office (CO) level, understood as the physical place where all the devices, not just the optical ones, are located and interconnected. What is included in this deliverable concerns the Data Plane of the optical layer and system level solutions for its implementation.

Four network segments are considered, namely: Access; Metro Aggregation; Metro Core; and Backbone; and three CO types (Access; Regional; National/Cloud COs) with different optical node roles Access (A), Hub (H), Regional (R), and National (N). This classification follows from the assumption that the optical topology of the Metro Aggregation segment is of the horseshoe type, with the access optical nodes (A) in Access CO collected by a horseshoe terminating in two hub nodes (H) which are located on Regional or National COs.

WP2 provided also an estimate of traffic needs for each of the network segment and optical node type for short, medium and long term scenarios (3, 6, 9 years respectively).

Based on this classification and traffic evolution, B5G-OPEN is proposing solutions for the optical data plane in the form of a set of node architecture, technologies and network paradigms.

The solution for the optical data plan developed within B5G-OPEN offers the following features and benefits:

a. Its flexibility to adapt to the specific network domain with the proposal of different optical switching technologies in order to cope with the specific needs in term of node size, scalability, cost, power consumption and numerosity. B5G-OPEN is proposing filterless A type nodes based on an semiconductor optical amplifier (SOA) in the metro aggregation, or an alternative low-cost reconfigurable optical add drop multiplexer (ROADM) again based on SOA supporting multi band operation; for the other network segment more traditional wavelength-selective switching (WSS) based architectures are considered suitably extended to cope with multiband operations.
b. The support for transparent interoperation (Optical Continuum) allowing transparent crossing of network domains with an expected relevant cost saving. The impact of this requirement is for example on the types of optical transceivers that should include also module suitable for long reach application even if they are deployed in metro aggregation nodes. Lower cost and performance transceivers are used in shorter applications like for traffic flows starting and ending within the same metro aggregation domain or directed toward the access segment.
c. The native support for optical disaggregation with horizontal and vertical standard interfaces and in particular the integration with the packet layer (IP over dense wavelength division multiplexing, DWDM). B5G-OPEN is considering existing and evolving standards for pluggable coherent modules exploring their evolution (in particular, in the direction of new functionalities like Point to Multi Point optical capabilities).

d. The introduction of Point to Multi Point (PtMP) at the optical layer thanks to innovative interfaces provides by partners. PtMP can efficiently provide traffic in the metro aggregation segment and particularly in short and medium term. Its extension to metro core has been extensively explored by B5G-OPEN with the introduction of new ROADM architecture suitably design to support PtMP trees in meshed optical networks.
e. An efficient use of available optical bands (Multi band). This is a very complex topic extensively studied theoretically and experimentally by B5G-OPEN. Not claiming to provide a conclusive word on the topic, the project contributed significantly to clarifying the limitations of the approach and evaluating the impact in terms of performance, ease of upgrade and cost of possible solutions, even in conjunction with a certain degree of spatial division multiplexing.
f. An advanced monitoring system is another key topic extensively explored by B5G-OPEN. Multi Band, Optical Continuum and a significant traffic increase in large networks are strongly increasing the interest in increasing the monitoring capabilities of optical equipment to leverage the collected data into insightful explanations. To do so, B5G-OPEN explored massive monitoring implementations either with dedicated low-cost hardware or more interestingly via the coherent transponders.
g. A common management and control of the complete infrastructure through standard and open APIs and a common and integrated planning tool are necessary functionalities in order to manage such a complex, large and disaggregated optical network together with the packet layer. These topics are covered in WP4, and not part of this deliverable.

The first two sections of the documents are giving a summary of all these aspects of the final B5G-OPEN data plain solutions, addressing only in some details a selected subset of them. In fact, practically all the topics have already been covered in considerable detail in the previous deliverables and in the literature published by the project. It has been therefore decided not to repeat a complete discussion here, but to refer the reader to the relevant documents where the detailed description is found.

The rest of the document (sections 3) discusses a miscellaneous of technical topics not yet included in previous deliverables.

In particular it covers:

a. New results and studies on optical subsystems, switching and amplification with a strong emphasis on solutions for the metro aggregation network segments (Multi-Band Sliceable Bandwidth Variable Transceivers, MB-SBVT; Filterless and ROADM based on SOA).
b. New results and studies on integrated access and cross-hauling options with emphasis on programmable packet-optical solutions and photonic integrated solutions and advancements on LightFidelity (LiFi).
c. New results and studies on advanced monitoring solutions including integrated monitoring in IP over DWDM and a cost analysis of the introduction of longitudinal link power monitoring in optical transport networks. Last section of chapter 3 covers a new approach for monitoring of chromatic dispersion in multiband networks based on the OFDM MB-SBVT developed in the project.

Last chapter of the document (Chapter 4) gives the complete list of “prototypes” developed by the partners in collaboration with other WPs during the entire duration of the project. It is reported in the form of a table updated of the one already included in D3.2.

1 B5G-OPEN HIGH-LEVEL ARCHITECTURE

This introductory chapter presents a summary of what is defined by the project in terms of high-level architecture. High-level architecture constitutes a premise to the final solutions identified by the B5G-OPEN project for the Data Plane which is described in a following chapter.

High-level architecture concerns both the network level (i.e., central offices and geographical connectivity between them) and the central office level, understood as the physical place where all the devices, not just the optical ones, are located and interconnected. What is included in this deliverable concerns the Data Plane of the optical layer and system level solutions for its implementation; as regards the Control Plane, into which the Data Plane must be integrated, the reference is WP4 and related deliverables. Therefore, the high-level architecture is understood as the hierarchy of the Central Offices (CO)s hosting Telco equipment of all types (not just DWDM optical), and also the architectures inside the individual Central Offices, which, playing a different role in the hierarchy, are characterized by different complexities and sizes.

Figure 1-1 shows the high-level network architecture defined in D2.1 [D2.1]. It includes four network segments: Access, Metro Aggregation, Metro Core and Backbone, and four levels of Central Offices (i.e., Telco exchanges): Access, Regional, National and Cloud (the latter is a backbone level site which hosts a national level Data Center (DC) hosting Telco and Service Cloud Functions). The same figure, in the bottom part, highlights the areas in terms of Telco and Service Cloud infrastructure, i.e. the Main Cloud (big DCs which are connected to the national backbone), the Edge Cloud which relies on National or Regional level COs, and the Far Edge Cloud which extends up from the Regional to the Access COs.

Deliverable D2.1 gives an in-depth description of Figure 1-1 and in particular (through Table 1.1 of D2.1) it gives parameters characterizing the various COs, such as number of COs of each type in a typical National network, estimated population covered by a CO type, max distance from the Access Point to each CO type, and other parameter as expected reliability/availability and the typical round trip time (RTT). In addition, D2.1 provides (through Fig. 1.2 of the deliverable) the mapping of the current networks of the three operators belonging to the consortium onto the high-level network view (i.e. Figure 1-1 of this document).

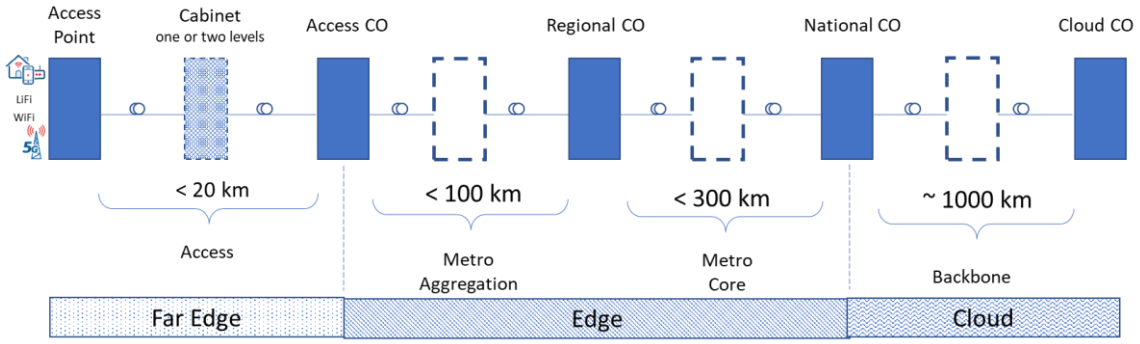

Figure 1-1: High-level B5G-OPEN general architecture defined in D2.1.

Deliverable D3.2 [D3.2], referring to the framework of Figure 1-1, defines the possible architectures of COs. CO architecture is defined in terms of DWDM optical equipment, seen as technology-agnostic nodes performing the switching functionality and transceivers classified by

their (approximate) reach, and other pieces of equipment that perform the functions of the packet layer (IP single piece of equipment or fabric, e.g., switches connected in a leaf & spine topology) and of the Telco (T) and Service (S) Cloud (data centers at different scale: micro, mini or main/full).

Figure 1-2 shows the reference high-level architecture for the four CO types (National and Cloud have the same CO structure, so the models justly three). Four different optical node roles and correspondent (red) boxes in the figure are identified and placed within the COs: Access (A), Hub (H), Regional (R), and National (N). This classification follows from the assumption that the optical topology of the Metro Aggregation segment is of the horseshoe type, with the access optical nodes (A) in Access CO collected by a horseshoe terminating in two hub nodes (H) which are located on Regional or National COs (Please refer to D3.2 [D3.2] for details).

In each CO, irrespectively of the hierarchy role, pieces of access equipment are present including Passive Optica Network (PON) line side terminations and optical device for allowing a direct transparent connection of Access Points in client premises to remote Point of Presence (POP) of services in the Aggregation segment. Also, the presence of DCs of different size is considered for each kind of CO.

The traffic coming to an optical node can be treated at the packet level, and in this case, it needs to be locally optically terminated (Add/Drop) to be delivered to the co-located packed equipment through a suitable transceiver, or it can pass through the node transparently remaining in the same network segment or crossing segments thanks to bypasses between optical nodes, creating the so-called “Optical Continuum” (Please refer to D3.2 [D3.2] for details).

In Figure 1-2, different types of DWDM transceivers are considered according to their performance in term of capacity and reach: all of them are indicated as “pluggable types” for simplicity, but for long reach optical paths (mainly in the Backbone), transponders instead of pluggable modules on packed devices could be preferred for their better performance due to less compromise in term of size and power consumption compared to the small form factor transceiver here considered. In this case the connection to the packet switch is done using grey interfaces. Also muxponders could be employed in interconnection points between network segments to allow grooming of lower bit rate flows, need to cross domains, into higher hierarchy optical flows.

The reference reach of the transceivers is indicated assuming that the traffic is terminated optically and processed at the packet level in the same network segment before being forwarded again on the optical network. If this was.e. if optical pass-throughs were created, the transceivers used could be of a different type. For example, if from an optical access node (A) you wanted to reach a regional (R) or national (N) node other than the two regional (or national) COs ending the horseshoe aggregation structure the access node belongs to, the transceiver must have the corresponding reach (therefore, and depending on the case, a reach metro core level of ≈400 km or a reach backbone level of ≈1000 km).

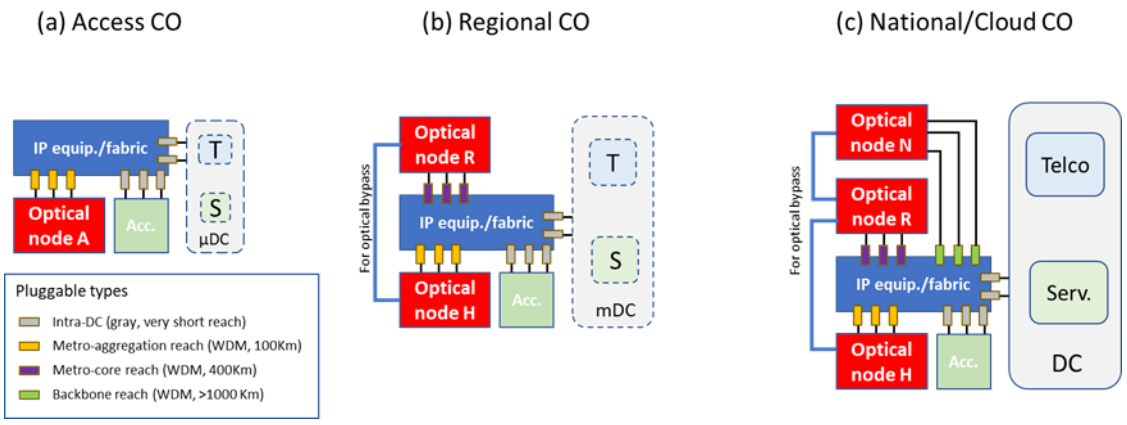

Figure 1-2: Reference architecture for Central Offices as defined in D3.2.

An analysis was carried out in D3.2 which identified the traffic that optical nodes of different types (A, H, R and N) are called upon to manage in three different time horizons: short term, medium term and long term.

The Table 1-1 summarizes for each type of optical node identified in Figure 1-2 the traffic to be handle in total and as add/drop.

Given the variability of traffic size reaching each CO even within the same network segment (i.e., the capacities of the nodes and the percentages of Add/Drop and optical bypass traffic can significantly vary), the traffic values in Table 1-1 refer to a maximum conceivable values for each type of node. Most of the nodes will therefore have lower or even much lower capacity requirements within each reference period. The technologies considered in B5G-OPEN must take into account these capacity requirements.

The main assumption made for table 1-1 are shortly recalled hereafter and are detailed in D3.2 to which the reader is referred for further details and.

Node N in national CO are assumed of nodal degree 4 (the node is supposed connected to other four correspondent N nodes hosted in as many National COs), traffic is balanced among the different degrees and pass-through traffic is twice the add/drop traffic. No optical bypass traffic coming from node R is assumed (although there might be) and the traffic exchanged with other national nodes N involves services delivered by National DC or directed to the gateways for reaching destinations outside the network (e.g., the Internet).

Node R in national CO is assumed receiving traffic from 24 nodes R (of different geotypes) from as many regional COs, there is no significant or not at all pass-through traffic coming from local H node (as these nodes are typically POP for telco and services functions) and so the traffic on line degrees equals the Add/Drop traffic. Alignment traffic for mDC and µDC, (possibly positioned in the Regional or Access COs, respectively) is neglected.

Node H in national CO is assumed to have no optical bypass traffic (i.e., Add/Drop traffic is 100%, all the traffic collected from nodes A of local COs by aggregation horseshoes) given that all the traffic collected by nodes A in access CO is managed on local network telco cloud functions.

Node R in regional CO is assumed collecting traffic from other 7 nodes on 4 nodal degrees and the traffic of the entire cluster of 8 nodes (assumed to be of the high-demanding Dense Urban geotype) is sent to by another nodal degree (5 nodal degrees in total) to a node R in a National

CO. Bypass traffic of access nodes of type A is also collected through local H node (100% of traffic optically-bypassed coming from 8 A nodes, or 50% of traffic coming from 16 A nodes).

Node H in regional CO is assumed to have 50% of bypass traffic (i.e., Add/Drop traffic is 50%) given that all the traffic collected by nodes A in access CO is managed on local network telco cloud functions.

Node A in Access CO has to handle half of the traffic generated by up to 7 other A nodes in pass-through (as 8 is the maximum number of A nodes in the aggregation horseshoe), plus the total traffic generated locally (two equal flows add/dropped and sent on horseshoe, one on East and the other on West direction).

Table 1-1: Maximum total and Add/Drop (A/D) traffic in Tb/s of the optical nodes in different Central Offices and for the three reference time horizons (short, medium and long term).

Type of optical node	Time Period (-term)	*Type of Central Office*					
		Access CO		*Regional CO*		*National/Cloud CO*	
		Total traff.	A/D traffic	Total traff.	A/D traffic	Total traff.	A/D traffic
Node A	Short	**4.5**	**0.5**	-	-	-	-
	Medium	**36**	**4**	-	-	-	-
	Long	**144**	**16**	-	-	-	-
Node H	Short	-	-	**8**	**2**	**8**	**4**
	Medium	-	-	**64**	**16**	**64**	**32**
	Long	-	-	**256**	**64**	**256**	**128**
Node R	Short	-	-	**40**	**1**	**74**	**37**
	Medium	-	-	**320**	**8**	**592**	**296**
	Long	-	-	**1280**	**32**	**2368**	**1184**
Node N	Short	-	-			**74**	**18.5**
	Medium	-	-			**592**	**148**
	Long	-	-			**2368**	**592**

Considering the high-level architecture and the consistency of the traffic briefly discussed in this chapter, in next chapter the proposed data plane infrastructure as elaborated in the B5G-OPEN project is presented.

2 B5G-OPEN TRANSPORT PLATFORM SOLUTIONS

In this chapter, the final B5G-OPEN "solution" is presented in the form of a list of guidelines. Note that we believe that a single solution for all situations is not the best choice.

Instead, B5G-OPEN believes that what is qualifying an innovative solution for the optical data plan is i) its flexibility to adapt to the specific network domain; ii) the support for transparent interoperation (Optical Continuum); iii) the native support for optical disaggregation with horizontal and vertical standard interfaces; iv) the integration with the packet layer (IP over DWDM); v) the introduction of Point to Multi Point at the optical layer; vi) an efficient use of available optical bands (Multi-band); vii) an advanced monitoring system; viii) the common management and control of the complete infrastructure through standard and open APIs; ix) a common and integrated planning tool.

In general, different technologies are proposed, sometimes in a concurrent way, for the different network segments in order to make them better suit to the specificity of each segment, in term of capacity, reach, scalability, power consumption and costs. Mixing of technologies within the same segment (for example, filterless systems with SOA and EDFA amplifiers in metro aggregation, with wavelength-selective switch based hub nodes) are considered where advantageous.

A detailed description of the qualifying characteristics of the proposed solutions has been already discussed in previous deliverables and in the associated literature. Here only some significant topics explored in B5G-OPEN are summarized for convenience, namely IP over DWDM, Optical Continuum, topics related to Multi-Band amplification and transmission performance and advanced monitoring techniques.

The high level architecture of proposed optical nodes for the identified network segments is then given as part of B5G-OPEN solution (from section 2.7 up to the end of chapter 2).

2.1 IP OVER DWDM PARADIGM

The recent evolution of transmission technology has driven the introduction of pluggable transceivers provided with a coherent detection strategy. Coherent transceivers are commercially available at rates of 400 Gbit/s in quad small form factor pluggable double density (QSFP-DD). Originally implemented for data center interconnection (DCI, up to 120 km reach) with a signal launch power of up to −10 dBm (400ZR), they rapidly evolved to support higher transmission power and longer optical reaches (400ZR+). For example, 400ZR+ QSPF-DD products have been successfully validated and deployed over few hundreds of kilometers relying on an output power of around 0 dBm. Furthermore, 800ZR+ transceiver have been recently commercialized, still relying on compact QSFP-DD (and OSFP) form factor.

All these types of pluggable coherent modules are suitable for metro-core reach (see Figure 1-2).

Lower cost and reach coherent pluggable modules are currently in an early commercial phase (100RZ [100RZ]) with reduced performance and in a QSFP form factor. These pluggable are ideal candidates for metro-aggregation reach (see Figure 1-2).

In the meantime, the Optical Internetworking Forum (OIF) has successfully defined the Common Management Interface Specification (CMIS) with related extensions for coherent modules,

Coherent CMIS (C-CMIS). CMIS is the management interface of choice for pluggable modules, supported by more than 10 Vendors with excellent interoperability performance.

These coherent modules represent an extremely attractive solution to be equipped directly within packet switching devices, including those designed for the wider data center market.

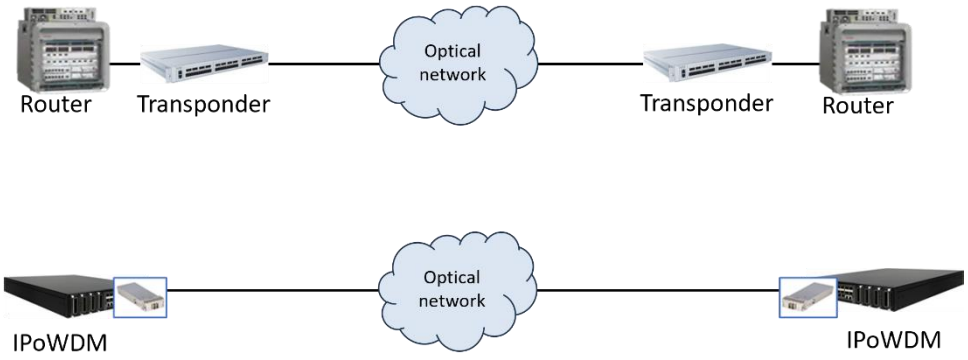

Figure 2-1: Evolution from Transponder-based optical networks to IPoWDM nodes equipped with coherent pluggable modules.

In B5G-OPEN, we specifically investigated the use of packet-optical nodes (typically called IPoWDM) in the Telco context, i.e. beyond the scenario of DCI. In particular, we have focused on the reduction/removal of transponders and muxponders as standalone network elements particularly in metro networks (see figure above).

The adoption of IPoWDM nodes leads to several remarkable benefits:

- reduced capital expenditure, through the elimination of expensive components like Flex-switchponders and possibly ROADMs and amplifiers in the OLS. The OLS comprises between 20-35% [HER20] of the total CAPEX in a MAN, so only this part offers important savings opportunities.
- reduced space in central offices, relying on a single IPoWDM box instead of two standalone elements with related interconnected fiber cables.
- reduced latency, since the queuing+processing+transmission of IP packets through 400 Gbit/s (and above) coherent pluggables will be in the order of 1 – 2 microsecs at most, very small compared with propagation delay [Kon24].
- reduced power consumption by avoiding the optical–electronical–optical (OEO) interconnection between gray router interfaces and colored transponder line interfaces (overall savings in the range between 50 and 150 W for every 100 Gbit/s of nominal traffic, depending on the line rate).
- tight integration between packet and optical networks, which is of special interest as transport is dominated by Ethernet and IP traffic.
- Introduction of advanced monitoring capabilities leveraging on programmable ASIC, as detailed in this document.

2.2 OPTICAL CONTINUUM

Optical Continuum is important in reducing cost of an optical transport solution. The following is taken from D3.2 and here reported for reader convenience.

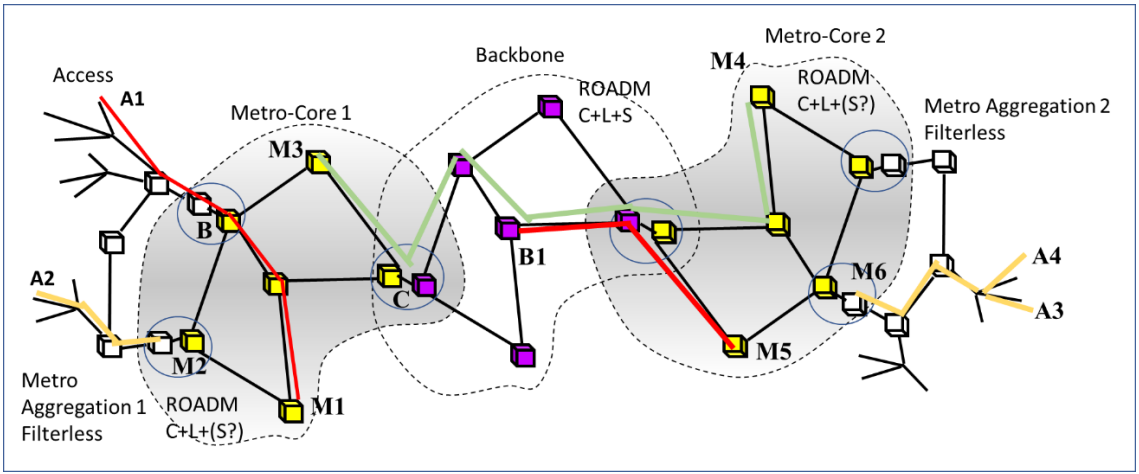

Figure 2-2: Continuum concept (from D3.2).

Figure 2-2 shows a network divided into access, metro and backbone segments and illustrates the Optical Continuum concept with simple graphic examples. At the left and right ends of the figure, the yellow lines highlight optically transparent connections created between access terminals and the first aggregation nodes (A2 to M2, and A3/A4 to M6). The redline on the left instead represents a transparent optical circuit which, starting from the access (A1), reaches the first aggregation node (B) and then also the more internal metro-core node (M1). Finally, examples of optical continuity between a single metro-core network and the backbone are represented (red line in the center of the figure, from M5 to B1) or even an optical continuity between two nodes that are part of different metro-core networks that pass through the backbone (M3 to C, B1 and M4).

To allow Optical Continuum, the B5G-OPEN transport solution includes sub-systems and strategies for as much as possible direct interconnection between DWDM systems of the two network domains (without the intermediation of a packet device or regeneration).

The major technological implications are:

- Lower bitrate flows (below 100 Gbit/s) of the metro aggregation network through nodes of the metro-core are multiplexed and mapped directly, at the interconnection with the metro-core network, into optical flows of a higher hierarchy (100-400Gbit/s or higher) using a muxponder of the metro-core network in order to reduce the number of electronic devices involved. This requires that the core network Muxponders be able to accommodate 10-100 Gbit/s color optics on the client side.
- Coherent flows at 100Gbit/s or higher in metro aggregation networks must be able to transparently cross the interconnection towards the metro core network in order to reduce the number of electronic devices involved. This requires that: i) the Core network must accept and manage coherent flows from the Aggregation network in the same way as Alien Lambdas; ii) metro-core reach pluggable coherent modules are employed.

- If the characteristics of the coherent signal at 100 Gbit/s or higher bit rate generated in metro aggregation networks do not allow it to reach its final destination, the flow must be able to be terminated on a client port side of a transponder/muxponder of the interconnection metro core node.
- In the hypothesis of having all network domains managed by the same vendor, the latter must guarantee an interconnection physical interface and adequate architecture of the nodes (Aggregation, Core and Backbone) and must allow joint management and routing through the two networks. The same should be true even in case of a multi-vendor environment; B5G-OPEN is proposing an open-source unified control plane and planning tool for this porpoise (see documents in WP4).
- Potentially nodes in the metro areas (metro aggregation and metro core segments) could be collapsed into a single node capable of managing both the segments (H and C nodes collapsed in Figure 1-2). In B5G-OPEN different transmission technologies and node technologies are considered in order to have a reasonable trade off between performance and costs. So different node types are employed in different network segments including H and C nodes.

2.3 Amplification in Multiband Systems

Multiband systems potentially allow an efficient use of the spectrum resource of fiber links. An efficient amplification scheme is therefore necessary. Due to the importance and complexity of amplification and its multi-face aspects, a summary of the main challenges and possible solutions explored in B5G-OPEN is given.

Rare–earth doped fiber amplifiers and Raman amplification are promising technologies for amplification in the S–band, the C–band, and the L–band [Rap21-2]. Capacity increase by these technologies comes most likely in two upgrade steps. The first deals with the short–term increase of capacity by implementing already available and qualified components. The aim of the second step, in contrast, is on the capacity enhancement in the mid–term [Rap21-1]. Therefore, components or proven concepts employed in this scenario are already available, but some of the components are not yet proved in the field or still need to be qualified according to the Telcordia standard.

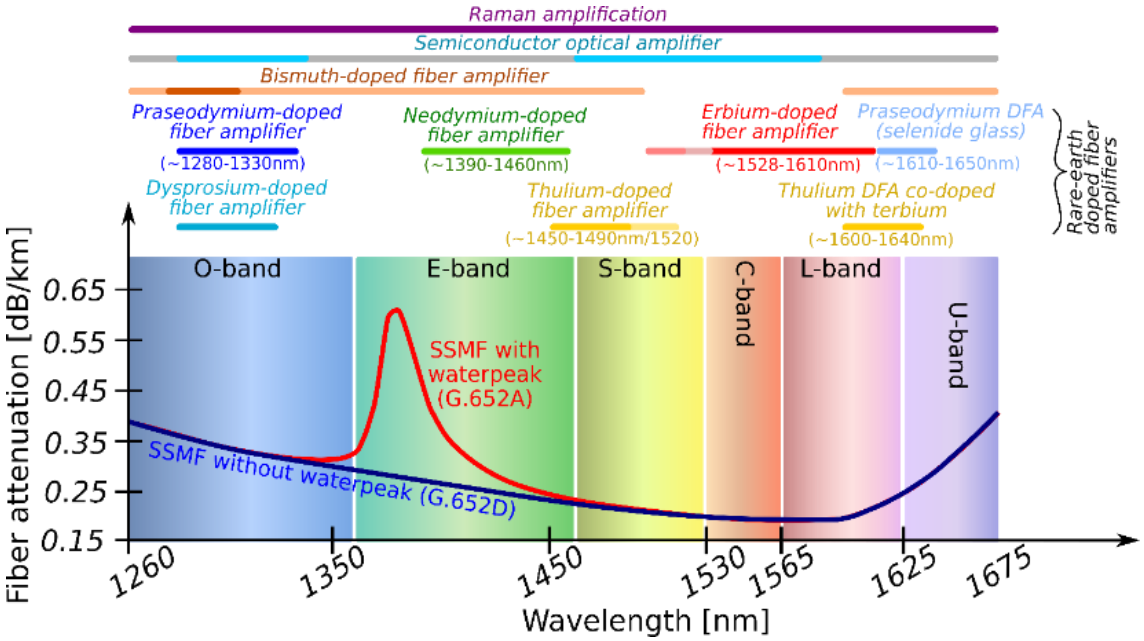

Figure 2-3: Amplifier technologies for different wavelength bands.

Figure 2-3 provides an overview over amplification technologies that can be employed for different wavelength ranges. The features of rare–earth doped fiber amplifiers, in particular erbium–doped fiber amplifiers (EDFAs), and Raman amplifiers are well explored. Bismuth–doped fiber amplifiers (BDFAs) have attracted a lot of attention during the last years. This is attributed to the fact that amplification can be realized at many wavelengths and this has been demonstrated at large amplification bandwidths. This metal introduces advantages over rare–earth based solutions in some wavelength bands even though still not all of its important features are fully understood.

The band gap of semiconductor amplifiers can be tailored for achieving gain in broad wavelength ranges. Such amplifiers, however, exhibit negative characteristics such a high noise figures and crosstalk. Hence, at the current level of development they are not yet considered promising candidates for inline amplification in long–haul systems. This in spite of that data transmission over a single span [Ren17] and in combination with Raman amplification over metropolitan distances [Ren19] has been recently presented.

2.3.1 C+L-Band setup with Improved Noise Performance

Presented results show degradation of the noise figure that can, however, be strictly limited by using a modified EDFA design with more than one gain–flattening filter [Rap22].

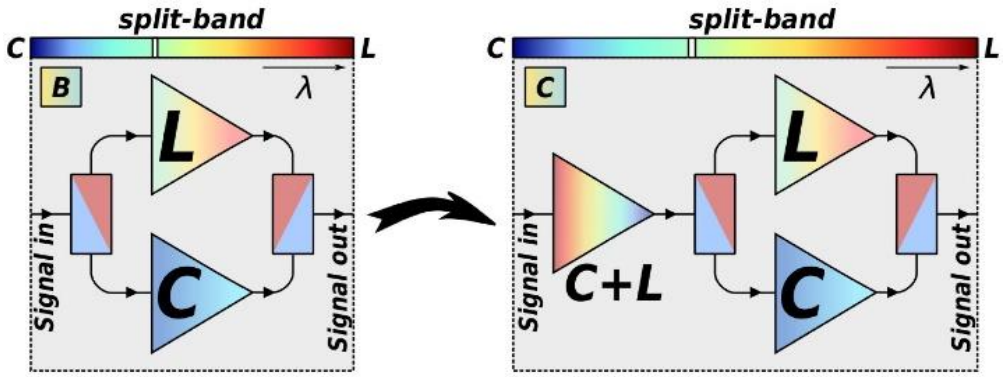

Figure 2-4: Extension of the split–band setup on the left side by introducing a common first amplifier stage in the setup on the right side for better noise figure.

The left side of Figure 2-4 shows a conventional setup for providing combined amplification in two wavelength bands, wherein a dedicated amplifier is used for each of the bands. However, this approach leads to increased noise figures due to the losses of the band splitter at the input of the amplifier setup. This drawback can be avoided by using a common pre-amplification stage amplifying both bands in front of the C/L–band splitter [Sun97], as shown in setup B. It has been revealed that such a promising approach in fact leads to improvement in noise figure. The data transmission in the wavelength range from 1529.6 nm to 1564.7 nm (C–band) and in a wavelength range of equal width from 1572.1 nm to 1609.2 nm (L–band) is analyzed.

For the following analysis, data transmission in the wavelength range from 1529.6 nm to 1564.7 nm (C–band) and in a wavelength range of equal width from 1572.1 nm to 1609.2 nm (L–band) is investigated.

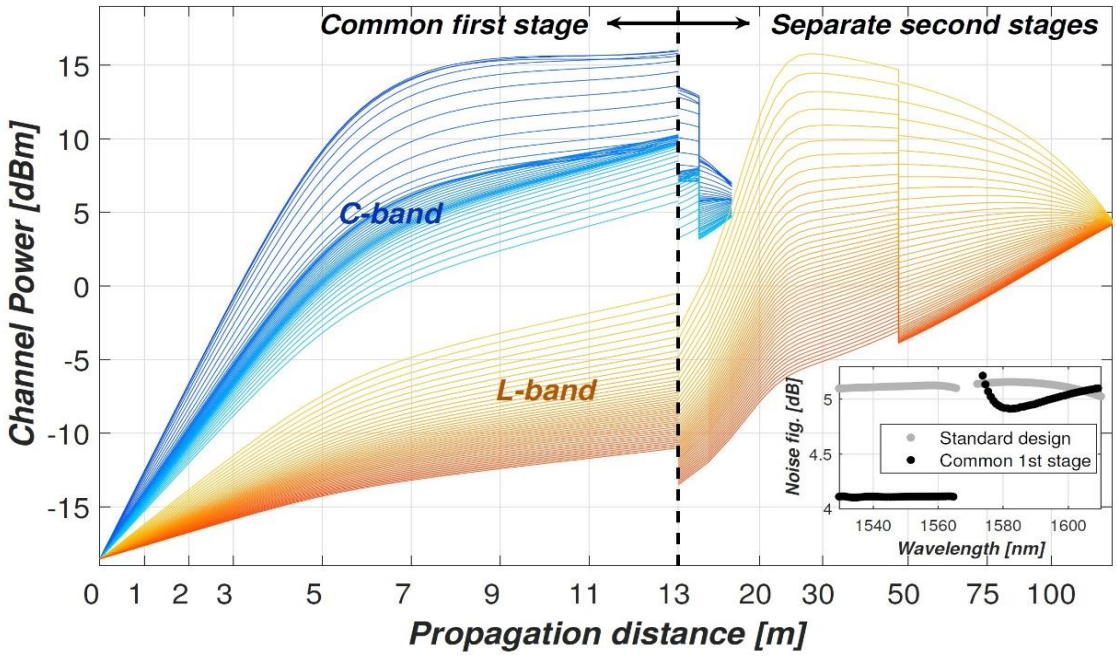

Figure 2-5: Power distribution of C–band and L–band channels in an amplifier design with a common first stage for both bands (setup C). Deformed x–axis for propagation distances longer than 13m.

Figure 2-5 reveals the major design challenge of a setup with common shared first stage. In this figure, the x–axis has been deformed for propagation distances after the C/L–band splitter, i. e. where the various wavelength bands are amplified in separate EDF coils of different lengths. In the first stage, significantly larger gain is realized at the C–band channels in comparison to the L–band channels. Thus, the gain of the L–band channels revealed before the C/L–band splitter is not sufficient to make the contribution of this passive component negligible according to Friis's formula. This problem could be overcome by making the first stage longer, but this would have a negative effect on the C-band and makes correct control in some operating conditions impossible.

While black dots in the inset of Figure 2-5 illustrate noise figure across both bands with a common first stage, gray dots indicate the noise performance for a setup with two completely separate amplification branches. It is worth mentioning that using a common first stage leads to improved noise figure in the C–band, but there is no significant benefit in the L–band. As a summary, both setups feature very similar maximum noise figure value arising within the target wavelength range of operation. However, extended C–band amplifiers are the better choice for required bandwidths up to around 60 nm at smaller output powers and up to 50 nm at higher output powers in comparison with split–band approaches designed for enabling amplification over 70 nm or more.

2.3.2 Band Splitting Setups – Performance and Handling

Upgrading existing links by implementing new wavelength bands is challenging due to the need for additional slots in subracks. For such an upgrade, only few already installed amplifier cards are prepared which will involve traffic interruption. Employing the amplifiers on individual cards allows for a stepwise upgrade of capacity and introduces relatively low initial cost. To avoid speed limitations, amplifier control is preferably performed on each card individually. However, determining the tilt and gain settings of each amplifier demands prior knowledge about the current total power in each wavelength band. Given that the input power of each band is measured on a dedicated card, the measured power levels need to be shared among the cards.

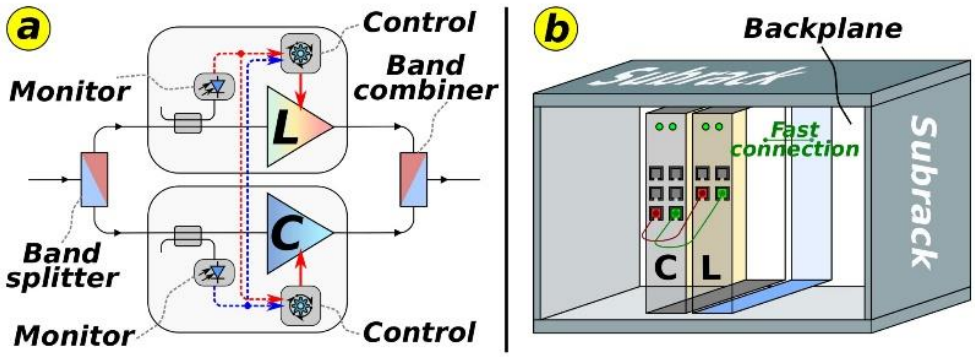

Figure 2-6: Implementation of a broadband amplifier comprising two amplifiers operating in parallel and each of them amplifying one wavelength band. (a) Required communication paths (b) Card split and system setup in a subrack.

Figure 2-6 (a) and Figure 2-6 (b) illustrate this concept. Such an approach requires a high–speed connection between the amplifier cards. One obvious solution is to transmit data via the backplane. The challenge in this option is that the speed of typical backplane connections is not

sufficient and some extra high–speed connections are demanded. Furthermore, this approach might introduce limitations on the placement of the cards in the subrack. By exploiting electrical radio frequency (RF) cables or even extra optical fibers, data can be transmitted from one card to another. Due to possibly wrong connections, this option introduces extra effort during commissioning and additional sources of failure. Thus, the connections that are established automatically between the cards when equipping the subrack becomes attractive [Rap24-1].

2.3.3 Extended C-Band Amplifiers

Increase of the traffic demand does not require in all links to add a complete band. In many link, increasing the available bandwidth by around 50% should be sufficient for the next years. However, some documents mention a significant deterioration of noise figure when increaseing the bandwidth of C-band EDFAs by 10 nm. With the work done in B5G-OPEN, it has been shown that even an increase by 20 nm is possible with only small impact on noise figure when designing the amplifier appropriately [Rap22].

Figure 2-7 reveals the distribution of the total signal power (upper curves) as well as the power of the individual wavelength channels (set of lower curves) for a conventional amplifier design with one gain-flattening filter and for a design with two of these filters. It is displayed for a maximum power of 950 mW pump power available for the first stage and for an upper limit of the target wavelength range of 1585 nm (represented in red). With this modification, the minimum signal power level after the first stage is by almost 10 dB higher as compared with previous setups (presented in green) so that the noise figure of the overall amplifier is only 0.28 dB higher than the noise figure of the first stage for an extended wavelength range up to 1585 nm. Moreover, the noise figure of this optimized configuration is by 1.78 dB improved as compared with the default setup comprising two stages and one GFF. The comparison of this design is optimized for an extended C–band up to 1585 nm with an EDFA design according to initial setup which is considered for the standard C–band. Here, the EDFA is operated at the same per channel power and hence at a reduced total output power.

In the following, the extended C-band amplifier is compared with a standard C-band amplifier design. In order to get a fair comparison, identical power is assumed per channel. Thus, the modified setup for the extended C–band and thus larger maximum channel count is operating at a total output power of 24 dBm, whereas the total output power of the standard setup amounts to 22 dBm. This yields a maximum noise figure of 4.18 dB in this operating point. As a result, extending the available bandwidth by 20 nm leads to an increase of the maximum noise figure by 0.48 dB. It is expected that further optimizing the filter function of the GFFs leads to a further decrease of the noise figure. Consequently, the modified setup enables an increase of the bandwidth by 60% with only minor degradation of the noise figure. A disadvantage of the approach, however, is the associated increased cost due to additional components such as an additional filter and an additional WDM coupler, and by the higher pump power required for pumping the second stage.

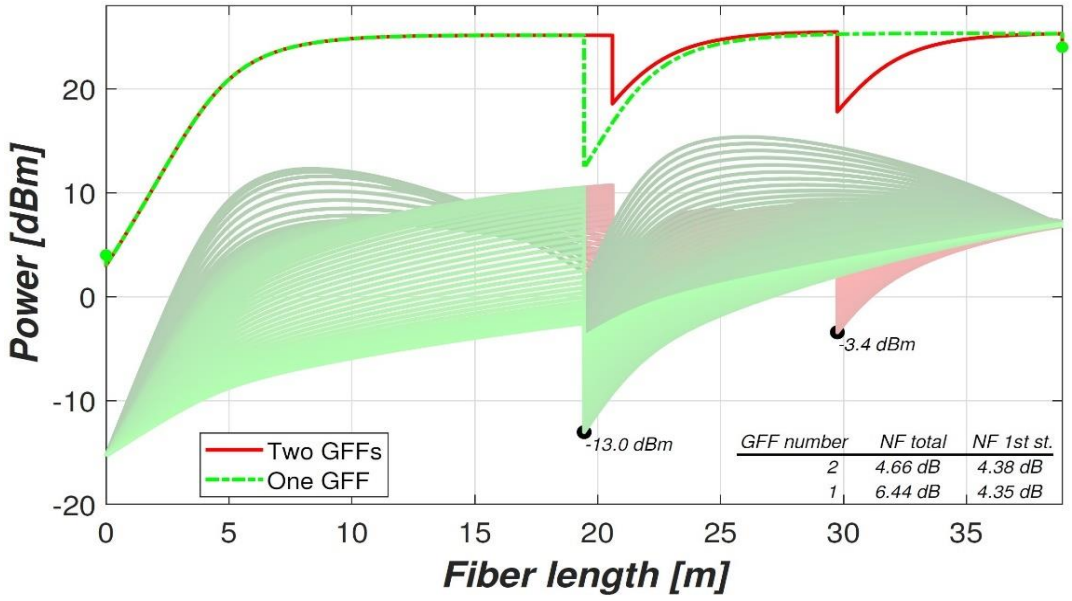

Figure 2-7: Power profiles in EDFA setups using one (setup A.1 [Rap22]) or two (setup A.2 [Rap22]) gain–flattening filters, respectively, for scenario 1 with a maximum wavelength of 1585 nm. Pump power in first stage: 950 mW, Gain: 20 dB.

2.3.4 Energy Efficiency

Energy efficiency of a wideband erbium–doped fiber amplifier (EDFA) for the L–band has been explored to be around 25% smaller as compared with a C–band EDFA [Rap23-1].

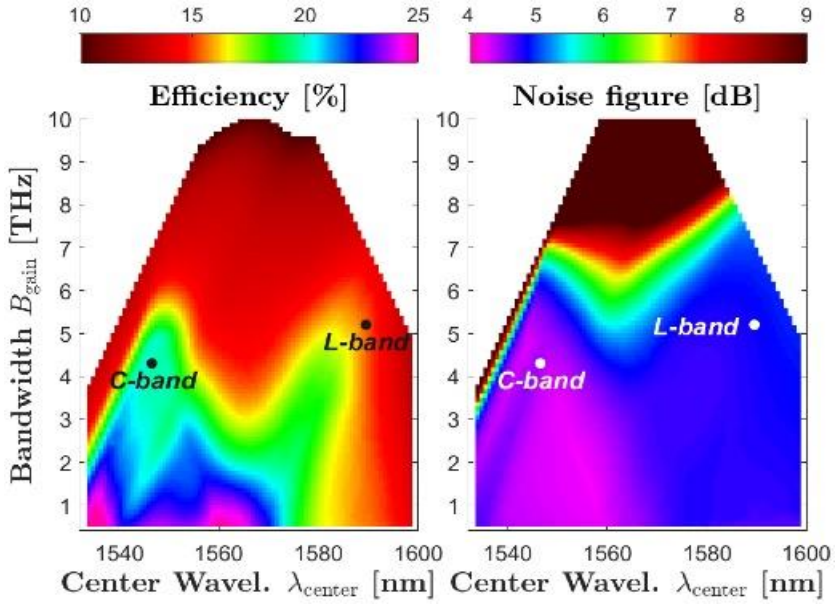

Figure 2-8: Color coded three–dimensional plots showing energy efficiency (left side) and noise figure (right side) of a wideband EDFA as a function of the two parameters center wavelength λ_c and optical bandwidth B_{gain}.

Figure 2-8 (left) illustrates the energy efficiency as a function of center wavelength λ_c and bandwidth B_{gain} of the gain range in form of a color coded plot for a constant output power of

20 dBm. Irrespective of the center wavelength λ_c, decrement in energy efficiency with increasing bandwidth B_{gain} is revealed. This is attributed to the growing average attenuation of the GFF. For small bandwidths, energy efficiency is significantly larger for center wavelengths λ_c in the C–band in comparison with the L– band. However, there are two spots at larger bandwidths in the range from 3 THz to 5 THz where similar energy efficiency is realized in both bands for center wavelengths of 1550 nm and 1583 nm. Nevertheless, noise figure is slightly smaller for small bandwidths at center wavelengths below 1565 nm, as illustrated on the right side of this figure. On the contrary, noise performance is enhanced for larger center wavelengths if the bandwidth exceeds 7 THz (bandwidths equivalent to combined C+L–band).

So far, constant output power has been assumed for general comparison irrespective of the actual bandwidth. Conversely, the number of channels scales almost linearly with bandwidth. Given the fact that the per channel power is limited by nonlinear fiber effects, it is still adequate to assume constant channel power if SPM is the dominant effect. As a result, the amplifier output power is a linear function of the channel number and of the bandwidth.

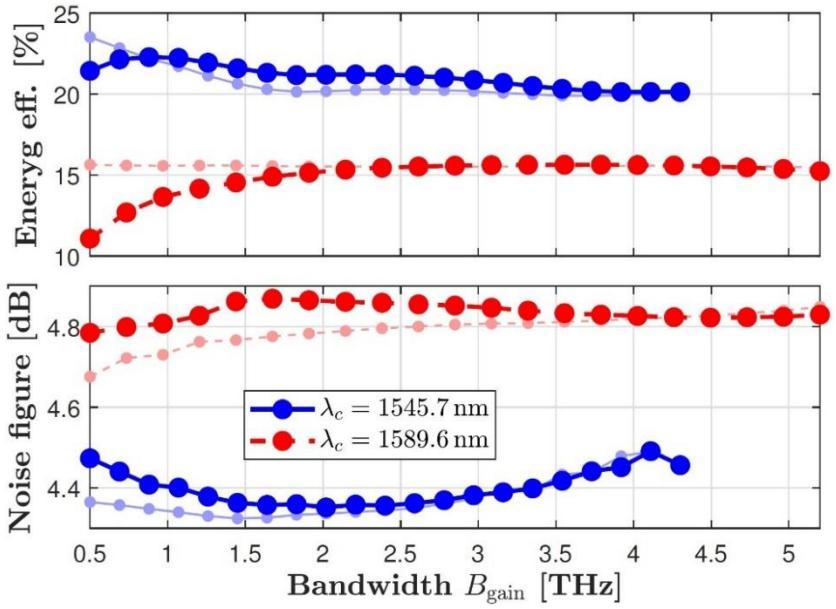

Figure 2-9: Energy efficiency and noise figure versus bandwidth B_{gain} for a center wavelength λ_c of 1545.7 nm (in C–band) and a center wavelength λ_c of 1589.6 nm (in L–band) with adaptive output power. Curves in light color represent results at constant output power.

For such a scenario, curves displayed in bold colors in Figure 2-9 reveal energy efficiency and noise figure versus gain bandwidth B_{gain} for center wavelengths of 1545.7 nm (in C–band) and 1589.6 nm (in L–band). In both cases, the amplifier output power amounts to 20 dBm at a gain bandwidth of 4.3 THz. Faint colors are used for representing results for a constant output power of 20 dBm for comparison purposes.

2.3.5 Raman Amplification and Compensation of Signal Distortion

Higher–order pumping schemes for codirectional Raman amplification are suitable for enhancing the optical signal–to–noise ratio (OSNR) in existing fiber links and consequently for increasing capacity or link length [Rap23-2]. However, this potential advantage has not achieved the desired output due to phase variations associated with intensity fluctuations of the

fundamental pump. A technique for compensating the impact of the phase noise by comparing the phase errors in two neighboring channels has been developed. Based on this technique, an improvement of the required signal–to–noise ratio (SNR) by up to 3 dB has been presented by means of Monte Carlo simulations. This enables an improvement in the OSNR with higher–order codirectional Raman amplification.

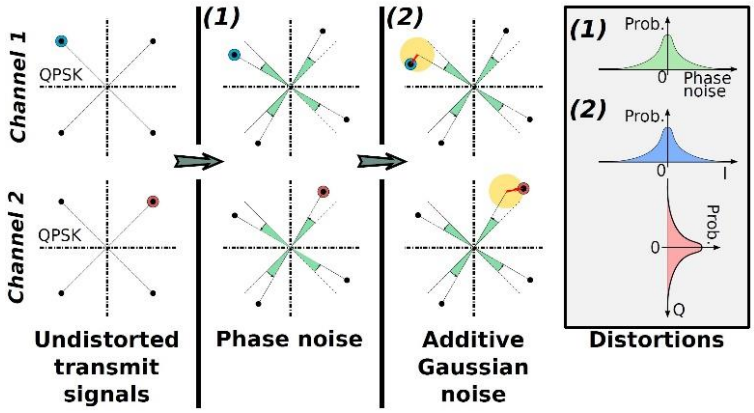

Figure 2-10: Modeling of the impact of phase noise on a QPSK signal.

Figure 2-10 illustrates modeling of the constellation diagrams for two copropagating channels influenced by phase noise and additive noise. The original symbols are represented by blue and red dots. In the first step, both symbols are rotated by the same random phase shift that is assumed to fulfill a Gaussian distribution. In the next step, a superposition of uncorrelated Gaussian distributed noise vectors to each of the two symbols is shown. By iterating these steps with random numbers of phase noise and additive noise, a large number of test samples is generated. Due to phase noise of the respective transmit and local oscillator lasers, both channels may further experience statistically independent phase variations. Nevertheless, the impact is very similar to additive noise. Thus, these contributions maintain the general functionality of the compensation algorithm.

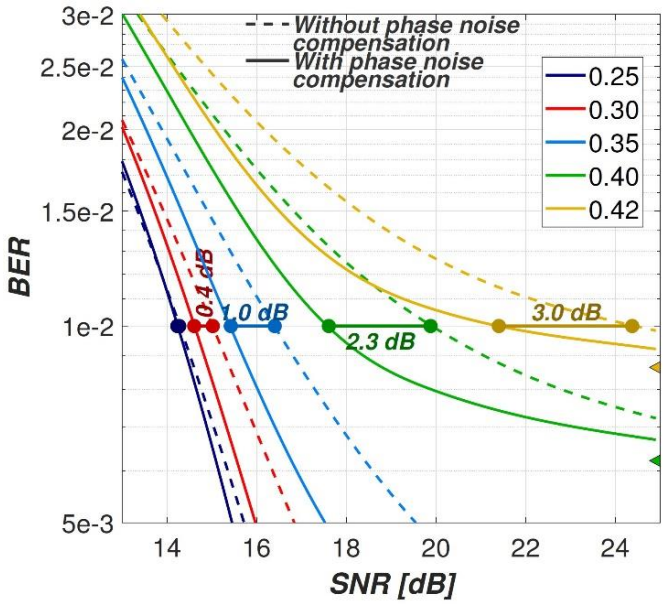

Figure 2-11: Pre–FEC bit error ratio (BER) versus signal–to–noise ratio (SNR) for different standard deviations σ_{PN} of the phase noise.

As a result of Monte Carlo simulations, Figure 2-11 illustrates BER versus signal–to–noise ratio (SNR). It is relating signal power to the power of the additive noise for different standard deviations σ_{PN} of the phase noise without (dashed curves) and with (solid curves) phase noise compensation. For the plots, ideal CPE is assumed and on the right side, there is an error floor indicated by triangles that increases with boosting σ_{PN}, which in turn limits the maximum realized improvement. As presented in this figure, the algorithm enables the reduction of the required SNR by up to 3.0 dB at a BER of 10-2. In order to fulfill this improvement, the clock phases of jointly processed neighboring channels need to be aligned at the transmitter side such that the symbols detected at the end of the fiber link are induced by the same pattern of intensity fluctuations of the high–power pump. Moreover, timing offsets emerging from different propagation delays need to be compensated. Additionally, the polarization axes of the two signals preferably needs also to be identical at the input of the transmission fiber.

2.4 Transmission Performance in Multi-Band Systems

2.4.1 Achievable Bandwidth Increase as Function of Margin

Expanding the capacity of fiber links using additional wavelength bands is cost-efficient and doesn't require reworking existing infrastructure. However, larger channel numbers can lead to increased signal distortions and reduced signal-to-noise ratio (SNR), limiting capacity upgrades. Nonlinear fiber effects, such as stimulated Raman scattering (SRS), can limit capacity in multi-band systems. To compensate this effectz, a tilt in the optical spectrum is introduced, producing a flat optical spectrum and constant optical signal-to-noise ratio (OSNR) at the receivers. To control nonlinear effects, average channel power must not exceed a characteristic power limit.

The links are based on standard single-mode fibers (SSMFs) with 0.2 dB/km attenuation at 1550 nm and transmitting wavelength channels with a data rate of 400 Gbit/s using polarization multiplexed 16QAM signals. The required OSNR is 21.5 dB, including a 1 dB penalty for nonlinear

fiber effects. The channel map covers the C–band, L–band, and S–band, see Figure 2-12 (A). Power exchange among channels is determined numerically using coupled differential equations [Man03]. Nonlinear interference accumulates incoherently and its contribution to the SNR scales quadratically with channel power [Pog14]. The OSNR versus transmission distance resulting from variable span numbers is illustrated in Figure 2-12 (B) and Figure 2-12 (C).

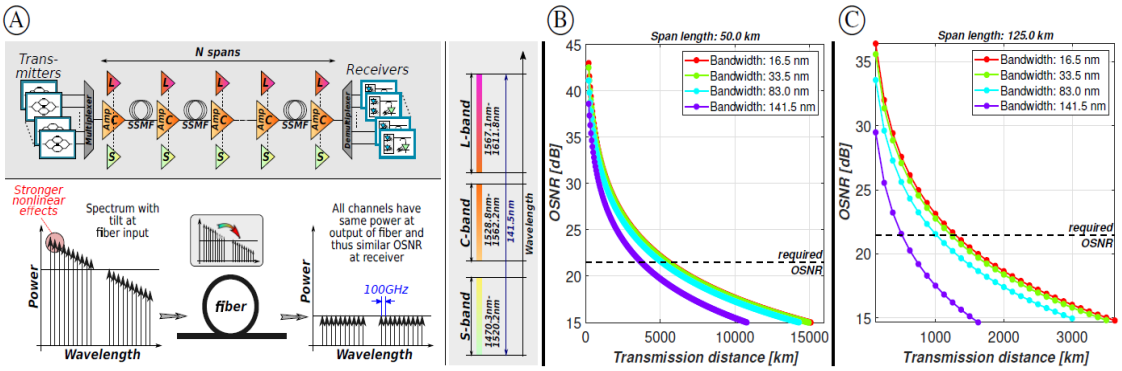

Figure 2-12: (A) Multi–span system setup and pre–tilting of the spectrum for SRS compensation (right side: considered wavelength bands), (B+C) OSNR at the end of a fiber–optical transmission link total link length for span lengths of 50 km and 125 km.

The study demonstrates in Figure 2-13 (A) that increasing the bandwidth leads to a stronger decrease in the OSNR as the span length increases. The decrease in maximum transmission distance is largest for the minimum span length, when adding L-band and S-band to a C-band system, as illustrated in Figure 2-13 (B). However, Figure 2-13 (C) shows that the relative reduction of the maximum transmission distance decreases with increasing span length. The study also shows in Figure 2-13 (D) that for short spans of 50 km, an OSNR margin of 2.5 dB is sufficient for upgrading the system to data transmission in all three bands, while a higher margin of more than 5.0 dB is required for achieving the same capacity increase.

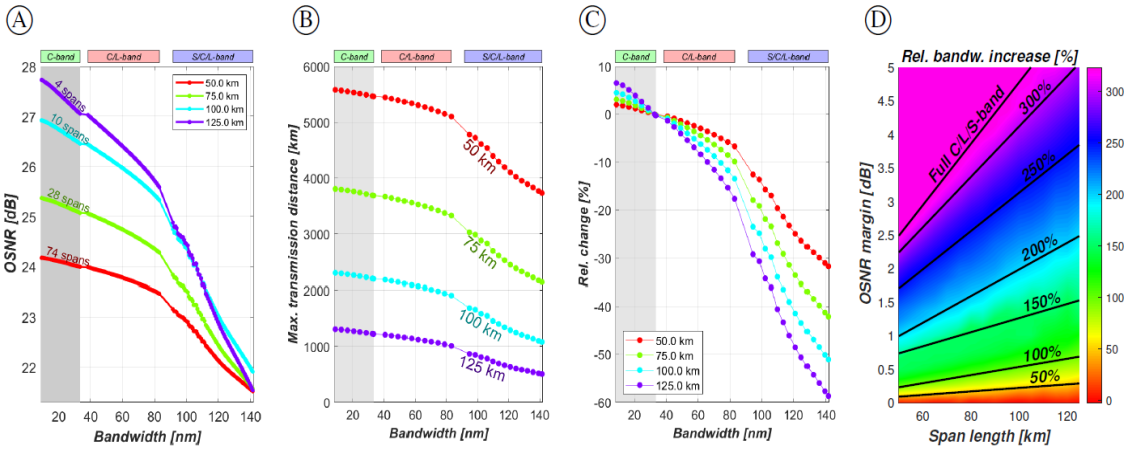

Figure 2-13: (A) Decrease of OSNR with increasing bandwidth for different span lengths and number of spans, (B) Maximum transmission distance versus bandwidth, (C) Relative change of maximum transmission distance versus bandwidth, (D) Achievable relative bandwidth increase versus span length and OSNR margin. Parameter in A-C: span length.

The study reveals that increasing the optical bandwidth of fiber links can lead to reduced OSNR due to SRS. The reduction is determined for different fiber lengths per span, with a 2.5 dB OSNR

margin required for 50 km spans to fully operate in full C/L/S-band, and even more than 5.0 dB for 125 km spans. For a typical 80 km span length, the necessary margin is approximately 3.9 dB.

2.4.2 Impact of band-gaps

The majority of commercial wavelength-division multiplexing (WDM) systems operate in the C-band, which has the minimal attenuation of a SSMF. The L-band and S-band, two more wavelength bands, provide somewhat slightly larger signal attenuation. O-band, E-band, and U-band are three more wavelength bands that can be used for data transmission, however the loss is much larger.

SRS in transmission fibers causes power transfer from shorter wavelengths to longer wavelengths [Rap07], resulting in higher effective attenuation for channels at shorter wavelengths. The slope of this attenuation is linearly dependent on total power launched into the fiber [Zir98], as long as the total optical bandwidth is smaller than the Raman shift. To compensate for this, optical amplifiers can introduce a tilt in their output spectrum, achieving a constant OSNR at receivers.

The power difference among channels increases with total power, even if the total power remains constant. This difference increases when channels are spread over a larger wavelength range. This is because the maximum launch power per channel is limited at the fiber input due to nonlinear fiber effects like SPM and XPM.

In a scenario where channel maximum power is limited by single-channel nonlinear effects, power exchange among channels is determined numerically by solving coupled differential equations [Man03]. The launch powers of channels are controlled to ensure all channels have equal power at the fiber output [Chr92] Adding L-band channels to a C-band system reduces receive power by 2 dB, resulting in a decrease in OSNR by around 2 dB, as shown in Figure 2-14. However, a C+L-band system provides better OSNR due to its larger wavelength range. Additionally, OSNR decreases by around 1 dB when introducing a gap between channels, as demonstrated by a C+E-band system. Therefore, gaps between wavelength bands should be avoided, and these observations apply to systems using three or four wavelength bands.

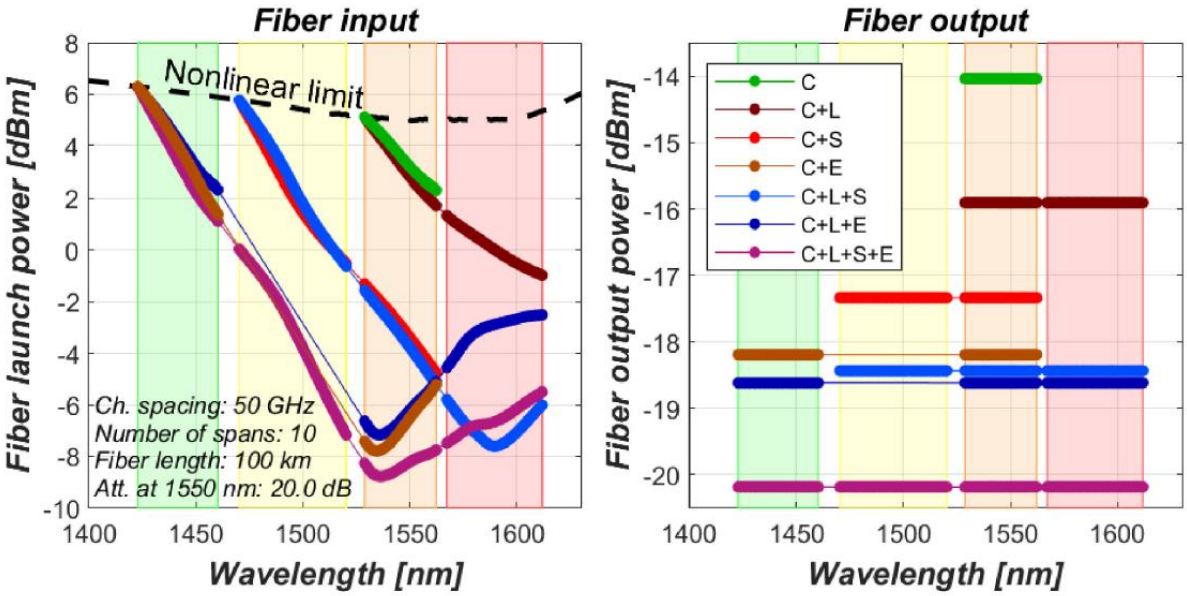

Figure 2-14: Pre–tilted input spectrum for various channel maps (left side) and spectral power distribution at the output of the transmission fiber (right side).

2.4.3 Capacity Upgrade Scenarios

Multi-band (MB) transmission offers cost-effective capacity upgrades over the existing fiber infrastructure in terrestrial networks, but it is not always the best solution. Capacity upgrades by multi-band transmission are less competitive in submarine links, where embedding new amplifiers is difficult. This makes space-division multiplexing (SDM) attractive. Multi-core fibers (MCFs) have found their first application in this field, but MB transmission is even not always the optimum solution in terrestrial networks, as shown in Figure 2-15.

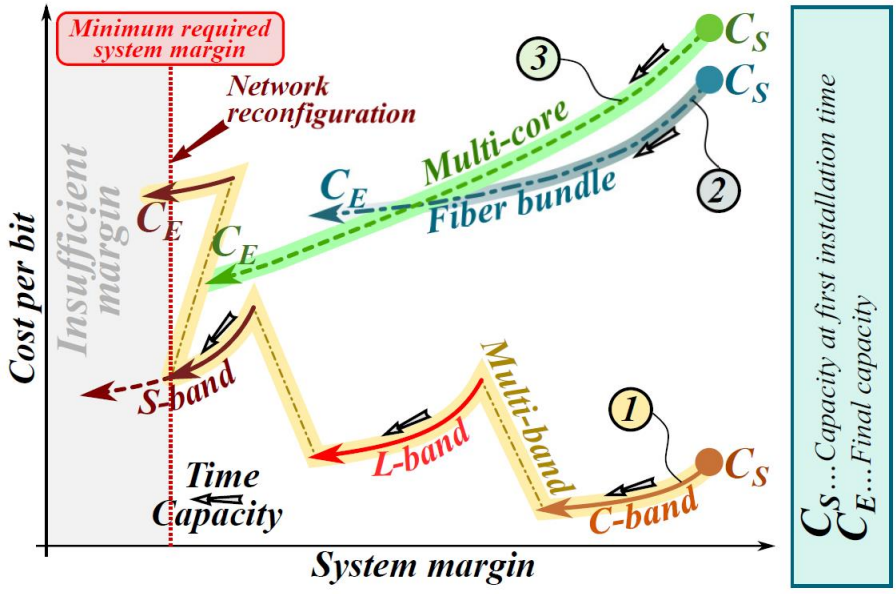

Figure 2-15: Parametric representation of an exemplary capacity upgrade scenario in a terrestrial network.

System margin and cost-per-bit are crucial parameters in evaluating transmission performance and economic potential of a transmission technology. Changes in these parameters are indicated by parametric presentations, with time and capacity increasing as the curves in the direction of dark arrows change. The cheapest solution is filling up the C-band, but it reduces system margin due to nonlinear fiber effects. Opening the L-band leads to a sharp decrease in system margin, followed by a further decrease with increasing channel count. The introduction of the S-band further decreases system margin and increases cost-per-bit.

The increasing number of channels in the S-band may lead to a decrease in system margin, making error-free data transmission impossible. To remedy this, network reconfiguration and additional 3R regenerators can be installed, but they increase cost-per-bit. Fiber bundles or MCFs may provide a more cost-efficient solution, but both have increased costs at smaller capacity due to cable installation costs.

2.5 Transient control in Multi-Band Networks – Experimental Verification

A fibre optical link with N spans consists of SSMFs with 0.2 dB/km attenuation at 1550 nm. The WDM signal is split into C-band and L-band parts, with power restored by amplifiers. Maximum launch power is limited by nonlinear fibre effects and decreases with more spans. A tilt compensates for SRS power transfer. This is illustrated in Figure 2-12 A.

In a meshed optical network, some channels may be dropped due to traffic interruptions in another optical multiplex section (OMS), requiring error-free data transmission of the remaining channels. To ensure this, amplifiers must be designed to cope with variations in channel numbers and total power levels. In multi-band scenarios, adjusting the gain and tilt of all amplifiers amplifying surviving channels is necessary. The power spectrum at the input of the transmission fiber must be adjusted, which is illustrated in Figure 2-16, with the tilt of both amplifiers set to the same reduced value [Anc22]. The gain of C-band amplifiers must be reduced, while the L-band amplifier's gain is increased. An amplifier optimized for a specific point of operation must compensate for the complete fiber loss, although a smaller gain would be sufficient under normal operation with all channels present.

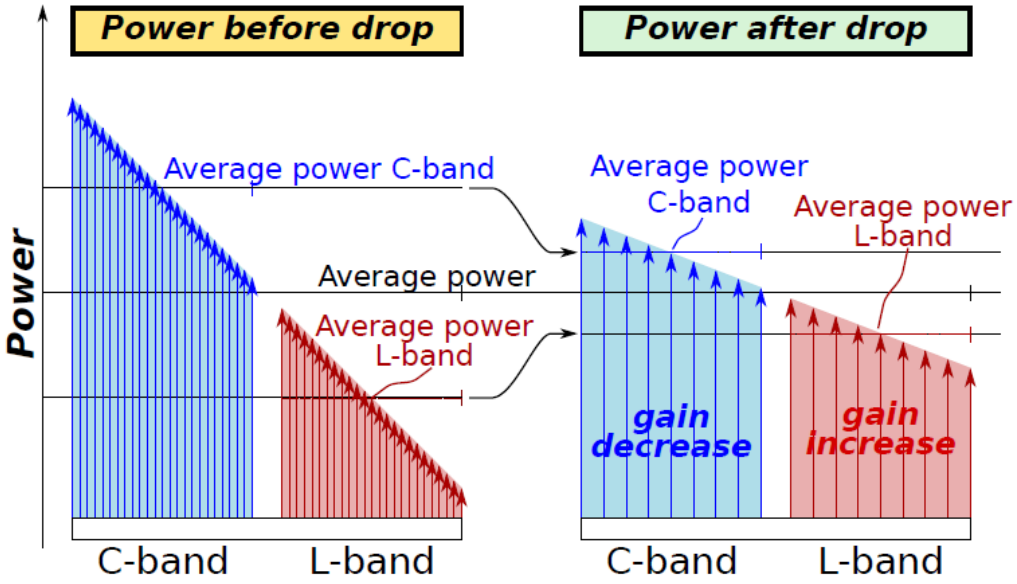

Figure 2-16: Tilt and gain adjustment in a C+L–band system when dropping an equal share of the channels in both bands.

The power exchange within a transmission fiber is determined using a numerical model based on coupled differential equations [Man03] considering wavelength dependence of all parameters. The attenuation coefficient is determined from wavelength-resolved measurement results for a typical SSMF, and the Raman gain coefficient's dependence on frequency separation between two lightwaves is considered for improved accuracy [Agr13].

Fast reaction is achieved through feedforward control, which determines pump power based on input parameters like input power. Look-up tables or mathematical relations are used, and a larger time constant feedback control is used. The tilt coefficient for the channel map before the drop is known, and the estimate of the tilt coefficient for the channel map after the drop can be directly calculated.

The equations for calculating total output powers from input powers in an electronic controller are presented in [Rap24-2]. Equal distribution of channels is assumed within the same band over the frequency range from a given minimum to maximum. The total output after channel drop can be determined from measured input powers. The relative contribution of two bands to total output power is determined by certain parameters. The results and measured input powers allow for easy calculation of the value for the integrated variable optical attenuators (VOAs).

The equations assume equal distribution of surviving channels across different wavelength bands. Three scenarios are considered for verification, starting with fully populated bands and covering depopulation of the C-band or L-band. Different options for depopulating one band are considered, with scenarios varying in number of channels and coverage. The study calculates the total power needed to achieve equal channel powers in the C-band and L-band for different scenarios and depopulations. The total power is divided by the total power launched into the transmission fiber. The results are illustrated in Figure 2-17, with dotted, dashed, and dash-dotted lines versus a parameter "power ratio". This parameter relates the total power in the depopulated band to the total power in the fully loaded band at the input of the amplifiers. The

power levels calculated match the total output powers, resulting in optimum compensation of SRS.

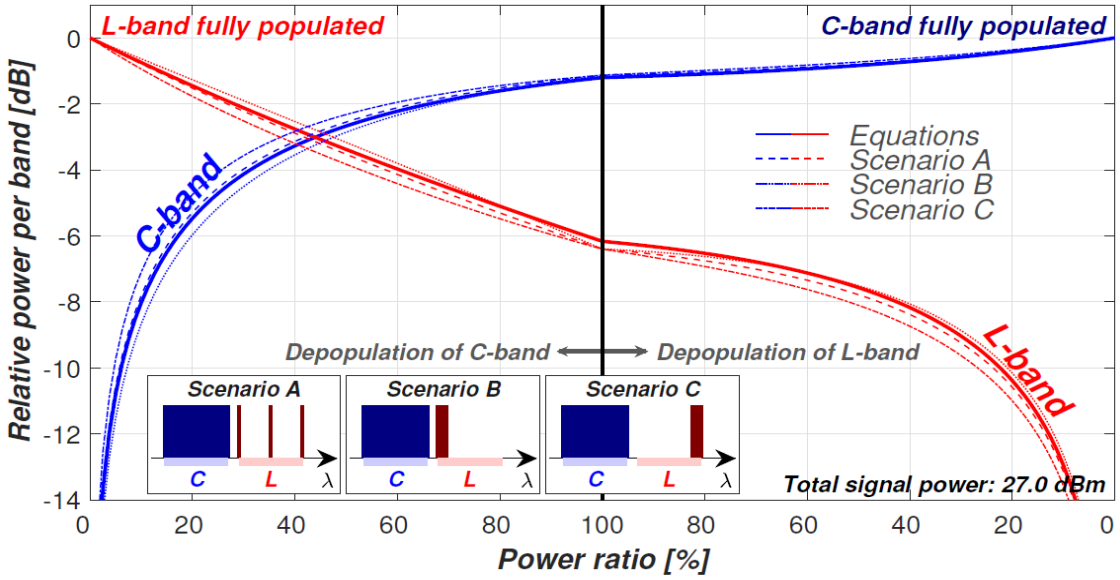

Figure 2-17: Output power per band normalized to the total launch power and represented in logarithmic units for a C+L–band system for three different drop scenarios. The three scenarios are illustrated for three channels in the depopulated L–band.

Further results are already contained in unpublished papers and will be presented in the future. Verification using a setup in the C+L+S bands is part of B5G-OPEN.

2.6 ADVANCED CHANNEL MONITORING

During the lifetime of an optical network, the performance varies due to multiple reasons like fiber cuts, equipment aging, soft-failure events, etc. Today, it is difficult to understand the underlying reasons of soft-failure events as little information from the physical layer is known. Current commercial transponders monitor signal performance (bit error rate and error vector magnitude), powers, polarization mode dispersion. Therefore, a key interest is to largely increase the monitoring capabilities of optical equipment to leverage the collected data into insightful explanations. To do so, B5G-OPEN proposes to study monitoring methods in C-band and see how it can evolve into multiple bands.

Massive monitoring can be implemented either with dedicated low-cost hardware or more interestingly via the coherent transponders. The latter area of research has attracted significant research works in the last years. Among these, a very promising technique is longitudinal power profile estimation which offers an estimate of power but also an accurate localization of this estimation (~1-2 km precision). The technique first introduced in the C-band [Tan19] has been extended to multiple bands [Sen22], and see Section 3.3 for the newest results from B5G-OPEN project. With such a technique, it offers plenty of monitoring applications such as power profiles, span-wise CD maps, gain spectrum of each amplifier in the transmission line under interest, excessive polarization loss with its location multi-path interference, etc.

For instance, in B5G-OPEN we performed a multi-channel transmission over C + L bands. The experimental setup is described in Figure 2-18. The channel under test (CUT) is PDM-16QAM modulated at 64 Gbaud shaped with a root-raised-cosine filter of 0.1 roll-off factor. Sequences of 2^{15} symbols are used for the transmitted signal. Digital pre-dispersion is applied and equals 800 ps/nm. The CUT is swept from 1537.83 nm to 1600.50 nm, with steps of 2.36 nm, and the rest of the channels are loaded with amplified spontaneous emission (ASE) channels. We consider in total 42 channels including CUT with a 1.18nm (~150 GHz) channel spacing where 20 channels are in the C-band and 22 channels in the L-band. The launched power is spectrally flat, i.e. no launch power optimization was performed, and the launch power per channel after the 3 dB coupler is 1.05 dBm in average over the C+L band. Between C- and L-band, we create a gap band of 13.52 nm (~ 1.645 THz). The channels are sent through a 4-span transmission line of 280 km in total over standard single mode fiber (SSMF). The EDFAs are configured in automatic current control mode. At the receiver side, the optical power of the WDM grid is boosted by an EDFA before being filtered through a bandpass filter (BPF) for the selection of the CUT. The signal before the filter is also used for optical signal-to-noise ratio measurements through an OSA. The CUT is sent to an offline receiver with 70 GHz bandwidth and 200 Gsample/s real-time oscilloscope (RTO) and is processed offline. We record 10 acquisitions at 1SPS for each of the 21 channels.

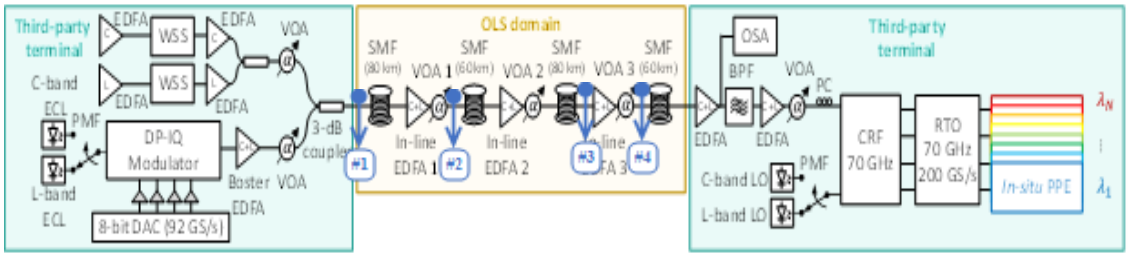

Figure 2-18: Multi-channel C+L experimental setup. Points #1, #2, #3 and #4 at the fiber span input underline where the power is estimated.

We processed the whole WDM multi-channel experiment. The traces are processed for a Δz = 2km with (2SPS, λ=5.10^{11}) and the obtained profiles are average for each channel. We then performed the estimation of the launch power per channel.

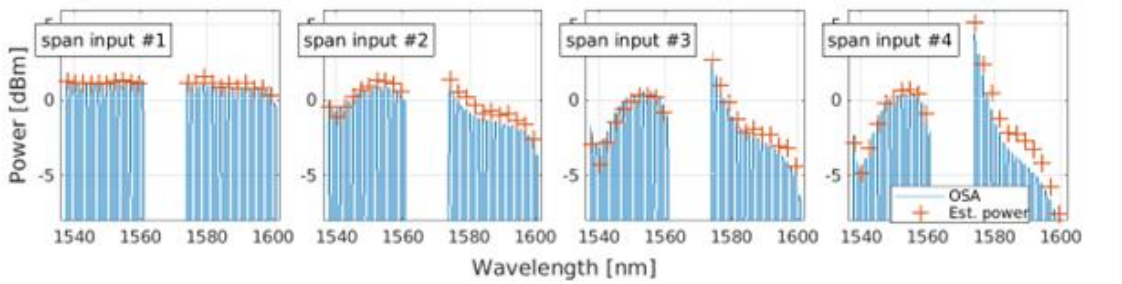

Figure 2-19: Estimated power at fiber span input along the transmission link.

In Figure 2-19, we plot the estimated power at the input of each span (red plus markers) as a function of the central channel wavelength. We superposed the OSA traces recorded at each fiber span input. We observed that the shape of the spectrum is well reconstructed, and the estimated power is in very good agreement with OSA measurements. The average channel

launch power in C+L-band is estimated at 1.01 dBm in excellent agreement with measured one of 1.05 dBm, leading to only 0.04 dBm error at the first amplifier. Lastly, we compute the min, max and average error on the channel power estimation. We observed that the maximum error increases with the distance. For span input #1 it equals 0.55 dB, up to a maximum error of 1.62 dB for the last amplifier where the largest tilt occurs. The average estimation error is 0.04, 0.51 and 0.4 and 0.76 dB for span input #1 to #4, respectively. These results have not been published yet.

2.7 BACKBONE NETWORK SEGMENT

Having as a reference the values of node capacities reported in Table 1-1 and assuming an optical backbone node (Node N in National CO as in Figure 1-2) of 4 nodal degrees, we conclude that the required capacity on each backbone topological edge, if traffic would be equally balanced among the four directions, is of 14 Tbit/s, 111 Tbit/s and 444 Tbit/s in short, medium and long term respectively. Additionally, the add-drop blocks should be capable of handling traffic loads of 18.5 Tbit/s, 148 Tbit/s and 592 Tbit/s in the same corresponding time periods.

Assuming the use of the ultra-wide C-Band only (6 THz), a 24 Tbit/s capacity is potentially available on a single fiber line system (for an average SE of 4 bit/s/Hz). Single C-band systems would therefore be able to satisfy traffic needs in the short term. However, if the traffic is higher than the one estimated with the hypotheses on which Table 1-1 is based on, something that cannot be ruled out a priori, a higher transmission capacity system would be needed.

The optical node architecture for the short term should be the one depicted in Figure 2-20 (b), where the route and select WSS based switching matrix is used as core switching system of the node and appropriate add and drop blocks are used (they can be made by multicast switches (MCS) or of WSSs and accompanied by optical amplifiers). The scheme of the switching matrix structure, based on route-and-select (R&S) architecture, is shown in Figure 2-20 (a). Optical amplifiers placed at the input and output of the WSSs assure the recovery of line losses (input) and the appropriate launch power (output).

According to Table 1-1, using a single band of a single optical fiber is not sufficient in the medium and long term for data transmission on topological edges of the backbone. Consequently, solutions that use multiple fibers (or a single multi core fiber) and/or multiple bands, in addition to C-band, must be adopted.

Figure 2-20 (c) illustrates a node architecture that exploits single-band WSS switching systems in parallel and combine SDM and MB. MB is implemented with appropriate band filters that separate and recombine the bandwidths at the input and output, respectively. SDM is obtained through parallel systems leveraging on a multi-fiber bundle or a single multicore fiber on the topology edge.

In the medium term, MB solutions consisting in the use of at least three bands (e.g., C, L and S), should be suitable for most transmission scenarios, but not all. Alternatively, the SDM solution making use of parallel fibers or cores should be capable of addressing all cases but, cost-wise, will most likely not be the ideal solution in same scenario. Consequently, a combination of the two solutions, SDM and MB, could be a preferable solution as it guarantees greater scalability.

In the long term, a SDM solution making use of several parallel fibers (more than ten) or, even better, a solution based on the combination of SDM and MB, will be required. According with

numbers in Table 1-1, in long term, exploiting three transmission bands (C, L and S) or more, and five to ten fibers/cores will be required on each topology edge of the most demanding optical backbone nodes.

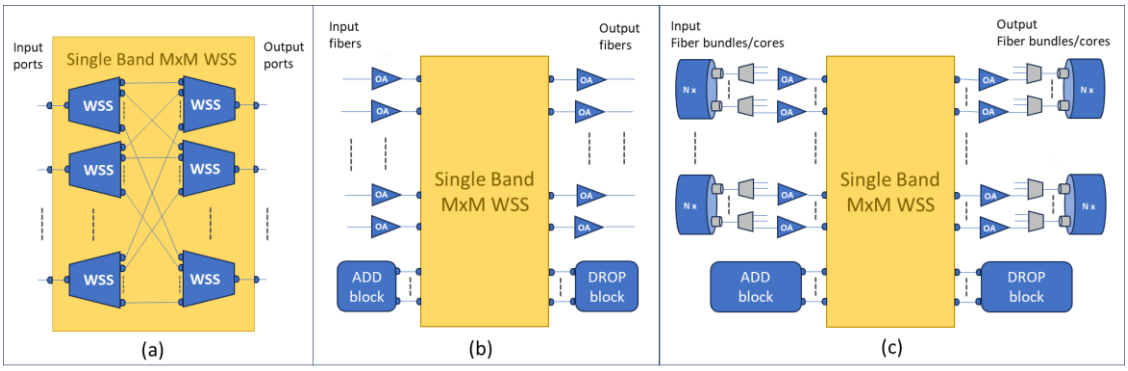

Figure 2-20: Optical node architectures for high capacity systems: (a) Single band MxM WSS route and select switching system, (b) optical node architecture for single band and single core/fiber line systems, (c) optical node architecture for multi-band and multi core/fiber line systems.

However, the node design shown in Figure 2-20 (c) suffers from scalability issues concerning the increasing spectral and spatial dimensions. One of the constraints to consider is the fact that WSSs have a limited number of ports (today around 30) and therefore a completely directionless and contentionless node structure becomes difficult to implement in many situations. Given the likelihood that in the future the wavelengths allocated on the entire spectrum of a fiber/core in input could be directed to a fiber/core in output without the needs to be optically processed (i.e., a pass-through of the entire band is what it is required from the node), specific input and output fibres/cores may be directly interconnected (via fiber/core switching), bypassing the WSS and the A/D structure. This direct connection holds the potential to simplify the node by reducing the WSS port count and enhancing optical performance for signals bypassing the WSS, thereby minimizing additional losses. Two examples of such Multi-Band over Space Division Multiplexing (MBoSDM) architectures are given in Figure 2-21. These architectures rely on a Spatial cross connect (S-OXC) and differ from each other by the employment of a single band WSS switch matrix or a multi-Band WSS switch matrix. Advantages and drawbacks of the two structures, and of another one that implement interconnections between input and output fibers/cores by means of a patch panel instead of S-OXC (not reported in Figure 2-21), are investigated in [Sou24] where scalability and cost issues are extensively discussed.

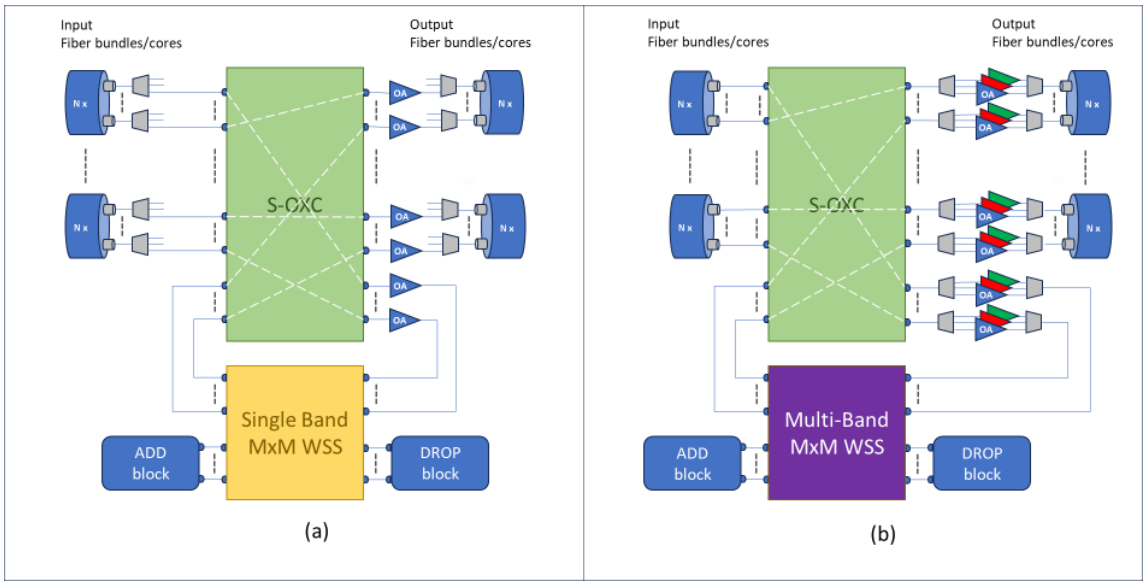

Figure 2-21: Combined MB over SDM (MSoSDM) node architectures: (a) single-band matrix-switch-based MBoSDM node with a S-OXC, (b) multi-band matrix-switch-based MBoSDM node with a S-OXC.

2.8 Metro Core Network Segment

A node architecture suitable for a Metro-Core segment, in case of meshed network requiring very high capacity node architecture, can be a single or multi-band WSS based switching architecture as the one presented for Backbone network segment. In this case, the internetworking will be done with conventional point-to-point transponders operating in the C, L, S or other bands and the number of bands and fibers/cores used in a specific context depend on the capacity needed. Data rates suitable for metro core transceivers would be in the range of 200 Gbit/s-800 Gbit/s (and even higher in the long term), with a SE of up to 5 bit/s/Hz (or even slightly higher).

Looking at the needs of the R nodes in National CO reported in Table 1-1, the total capacity required in short, medium and long term is the same of the capacity required by the Backbone nodes N. The difference is on the percentage of Add/Drop traffic that is much higher for Node R as they deliver all traffic to telco and service functions. This metro core nodes require the same solutions of backbone nodes.

The maximum needs of the R nodes placed in Regional CO, always with reference to values reported in Table 1-1, are lower than the R nodes in National CO. In this case, the single band single fiber node architecture (as the one of Figure 2-20 (b)) allows to cope with traffic needs of node R up to medium term, while only for the long term a MB (or SDM) node system will be required. The traffic requirements in Table 1-1 are for the R nodes in regional COs requiring higher capacity, i.e. those R nodes that act as transit for traffic coming from other more peripheral R nodes. For the latter, the traffic requirement is even lower and therefore, even more so, single band systems seem to be sufficient. In the medium and long term, the problem could be to make peripheral single-band nodes interwork with more central multi-band nodes. This issue requires special architectural solutions.

In addition to the solutions identified above, which use conventional point to point networking and ROADM or their extensions (i.e., MBoSDM nodes) in the metro core segment, in B5G-OPEN point-multi-point coherent optics (DSCM/XR) were also considered as a solution for the entire metro environment (aggregation and core).

The context here is no longer that of the separate metro access and metro core segments but provides a solution that integrates both. In such case the topology is not restricted to be a linear chain, typically an horseshoe ended by two hubs with many leaves in-between as it is in the aggregation, but it is a mesh, and light-trees have to be created to allow the subcarrier's internetworking of many leaf transceivers (each terminating one to some SC on the same wavelength) with the hub transceiver (which terminate all active SCs coming from leaves of the corresponding three wavelength).

The extension from the aggregation segment to the metro core segment of the point to multipoint coherent optics networking requires modified WSS-based ROADM architectures. The challenge to investigate ROADM structures suitable for point to multipoint networking have been addressed in B5G-OPEN and reported hereafter.

Conventional ROADM are based on Wavelength-Selective-Switches (WSS) which impose an internal blocking situation in most of the commercial equipment deployed: WSSs cannot switch two signals in the same wavelength, coming from two different ports, to the same output. This means that two DSCM signals using different subcarriers in the same wavelength cannot be merged by these WSSs.

To circumvent this limitation in conventional broadcast-and-select ROADMs, some options have been examined:

- Architecture (a) shown in Figure 2-22: WSS-based directional add/drop with posterior add. This option consists in reusing conventional ROADMs as-is but using spare components to add the transmission side of the DSCM signal in an external coupler after the WSS. The solution is very simple, but the wavelength-tree is constrained to be linear, and the hub must be at the end of the node chain. (Not yet commercially available a system, but easy to be implemented from spare components).
- Architecture (b) shown in Figure 2-23: WSS-based directionless drop/directional with posterior add. This option is exactly the same as the previous one in the add section but it gains the directionless property for dropped wavelengths through the WSS followed by the splitter in the drop section. (Not yet commercially available a system, but easy to be implemented from spare components).
- Architecture (c) shown in Figure 2-24: Degree-N WB-based directionless add/drop. The solution requires N^2 wavelength blockers (where N is nodal degree) and it is suitable for arbitrary trees with hub at the end (all subcarriers of the same wavelength (the tree-wavelength) must be received from the same degree at the Hub). (Not yet commercially available, needs to be developed).
- Architecture (d) shown in Figure 2-25: Degree-N WB-based directionless add/drop. The solution requires N^2 +N wavelenght blockers (where N is nodal degree) but it is suitable for arbitrary trees and arbitrary hubs. (Not commercially available, needs to be developed).

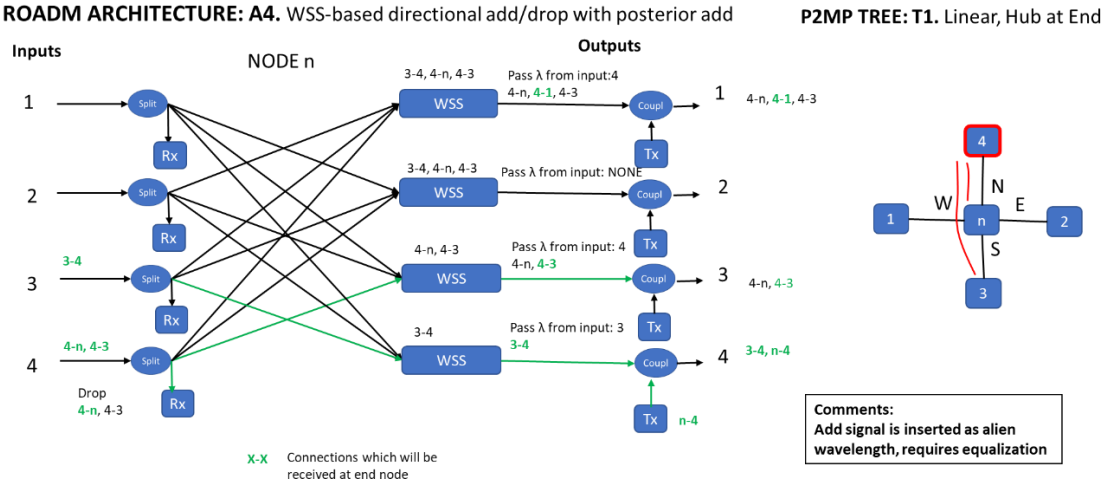

Figure 2-22: Modified ROADM with WSS-based directional add/drop with posterior add.

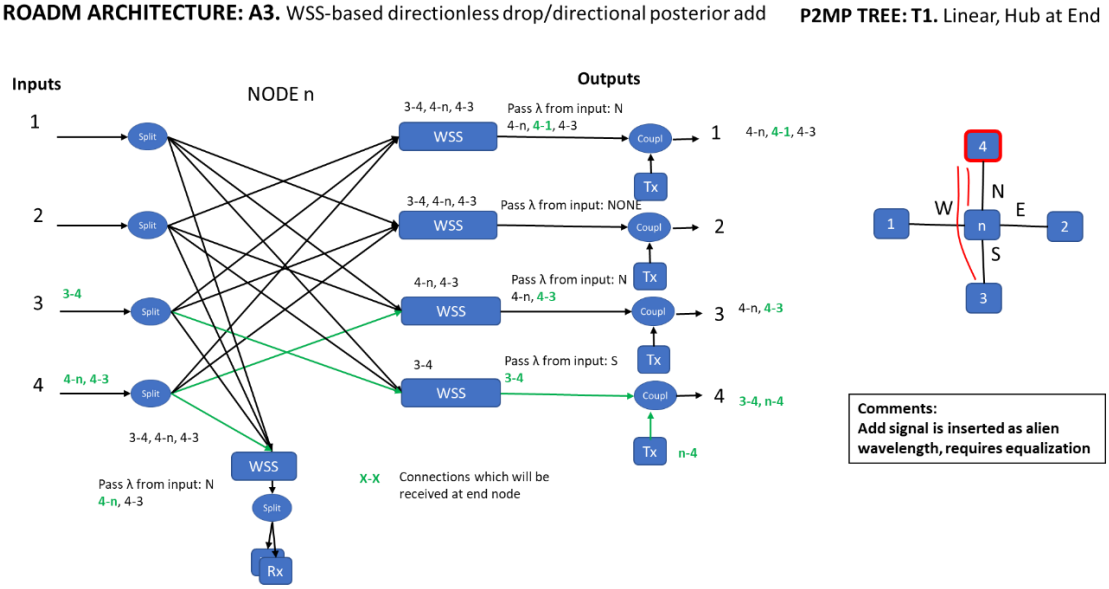

Figure 2-23: Modified ROADM with WSS-based directionless drop/directional with posterior add.

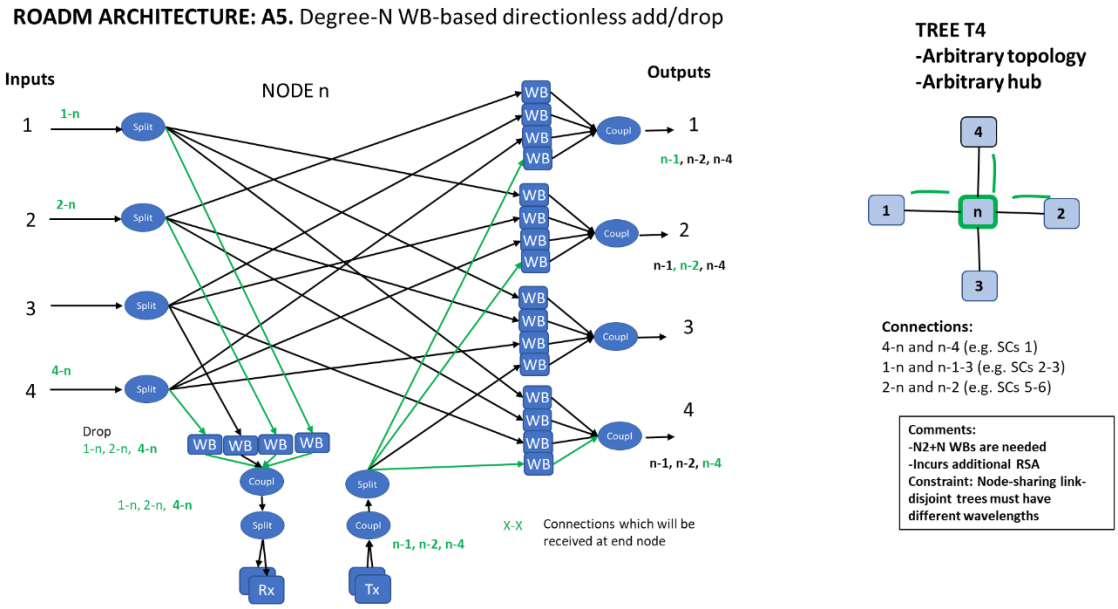

Figure 2-24: Modified ROADM with Degree-N WB-based directionless add/drop.

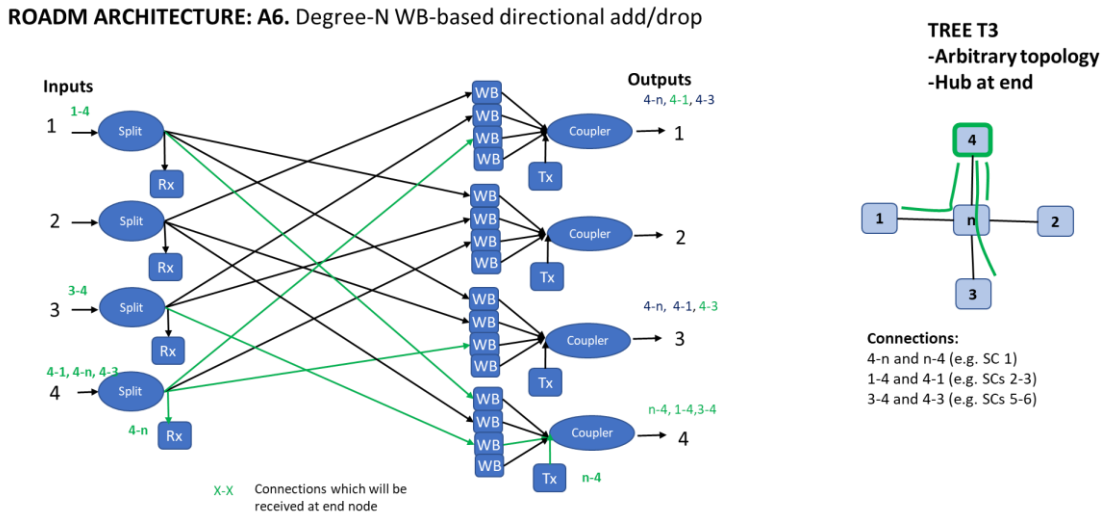

Figure 2-25: Modified ROADM with Degree-N WB-based directionless add/drop.

Considering the systems currently available or bing in the last R&D stage (i.e., 400 Gbit/s Point to Multipoint hub transceivers), this solution is suitable for a short-term scenario and in situations where traffic is not very high (for example for gathering the traffic in suburban or rural areas), but in future, with higher data rates of hub transceivers (for example with 800 Gbit/s or 1.6 Tbit/s), this type of solution will be applicable in all contexts (including urban or densely urban areas) and also in the medium and long term.

2.9 Metro Aggregation Network Segment

In the metro-aggregation network segment, the low cost of the optical data-plane solution is an important driver, considering the high number of nodes comprised by this network segment. Moreover, the solution must suit the high variability in terms of traffic amount to be handled by different nodes, based on the different geotypes they belong to.

In D3.2 an estimation of upper limit in terms of traffic needs has been evaluated, both for the Access optical node and for the Hub optical node type, considering:

- a dense urban geotype,
- horseshoes topologies composed by up to 8 Access nodes and terminated by two HUB nodes,
- couples of Hub nodes terminating the traffic collected from up to 16 Access nodes, arranged in 2 to 4 horseshoe topologies.

This hypothesis lead to the estimation for a generic Access optical node of a maximum add-drop traffic of 0.5 Tbit/s, 4 Tbit/s and 16 Tbit/s and a maximum pass-through traffic of 4 Tbit/s, 32 Tbit/s and 128 Tbit/s in the short, medium and long term timeframe respectively (where short, medium and long term means respectively 3, 6 and 9 years from now), and for the Hub optical node, of a total handled traffic of 4 Tbit/s, 32 Tbit/s and 128 Tbit/s in the short, medium and long term timeframe respectively, divided in add-drop and pass-through based on the percentage of traffic transparently bypassed toward the national node. These evaluations can be considered upper limits with respect to an average metro aggregation network; in fact, in some suburban and rural contexts, a downscaling factor of 4 to 10 for these numbers can be considered reasonable.

The project has looked into optical add drop multiplexer (OADM) designs to support the increasing amount of required traffic. Initially, filter-less designs can support a number of stacked 400 Gbit/s or 800 Gbit/s p2mp subcarrier channels (p2mp-SC) in the C-Band. The number of p2mp-SC systems that can be stacked depends on multiple factors like the size of the aggregation metro network, i.e. the number of OADMs the traffic is crossing. The upgrade of the initial design presented in D3.2 is analysed here in Section 3.1.4. Assuming we could use four 800G p2mp-SC systems, this would lead to a metro-aggregation network with 3.2 Tbit/s capacity. This type of solution can certainly fit suburban and rural contexts, at least in the short and medium timeframe.

Increasing capacities will require a new design, where the OADM is based on wavelength blockers comprising fixed filtering mux/de-mux elements and SOAs and exploiting Multi-Bands, and SDM architectures based on parallel fibers. These types of solution are described in details in Section 3.1.5 and Section 3.1.6, reporting first experimental setup and performance evaluations.

These solutions are modular and can comprise modules working in O, S, C and L bands, which correspond to spectrum widths of 17.5 THz, 9.4 THz, 4.5 THz and 7 THz respectively.

So, considering the traffic estimation handled by a generic Access node in a dense urban context according to D3.2, corresponding to 36 Tbit/s in the medium timeframe (32 Tbit/s in passthrough and 4 Tbit/s in add-drop), in the hypothesis of 400 Gbit/s channels and 100 GHz of channel spacing, the Access OADM node architecture could relay on a C+L Multi-Bandwidth Wavelength Blocker (MB-WB) and without the need of parallel fibers, as shown in Figure 2-26.

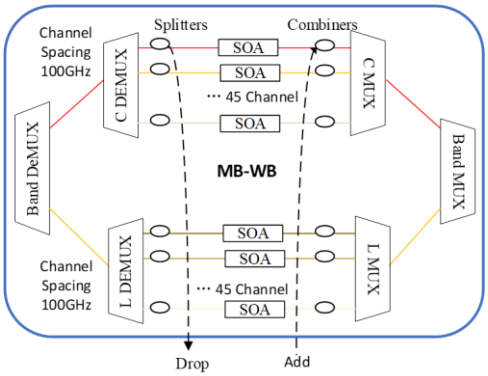

Figure 2-26: OADM architecture for an Access node in a dense urban context in the medium timeframe.

In order to scale to the total traffic handled by a generic Access node in a dense urban context in the long timeframe according to D3.2 estimation, corresponding to 144 Tbit/s (128 Tbit/s in passthrough and 16 Tbit/s in add-drop) an SDM architecture, based on parallel fibers, must be adopted, and possibly also the usage of more then two bands.

A possible solution, based on C+L bands, and four parallel fibers, is shown in Figure 2-27. Depending on the distance between adjacent Access nodes, this solution could comprise EDFAs preceding the nodes, to compensate the high attenuation introduced by the 1:5 splitters.

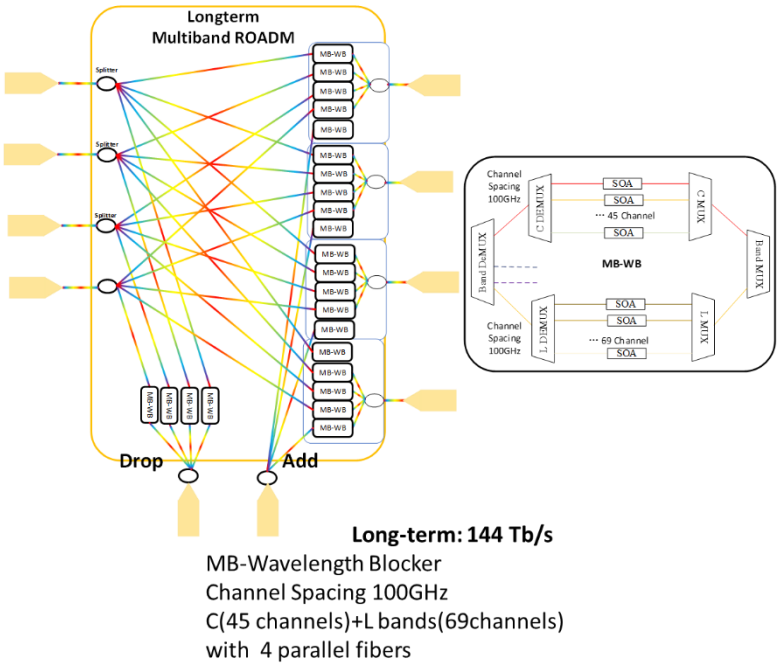

Figure 2-27: OADM architecture for an Access node in a dense urban context in the long timeframe based on C+L bandwidth and four parallel fibers.

An alternative solution, exploiting only two fibers, but three bands (O, C and L) is shown in Figure 2-28, where the usage of the O band is considered for shorter links, terminated on Access nodes

within 40 km from a Hub node, leaving the C and L bands for the transport of channels over longer links between the two Hub nodes.

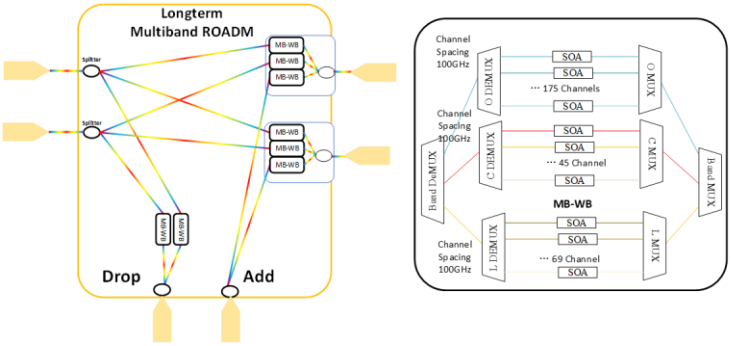

Long-term: 144 Tb/s
MB-Wavelength Blocker
Channel Spacing 100GHz
O(175 channel)+ C(45 channels)+L bands(69channels)

Figure 2-28: OADM architecture for an Access node in a dense urban context in the long timeframe based on O+C+L bandwidth and two parallel fibers.

As shown in the high-level architecture of B5G-OPEN (Figure 1-2) the hinge from metro aggregation and metro core is the optical hub node (node H) having the role of interconnecting several metro aggregation horseshoes to a single terminal metro core optical node. The function of the hub node is to allow a flexible dropping of flows needing a local processing in the packet layer or transparent bypassing toward the metro core network.

This node can have the same architecture and technology of Access node (Optical node A in Figure 1-2) as previously discussed or be a conventional WSS based ROADM single or multi-band node. One dedicated degree or add/drop client-side interconnection, are both options allowing transparent interconnection between the two network segments.

2.10 Access Network Segment

One of the key features of B5G-OPEN is the Integrated Access where any access technology system is seamlessly operated and controlled.

Access CO architectures were described in Section 4 of D2.1 [D2.1] distinguishing along time frames, and in considerable details in Section 5 of D3.1 [D3.1].

The reader is referred to above cited deliverable, were a complete a comprehensive discussion of the access network architecture is given.

3 THIRD YEAR RESULTS ON DATA PLANE INFRASTRUCTURE

3.1 OPTICAL SUBSYSTEMS, SWITCHING AND AMPLIFICATION

3.1.1 OADM-based filterless solutions for low-cost network architectures

As preparation for the system-level demonstration at BT-labs, we used the numerical simulation tool to carry out performance analysis with the aim of determining critical aspects from a transmission point of view. For the current analysis, even though we had previously decided to define a network with twelve leaf nodes and a downlink/uplink traffic, which could be covered by 16×25 Gbit/s subcarriers (see D3.2), upgrades were performed on the simulation tool to allow for an arbitrary number of leaf nodes and different traffic characteristics. Figure 3-1 shows the general illustration of the diagram describing the demo scenario. Note that the inner structure of the optical add/drop multiplexer has been previously described in D3.2.

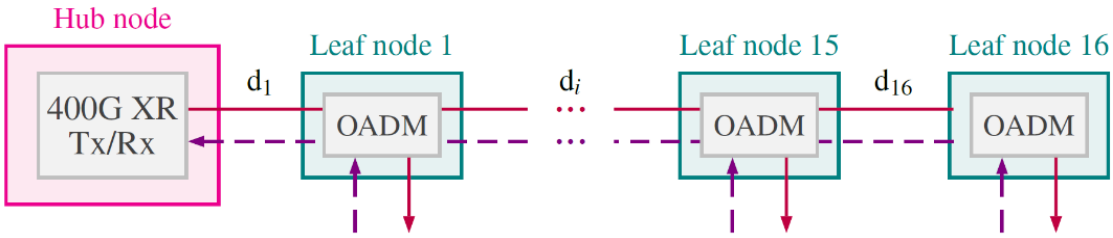

Figure 3-1: General diagram for evaluating the optical performance of a PtMP DSCM-based system for metro-aggregation applications. The solid line denotes the downlink, where the SCs originating at the hub node are broadcast to all leaf nodes; and the dashed line, the uplink, where a given number of subcarriers are uploaded at every node.

As mentioned above, the network under test is composed of 16 leaf nodes in serial configuration, which are connected to a single hub node in a dual-fiber configuration: one transmission line for the downlink (solid line in the Figure 3-1) and one for the uplink (dashed line in the Figure 3-1). The hub node features a DSCM-powered PtMP (Point to Multipoint) pluggable transceiver capable of generating and transmitting a 400 Gbit/s optical signal comprising 16×25 Gbit/s digital subcarriers that can be individually detected and processed at the receiver of the remote leaf nodes. In addition, the receiver of this high-speed pluggable can, at the same time, process up to 16 subcarriers that may originate at different leaf nodes, if the power imbalances and levels of distortions between them are within the spec range of the device [Sim24]. The Access nodes house OADMs, which consist of SOAs and combiners/splitters with suitable coupling/splitting ratios. In our investigation, the ratio has been set to 75:25, where 75% corresponds to the through path and 25%, to the add and drop paths. Regarding the operating conditions of the SOAs, the gain of the amplifiers has been configured to ensure a given total output power at the output of the OADM. Following this, in the uplink direction, the optical power levels (i.e., the power per DSC) between the input signal of a given OADM and the added DSC are equalized by adjusting the SOA at the input of the OADM. Since the application of interest is metro aggregation, the maximum distance of the transmission line (i.e., $d_1+d_2+...+d_{16}$) in our investigation does not exceed 400 km, and each fiber span distance d_i does not exceed 80 km.

For the system evaluation, we have assumed a total launch power value (i.e., power at the output of an OADM) of 0 dBm, and a fiber loss coefficient of 0.25 dB/km; aside from the optical coupling losses, all other losses have been ignored (e.g., due to connectors, splices, etc.). Furthermore, impairments such as non-linearities and polarization-dependent loss have also

been accounted for and introduced in the simulation tool as performance penalties compared to the optical back-to-back performance of the pluggable transceiver. Both penalties are considered on a segment-by-segment basis (i.e., fiber segment between leaf nodes) and added at the end of the simulation. Finally, to generalize the performance analysis of the network, we have defined the distances of the fiber segments according to a Gaussian distribution with a mean of 20 km and a standard deviation of 5 km, which allow us to approximate the distances of horseshoe-like networks in the metro-aggregation domain.

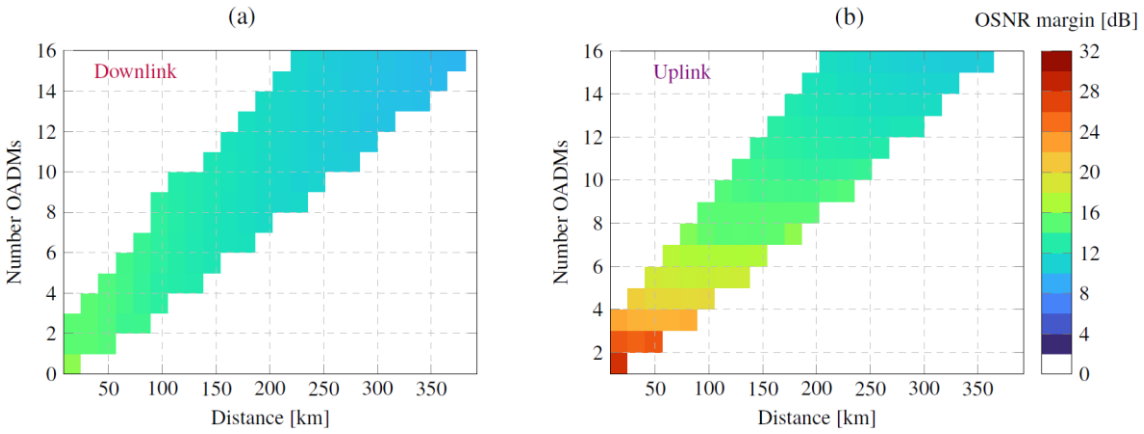

Figure 3-2: OSNR margin corresponding to Figure 3-1 for the (a) downlink and (b) uplink directions.

Due to the statistic approach to the network design, we have carried out 10,000 simulations, where we have calculated the optical signal-to-noise ratio (OSNR) margin of the transmission line under analysis for both downlink and uplink as a function of the total number of OADMs and the total transmitted distance. In both scenarios, we observe that distances in the metro-access range can be well served by DSCM-powered transceivers, exploiting the advantages of a PtMP network paradigm in terms of fewer number of pluggable units and power consumption [Cas24], exhibiting OSNR margins > 9.3 dB after 16 OADMs and over 350 km. In the results reported in Figure 3-2, the downlink case shows a slight signal degradation along the complete transmission line, which arises from acceptable noise figure levels and negligible impact of non-linearities due to the low launch power per subcarrier (~ -12 dBm, since there are 16 subcarriers). For the uplink, on the other hand, the degradation of the OSNR margin quickly increases when combining subcarriers at the leaf nodes using optical couplers. Like for the downlink scenario, non-linearities do not play a significant role at a total launch power of 0 dBm; instead, PDL introduces noticeable penalties (> 1 dB in terms of OSNR margin). This can be explained by the structure of an OADM: the uplink path requires an additional amplifier to fulfill the constraints regarding power equalization and launch power; this causes the signal to traverse twice as many amplifiers along the transmission line compared to the downlink path. Nevertheless, as previously stated, the system does exhibit reasonable performance margins to ensure robustness in the distance range of 350 km, while simultaneously connecting to 16 leaf nodes. The results of this study allow us to confidently plan the demonstrator in accordance with a desired performance for a given system application and a desired total reach.

3.1.2 The MB sliceable bandwidth/bitrate variable transceiver (S-BVT)

An innovative, multi-band (MB) sliceable bandwidth/bit rate variable transceiver (S-BVT) has been developed within B5G-OPEN project to extend the capabilities of current networks towards including MB operation and provide suitable capacity scaling. The proposed transceiver architecture is flexible, scalable and adaptable consisting of different bandwidth/bit rate

variable transceivers (BVTs)/building blocks that can operate beyond the C-band and can be enabled and disabled according to the traffic demand and network needs (more information and details can be found in B5G-OPEN deliverables [D3.1, D3.2]). This also promotes and efficient use of the available network resources maximizing network throughput. Additionally, its modular approach enables an easy integration of new technologies by suitably aggregating building blocks based on different implementations. Specifically, at the transmitter side intensity modulation (IM), amplitude modulation or IQ modulation are possible optical implementations that can be adopted. Also, either external modulation (i.e. adopting Mach Zehnder modulators, MZMs, and tunable laser sources, TLS) or direct modulation (i.e. by means of vertical cavity surface emitting lasers, VCSELs) can be included. At the receiver side possible configurations can be based on direct detection (DD) or coherent detection, trading-off performance versus cost/complexity. This intrinsic modularity not only ensures seamless integration of novel functionalities and technologies but also provides an agile platform for accommodating emerging network requirements (i.e. in terms of bandwidth, capacity) significantly enhancing operational efficiency and agility.

A crucial element of the proposed transceiver is the MB optical aggregator/distributor that should facilitate MB operation and the generation of a high-capacity flow (composed of diverse data streams from multiple BVTs) and distribution across the network. The generated data flow can be also received to different network endpoints by suitably disaggregating specific contributions at intermediate network nodes facilitating both point to point (PtP) and point to multipoint (PtMP) operation. To achieve this, different implementation approaches can be explored, ranging from traditional optical passive components like band-pass filters (BPFs) to more advanced programmable filters such as wavelength selective switches (WSSs). While current commercial WSS solutions are limited to the C- and L-bands, recent advancements have shown promising developments, including a WSS solution capable of continuous switching between 1300 nm and 1565 nm.

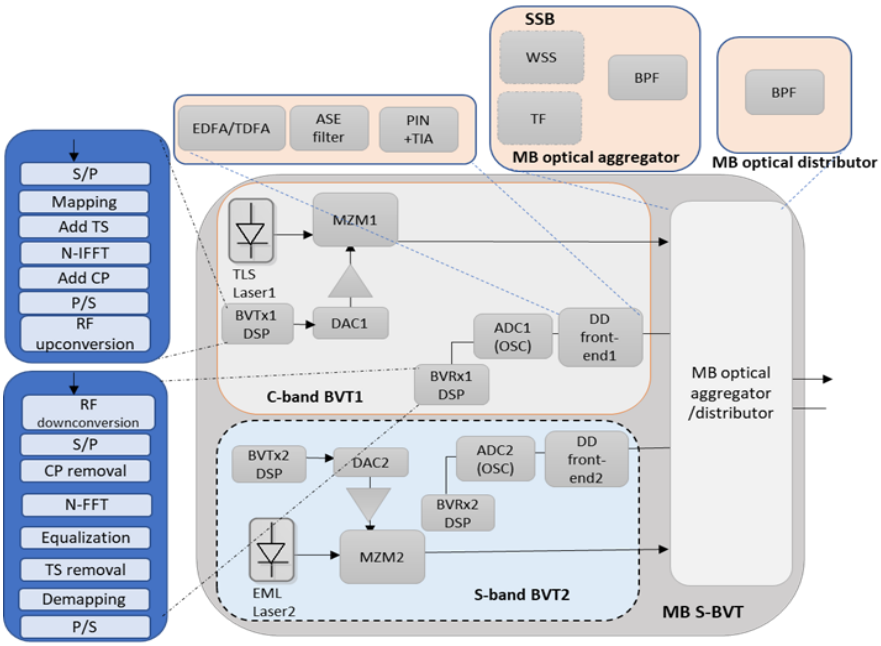

Figure 3-3: MB S-BVT prototype proposed in B5G-OPEN.

The last year of the project has been devoted to optimizing the prototype of the MB S-BVT [Nad23, Nad24]. The proposed MB S-BVT leverages advanced modulation formats based on orthogonal frequency division multiplexing (OFDM) to further enhance overall flexibility and performance. All the related transmission and reception digital signal processing (DSP) is detailed in both deliverables [D3.1, D3.2]. The final prototype is depicted in Figure 3-3. It includes two BVTs based on external modulation and direct detection. Each BVT operates in the C- and S-bands, respectively by including suitable and optimized technology operating in each band. Specifically, the first BVT operates in the C-band and the transmitter front-end includes a MZM and a TLS with linewidth< 100 kHz and which central lambda can be varied within the whole C-band. The S-band BVT utilizes a MZM and a TLS with a linewidth of 150 kHz and which central lambda can be set within the whole S-band. For digital to analog operation, two channels of a digital to analog converter (DAC) at 64 GSa/s are enabled. The two slices (C+S) are aggregated by means of a MB optical aggregator, which integrates single side band (SSB) filters and a BPF to generate a multi-band high-capacity flow. In particular, a C-band WSS and an S-band tunable filter (TF) are used in the optimized transceiver version to perform SSB and enhance resilience against fiber chromatic dispersion (CD). The C-band receiver front-end utilizes an EDFA with automatic power control mode, a WSS for amplified spontaneous noise (ASE) noise filtering and a PIN photodetector, while the optimized S-band receiver front-end employs a TDFA with automatic current control mode (instead of the semiconductor optical amplifier, SOA, of previous versions), a static filter and a PIN. Two channels of an oscilloscope (OSC) at 100 GSa/s are enabled to perform analog-to digital conversion (ADC). The main features and specs of the proposed MB S-BVT prototype are summarized in the following table:

Table 3-1: Key features for the MB S-BVT prototype.

Key features	**SPECS**
Sustainability	• Cost reduction due to DD (compared to coherent solutions) • Increased resource efficiency due to MB
Slice-ability	• 2 slices
Scalability	• 80 or 160 C-band channels of 50 GHz (DSB) or 25 GHZ (SSB) • 175 or 350 S-band channels of 50 GHz (DSB) or 25 GHz (SSB)
MB operation	• C+S operation
Flexibility	• OFDM and adaptive loading implementation
Disaggregation	• BVTs within the MB S-BVT can be from different vendors
Programmability (OpenConfig)	• TLS central wavelength and output power • DAC channels enabled/disabled • ADC channels enabled/disabled
BER	• HD-FEC (4.62e-3) • SD-FEC (2e-3)

Bandwidth per slice	• 40 GHz (DSB); 20 GHz (SSB)

In [Nad24], we have demonstrated different network scenarios considering the optimized MB S-BVT prototype, as depicted in Figure 3-4. Several spans of standard single-mode fiber (SSMF) with lengths of up to 125 km have been evaluated considering the metro/aggregation segment target links. Emulating transmission over a multi-band (MB) network, a MB node is constructed using a 16x16 polymer switch photonic integrated circuit (PIC) prototype, along with a semiconductor optical amplifier (SOA) and a band-pass filter (BPF), as illustrated in Figure 3-4. In the figure, the MB node is replicated twice to simulate a two-hop network scenario. However, during experimental assessment, two distinct inputs/outputs of the 16x16 switch are utilized.

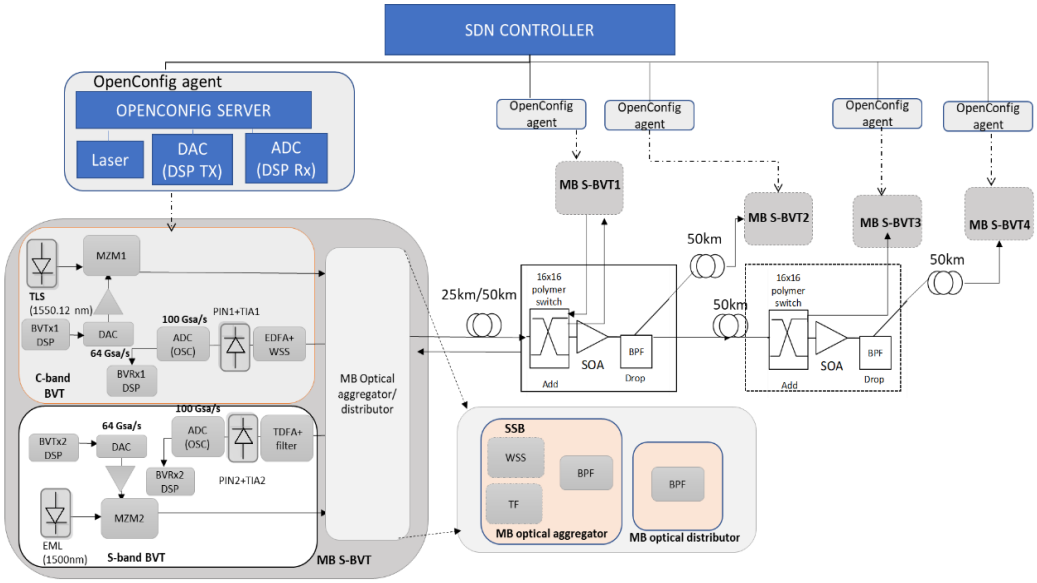

Figure 3-4: Experimental setup for the proof of concept assessment of the MB S-BVT prototype.

As a first step, a back-to-back (B2B) scenario is considered achieving maximum capacities per slice/band of 66.5 Gbit/s (C-band) and 65.7 Gbit/s (S-band) at a target BER of 4.62e-3. A second scenario targets MB transmission over a 1-hop 25 km path, achieving capacities of 48 Gbit/s (C-band) and 42.5 Gbit/s (S-band). The C-band contribution achieves 40 Gbit/s after 50 km of SSMF and 29.3 Gbit/s after a 2-hops path of 75 km of SSMF at the target BER. The S-band slice achieves similar performance obtaining 34 Gbit/s and 24.6 Gbit/s after the 1-hop 50 km and 2-hops 75 km paths, respectively. Finally, the C-band slice traverses an additional fiber span of 50 km achieving 20 Gbit/s after a 3-hops path of 125 km, demonstrating transceiver sliceability. Thanks to the modular and scalable transceiver approach, higher capacities can be envisioned enabling multiple slices within the different bands. In particular, 33.6 Tbit/s can be envisioned, comprising 160 C-band channels of 25 GHz (SSB) and 350 S-band channels of 25 GHz (SSB). MB transmissions of 22.6 Tbit/s and 18.3 Tbit/s can be anticipated after traversing 25 km and 50 km paths, respectively, by activating all available C+S-band SSB channels. However, additional transmission impairments such as stimulated Raman Scattering (SRS) should be taken into account, when enabling multiple wavelength division multiplexing (WDM) channels, that can limit the overall achieved performance.

This analysis shows the potential capabilities of the proposed MB S-BVT to increase the capacity of SoA transceivers up to 2× - 4× by exploiting multiple transmission bands while enabling appropriate slice/band selection according to the network path (B5GOPEN KPI 3.4 a).

3.1.3 The (semi-) filter-less add/drop node prototype

In D3.2 the (semi-) filter-less add/drop node prototype was introduced; in this part the prototype is integrated with a multiband testbed environment alongside a transceiver prototype, the prototypes have SDN agents allowing them to be controlled by SDN controllers.

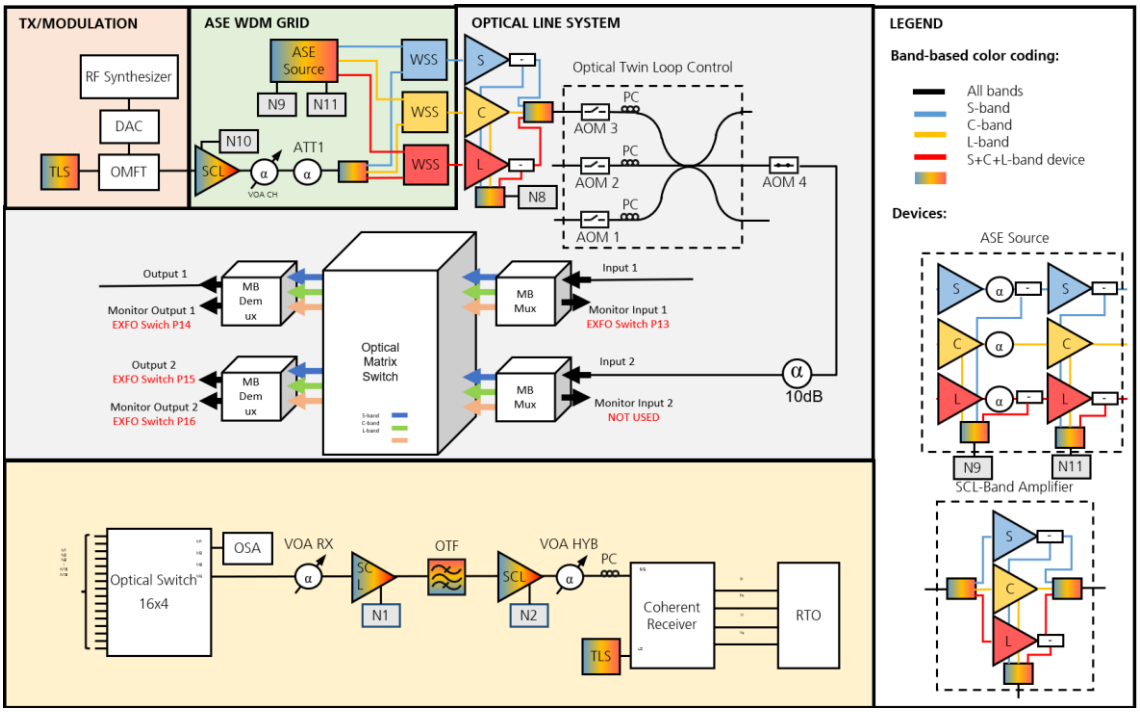

Figure 3-5: Experimental MB (S+C+L) set up integrating the node and the transceiver prototypes, The legend specifies the band-specific color scheme and diagrams for the ASE Source and SCL-band amplifiers.

Figure 3-5 depicts the mentioned setup in detail, the legend section details the diagram and components used as the S+C+L-band ASE source. Other significant components are the S+C+L-band amplifiers, these are designed as single-band amplifiers operating in parallel with multiplexing/demultiplexing of the individual bands at the input and output of the block, each block provides a monitor port to make sure we can monitor the testbed. Through the 16x4 optical switch, we can reroute the monitoring points within the testbed to the optical spectrum analyzer (OSA) to debug and keep track of what happens through the link. The monitoring points Nx in the setup are from each amplifying black, the ASE source, and the input and output ports of the node (except for input 2 monitor port is not used as it is already covered by monitoring point N8), the optical loop in the setup is used only as a through.

The prototype also includes full-band ASE WDM grids, populating all three bands with ASE dummy channels with pre-defined channel spacing, this will be used here as a demonstration of the band switching of the node prototype.

Controlling the node prototype is done via MATLAB script, utilizing our instrument control toolbox, allowing for band switching between the two input ports and the two output ports of the nude, it allows also for band dropping. The script allows for either a single band switching and dropping at a time or the whole spectrum change is also possible, so the routing control

function for example would be like: 'Fn(prototype,input,output,band)', where prototype is an object interfacing the node, input is "in1" or "in2" of the node, output is "out1", "out2" of the node, or "drop" referring to just dropping or routing to open port, and finally band is the selected band which can be "s", "c", "l", or simply "all".

Figure 3-6 shows a simple demonstration of the node in routing the ASE noise generated from the testbed above in Figure 3-5, the demonstration is done in three steps showing different functionalities of the node prototype. We start by showing the spectrum of the input ports in Figure 3-6 (a), the first step would be routing the whole spectrum to output port 2, meaning that, in relevance to example function stated above, the command 'Fn(prototype,"in2","out2","all")' is executed. The output of the first step is shown in Figure 3-6 (b). In the second step, we route or switch the S band to output port 1 in the node through the command 'Fn(prototype,"in2","out1","s")', this is shown in Figure 3-6 (c). Finally, and in the same way, we drop the C band from the grid, 'Fn(prototype,"in2","drop","c")', this can be seen in Figure 3-6 (d).

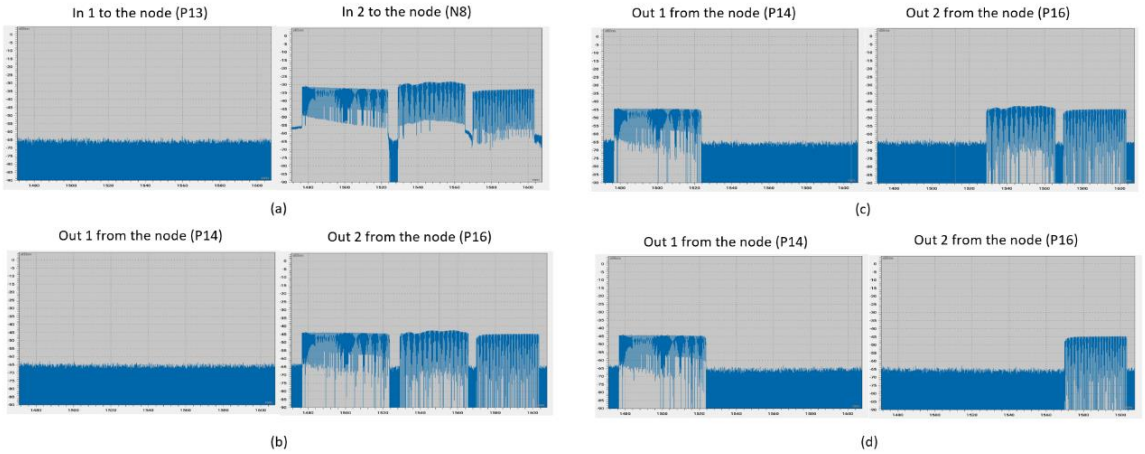

Figure 3-6: (a) Inputs to ports 1 and 2 of the node (b) Outputs from ports 1 and 2 of the node after the 1st command (c) Outputs from ports 1 and 2 of the node after the 2nd command (b) Outputs from ports 1 and 2 of the node after the 3rd command.

3.1.4 Filter-less OADM solution designs

The filter-less OADM was introduced in M3.3 and D3.2 and it applies in Metro-Aggregation networks (Figure 3-7) using the 400G Open p2mp-SC pluggable optics [Cas24].

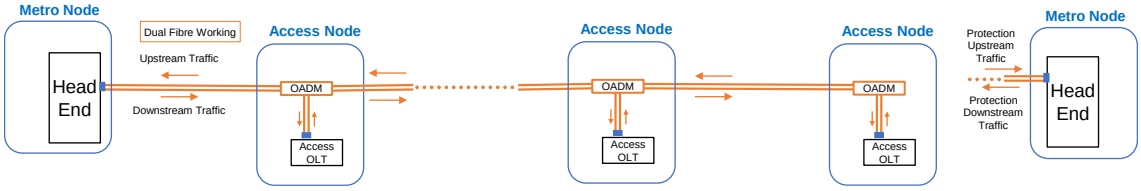

Figure 3-7: Metro-aggregation network with a horseshoe topology.

The initial design of the filter-less OADM was illustrated in D3.2. It consists of six unidirectional ports, three or four SOAs (SOA-2 is optional depending on the insertion losses of the following

link span), one optical splitter in the DS direction, and one optical combiner in the US direction (Figure 3-8).

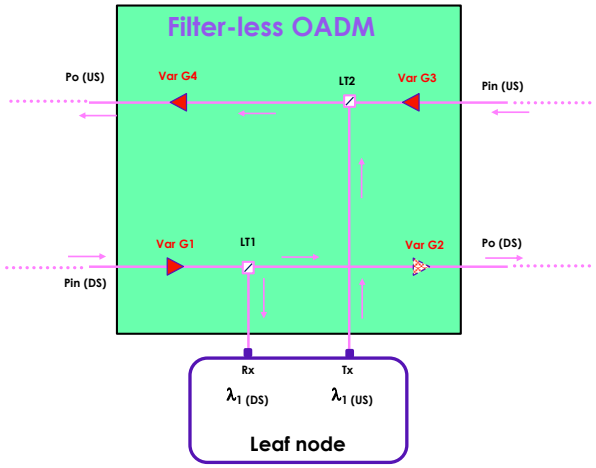

Figure 3-8: Initial filter-less OADM design.

The Downstream (DS) represents the West-to-East direction (bottom horizontal line in Figure 3-8), and it carries the optical signal from the Hub node in the Metro CO towards the Leaf nodes in each one of Access COs in the chain. The Upstream (US) represents the East-to-West direction (top horizontal line in Figure 3-8), and carries all the traffic from each Leaf node, East from the OADM, towards the Hub node in the Metro CO.

Upon entering the OADM the DS signal (bottom left in Figure 3-8) is amplified by the SOA-1 before being split at the LT1 to ensure enough optical power in the dropped connection hits the local receiver. The local receiver at the Leaf node will process the dropped digital subcarrier channels (up to four) according to the connection configuration. The input multiplex is broadcast to the DS output of the OADM. Depending on the length of the next fibre span, another SOA-2 can be used to boost the signal.

The US signal enters the OADM (top right in Figure 3-8) and hits the SOA-3, which is used to equalise the incoming digital channels with the added ones from the local Leaf node at the optical combiner at the output of SOA-3. The total optical signal gets boosted at SOA-4 to reach the next OADM in the chain or the receiver at the Hub node.

The SOAs have a variable and configurable gain. The DS signal crosses one or two SOAs, and their gain will be set depending on the losses of the next fibre span. The most critical SOA is the first one crossed by the US signal as it is used for equalisation of all the digital subcarrier channels, i.e. SOA-3. Therefore, its gain (G3) will depend on several parameters like the number of active channels in the input multiplex, the number of channels to be added, etc., and it is given by Eq. 3-1.

As reported in D3.2, the G3 can be obtained using the equation:

$$G_3(dB) = P_a(dBm) - P_{in}(dBm) + 10\log\left(\frac{n_i}{n_a}\right) + LT2_t - LT2_a,$$

Eq. 3-1

and the necessary gain of the second SOA is given by:

$$G_4(dB) = P_0(dBm) - 10\ \log\left(10^{\frac{P_{in}(dBm)+G_3-LT2_t}{10}} + 10^{\frac{P_a-LT2_a}{10}}\right).$$

Eq. 3-2

The parameters are explained in Table 3-2.

Table 3-2: Parameters for calculating the SOA gain to equalise US & added channels.

Parameter	Description
G_3	Gain of SOA 3 (dB) at the OADM input for the US path
G_4	Gain of SOA 4 (dB) at the OADM output for the US path
Pin	Total optical power at the OADM East input (dBm) in the US direction
n_i	Number of active channels at the OADM input in the signal multiplex in the US direction
Pa	Total optical power added from the local Leaf node (dBm)
n_a	Number of channels being added from the local Leaf node
LT2t	LT2 insertion losses in the Through path (dB) for the US direction
LT2a	LT2 insertion losses in the Add path (dB) for the US direction
Po	Total OADM optical output power (dBm) needed to overcome losses in the next link span for the US direction

Regarding the SOAs, the main considerations to be made are:

1. The saturation output power cannot be exceeded.
2. The Noise Figure to ensure enough OSNR at the receiver (both US & DS).
3. The total input optical power at the SOAs must be above the minimum depending on the required gain and maximum acceptable Noise Figure.
4. When adding digital channels in the US direction, the total optical power of the channel multiplex gets automatically increased.
5. Careful characterisation of the SOAs is needed to ensure that:
    a. channel equalisation is possible with any possible scenario in terms of the number of active input channels and added channels, as well as optical power levels at the input and added.
    b. the optical multiplex can reach the next access node in the chain overcoming insertion losses of the next link span.
6. SOAs can be used as optical attenuators (neg gain) if needed, for example to avoid saturation of the next SOA or overloading the receiver.

The initial filter-less OADM design works for a single instance of p2mp-SC optics. Therefore, it is necessary to investigate different methods of upgrading the OADM node when we need to increase either the number of local Leaf nodes or the total capacity of the Metro-aggregation network. Report D3.2 already pointed out at the different methods of upgrading the OADM node.

This design analyses concerns only the power levels and does not evaluate the degradation of OSNR due to ASE noise generated at the SOAs or the Polarisation Dependent Loss (PDL), which is left for further study at a future time.

3.1.4.1 Upgrading the number of Leaf nodes in the local access CO.

It may be the case when we need to install an additional Leaf node at an Access CO. There are two ways to increase the number of Leaf nodes at the access CO:

a) Use back-to-back filter-less OADM initial design.

The simplest way is to use two filter-less OADM (Figure 3-8) in a back-to-back configuration as shown in Figure 3-9. A first Leaf node is connected to the OADM on the left-hand side while the new Leaf node is connected to the additional OADM on the right-hand side. In this case, the SOA-2 in the left OADM could be omitted as there are hardly any losses to the input of the second OADM. The SOA-2 in the OADM on the right works in the same way as before, which is to overcome the losses of the next link span.

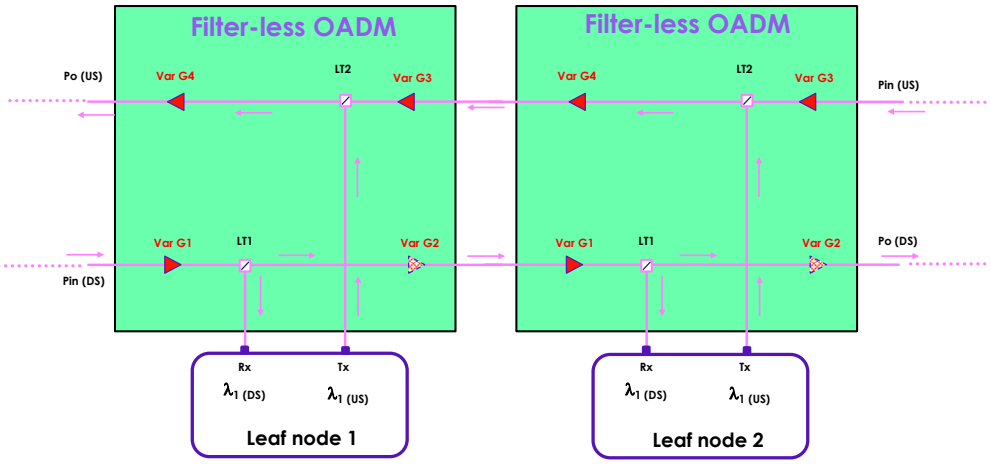

Figure 3-9: Additional Leaf node using back-to-back filter-less OADM configuration.

On the US, we can use the same equation Eq. 3-1 to equalise the incoming digital channels with the added ones. First it will be applied to the OADM on the right, and second to the OADM on the left.

b) Use OADM initial design and an external optical splitter at the local traffic port

A second method is to add an optical splitter (SP) at the local port of the OADM as illustrated here in Figure 3-10. Now we can connect two Leaf nodes through the optical splitter. It is important to note that both Leaf nodes are working at the same wavelength λ_1 .

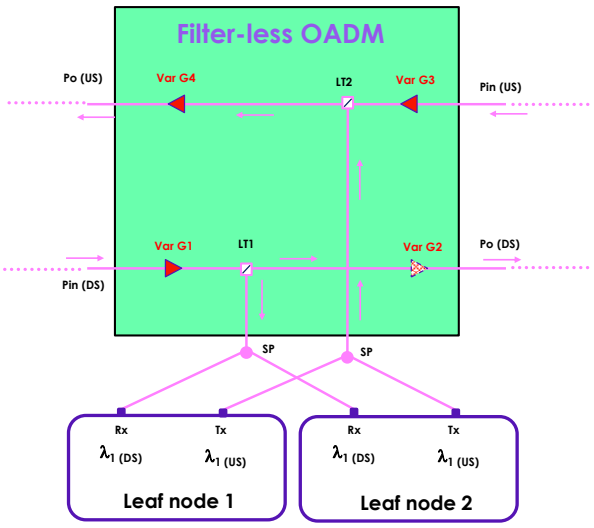

Figure 3-10: Additional Leaf node using a Splitter (SP) at the local traffic OADM port.

Now the equalisation of the digital channels in the upstream direction requires the use of more data as the launched optical power from the two Leaf nodes are interrelated. This is because we only have SOA-3 to equalise all the digital channels being added from the two local Leaf nodes and the ones in-line. This means that the launched optical power from Leaf node 2 is linked with the launched power from Leaf node 2 depending on the number of digital channels each node is adding. This relation is shown in Eq. 3-3 and Eq. 3-4.

$$P_{a2}(dBm) = P_{a1}(dBm) + 10\log\left(\frac{n_{a2}}{n_{a1}}\right),$$

Eq. 3-3

$$P_{a1}(dBm) = P_{a2}(dBm) + 10\log\left(\frac{n_{a1}}{n_{a2}}\right).$$

Eq. 3-4

Where the parameters are described in the next table.

Table 3-3: Parameters linking total added optical powers from the two Leaf nodes.

Parameter	Description
P_{a1}	Total optical power added from Leaf node 1 (dBm)
P_{a2}	Total optical power added from Leaf node 2 (dBm)
n_{a1}	Number of digital channels added from Leaf node 1
n_{a1}	Number of digital channels added from Leaf node 2

The gain of the SOA-3 used for channel equalisation is given by:

$$G_3(dB) = P_{a1}(dBm) - P_{in}(dBm) + 10\log\left(\frac{n_i}{n_{a1}}\right) + LT2_t - LT2_a - SPL,$$

Eq. 3-5

And the gain of the booster SOA-4 is given by:

$$G_4(dB) = P_0(dBm) - 10\ \log\left(10^{\frac{P_{in}(dBm)+G_3-LT2_t}{10}} + 10^{\frac{P_{a1}(dBm)+10\log\left(1+\frac{n_{a2}}{n_{a1}}\right)-LT2_a-SPL}{10}}\right).$$

Eq. 3-6

In both Eq. 3-5 and Eq. 3-6, SPL are the insertion losses, expressed in decibels, of the external splitter at the local traffic ports of the OADM.

3.1.4.2 Upgrading the total capacity of the metro-aggregation network

We have realised the first filter-less OADM design to be used with the 400G p2mp-SC optics in the horseshoe metro-aggregation network. It may happen that this capacity is not enough to support the traffic and thus the capacity needs to be upgraded.

a) Upgrade the p2mp-SC optics to 800G.

The first way of increasing the network capacity is to reüöace the p2mp-SC 400G optics with a 800G version, which may have an increased number of digital channels. Infinera have not yet developed such an 800G p2mp-SC optics and therefore here we can only speculate.

The same initial OADM design (Figure 3-8) can be used with no alterations. If we assume that each digital channel of a 800G p2mp-SC has a capacity of 25 Gbit/s per subcarrier, same as the 400G XR, then it leads to the conclusion that the DSCM multiplex can transmit up to 32 digital channels.

A consequence of this is that the digital channel multiplex has a 15 dB optical power range between carrying 1 channel to carrying all 32 channels, i.e. if the total optical power of the multiplex is 0 dBm, carrying 32 digital channels, it is carrying -15 dBm per digital channel.

If we call TTx the total optical power in the digital channel multiplex expressed in dBm, then the optical power per Digital Channel DCTc can be expressed as:

$$DCTx(dBm) = TTx(dBm) - 10\log(n),$$

Eq. 3-7

Where ‘n’ is the total number of digital channels active in the multiplex.

The increased optical power range is important for the channel equalisation in the upstream direction, and the SOA-3 would need to be designed such that it can equalise in any situation, i.e. regardless of the number of channels carried within the upstream multiplex, and the number of channels being locally added. Of course, being able to change the launched optical power of the local traffic being added onto the network, also helps with the equalisation.

The equation to work out the gain of SOA-3 to equalise the incoming digital channels with the locally added is the same as in the case of the 400G p2mp-SC optics, i.e. Eq. 3-1. The equation to find the gain of the booster SOA-4 in the US is also the same as Eq. 3-2.

b) Adding a second 400G p2mp-SC system at a different wavelength

A second option to increase the capacity of the metro-aggregation network is to add a second 400G p2mp-SC optics system at a different wavelength than the first one. In this case we can still re-use the same initial filter-less OADM design and we have two options.

b.1) using back-to-back initial OADM design

Because we are stacking two 400G p2mp-SC optics, they need to be operating at different wavelengths as shown in Figure 3-11. Equations Eq. 3-1 and Eq. 3-2 are still valid for the US direction and can be applied independently for the two different wavelengths. However, care must be taken that the total optical power at each wavelength is still enough to reach the next filter-less OADM or the Hub node receiver. A problem might arise depending on the number of OADMs in the chain and the optical powers difference between both wavelengths.

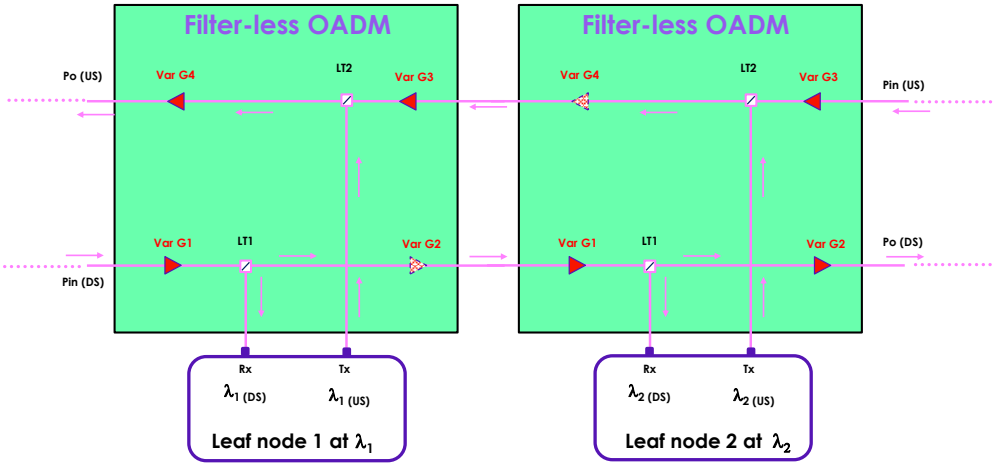

Figure 3-11: Back-to-back OADM for capacity upgrade using stacked 400G p2mp-SC optics.

On top of the considerations for the initial design, additional considerations to be made are:

1. SOAs amplify the total optical power, which include both wavelengths.
2. When we add channels at one of the two wavelengths through the Add path in the optical power combiner, the total optical power for that wavelength multiplex is automatically increased while the optical power at the other wavelength is not.
3. If no channels are added in one of the two p2mp-SC multiplex, the optical power difference between the two p2mp-SC systems multiplex at the output of the second OADM may be different (higher or lower) than the power difference at the input of the first OADM.
4. Power difference also varies if the added powers from the two local Leaf nodes are different.
5. Increased power difference when crossing OADMs may lead to limit the number of access nodes in the chain.

b.2) adding an external splitter to the initial OADM design

As before, another way of supporting two stacked 400G p2mp-SC optics at two different wavelengths is to use a single initial design filter-less OADM and adding a 1:2 optical splitter at the local port as shown in Figure 3-12.

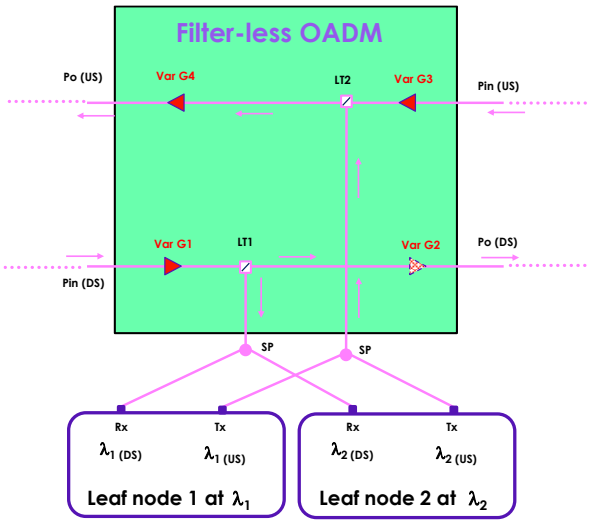

Figure 3-12: Splitter at local port of OADM for capacity upgrade using stacked 400G p2mp-SC optics.

Now again we only have SOA-3 to equalise the US in-line digital channels at both wavelengths with the added local channels from the two local Leaf nodes. This means that the added local optical powers are inter-related as expressed in the equations Eq. 3-3 and Eq. 3-4.

The gain of the SOA-3 used for channel equalisation is given by:

$$G_3(dB) = P_{a1}(dBm) - P_{in}(US) + 10\log\left(\frac{n_{i1} + n_{i2}}{n_{a1}}\right) + LT2_t - LT2_a - SPL,$$

Eq. 3-8

where:

Table 3-4: Parameters.

Parameter	Description
P_{in}	Total optical power across all wavelengths
n_{ij}	Number of in-line digital channels at wavelength "j"
n_{aj}	Number of digital channels added from Leaf node "j"
SPL	Insertion losses of the optical splitter in dB

and the remaining parameters are the same as in Table 3-2 and Table 3-3.

Finally, the gain of the booster SOA-4 is the same as Eq. 3-6.

3.1.5 Multiband Optical Node Architecture in Metro-Access Network

In addition to the filter-less OADM solution presented in the previous section, in Task 3.2 of B5G-OPEN, we also conducted investigations into new multiband optical switching solutions. These multiband optical switches are designed to operate across multiple bands, including the O-, S-, C-, and L-bands. This approach offers increased flexibility and higher capacity for B5G-OPEN networks, aligning with the stringent requirements of Beyond 5G (B5G) in terms of bandwidth, capacity, flexibility, and efficiency, all while maintaining transparent operation.

The node is equipped with a highly flexible multiband optical add/drop multiplexer (MB-OADM), which serves the purpose of adding, dropping, drop and continue, and bypassing traffic between Metro-Access and Metro-Core (metro aggregation segment). The schematic of the multiband optical network architecture, depicting the primary functional optical building blocks, can be found in Figure 3-7 and Figure 3-13. The modular design of the MB-OADM building blocks allows for efficient customization based on various factors, including traffic volume, the number of channels, channel granularity, the number of bands, and the number of ports (or the degree of the switch). Our primary focus has been on the design and implementation of a programmable multiband reconfigurable optical add/drop multiplexer (MB-ROADM), a multiband wavelength selective switch (WSS), and programmable multi-cast select switch (MCS) capable of operating across the O-, S-, C-, and L-bands, enabling seamless drop and continue operations.

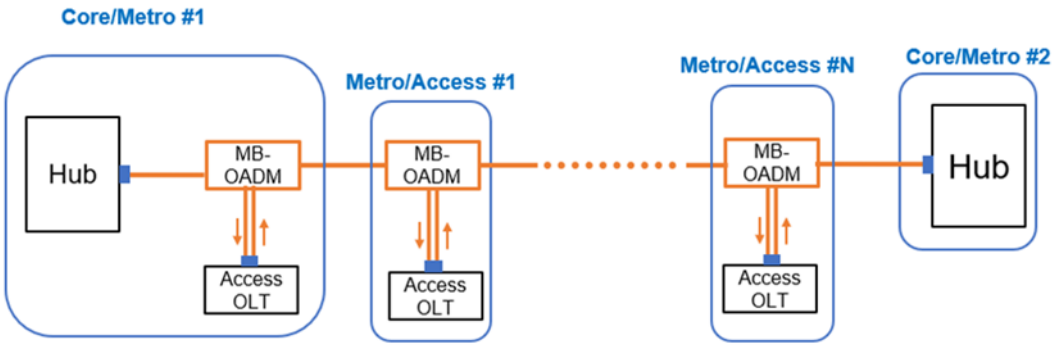

Figure 3-13: Optical network architecture based on MB-OADM in Metro-Access and Metro-Core Network.

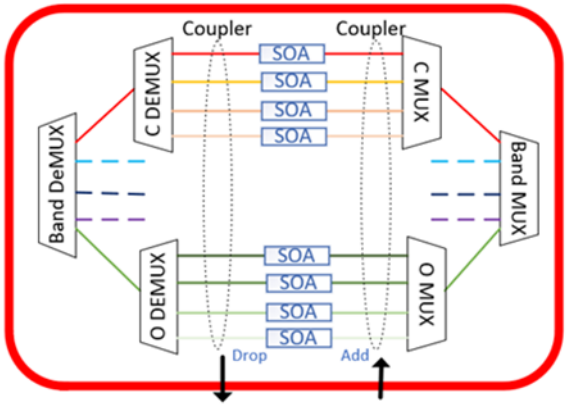

Figure 3-14: MB-OADM Node architecture.

As shown in the Figure 3-14, we designed MB-OADM. The MB-OADM Node consists of a band demultiplexer and multiplexer used to separate and combine the input MB signals. Commercial fused fiber WDM splitters can be utilized to implement the band demultiplexer/multiplexer. After separating the bands, each band's signals are directed to the respective OADMs operating at O-, S-, C-, and L-bands.

Each OADM is comprised of a demultiplexer, which separates the single-band signals into individual channels, an array of Semiconductor Optical Amplifiers (SOAs) that selectively and dynamically block or pass each channel, and a multiplexer for combining the channels. The drop stages are realized by a 3 dB splitter before each SOA, and the add stages are realized by a 3 dB combiner after the SOA and before the multiplexing stages. The SOAs compensate for the losses introduced by the muxes/demuxes as well as the 3 dB splitter/combiner.

It's worth noting that each SOA operates with a single channel, avoiding FWM (Four-Wave Mixing), XGM (Cross-Gain Modulation), and XPM (Cross-Phase Modulation) nonlinearities that can degrade signal quality. This implementation allows for the drop/add and continue operation of each individual channel.

Figure 3-15 illustrates the time-resolved response of the SOA-based ROADM/OADM during switching. As the other components in the SOA-based OADM/ROADM system are passive, the switching speed is predominantly influenced by the SOAs.

Figure 3-15 (a) shows a rise time of approximately 30 ns. Figure 3-15 (b) exhibits a fall time of about 30 ns. Figure 3-15 (c) presents both a rise time of around 30 ns and a fall time of approximately 25 ns. These results demonstrate that the switching speed allows the system to transition from low to high states in about 30 ns and from high to low states in 25-30 ns.

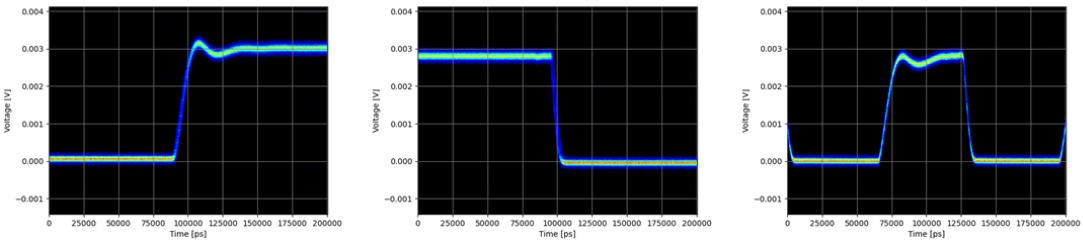

Figure 3-15: Switch speed of SOA-based ROADM/OADM.

Moreover, the modular architecture permits expansion in a 'pay-as-you-grow' approach to accommodate increasing traffic demands by processing multiple bands. Each module can handle the data channels of one of the multibands, starting from the C-band and subsequently expanding to the L-band, S-band, or O-band if needed. This design ensures a future-proof architecture capable of supporting traffic growth even in long-term scenarios.

3.1.6 3x1 Multiband Lossless ROADM Architecture for Optical Metro Aggregation Network

Optical metro and access networks already adopt metro hubs and multi-horseshoe network topology as shown in Figure 3-16 (a). O-band transmission can be exploited in short-link horseshoe metro-access networks leveraging C-band transmission for long links between hubs in the metro-core network [Xia23]. To transparently and flexibly operate the MBT metro

network in a cost-efficient way preserving both the ability to share edges among different connections and provide intra-node connectivity to flexibly route carriers across the network [Sch22], the metro hub node should be equipped with a multiband (O+C band) multi-degree ROADM architecture.

The 4-port Multiband ROADM architecture, depicted in Figure 3-16 (b), is designed to accommodate multi-band and multiple port network configurations. The architecture comprises three inputs originating from the Metro (as an example, considering Figure 3-16 (b), the inputs from Hub4, Access Network1, and Access Network 2), and the fourth input is the add port. The optical power of each input port is split using a 1X4 splitter to broadcast the MB channels to the corresponding multiband wavelength blockers (MB-WB) at the output ports (including the drop port). At each output port, four MB-WBs are employed to either block or bypass the traffic from the 3 input ports and the add port. The traffic passed by the MB-WBs is then combined using a 4X1 combiner to the output port. The Drop port is a 1X3 coupler and 3 MB-WBs for dropping traffic from three input ports.

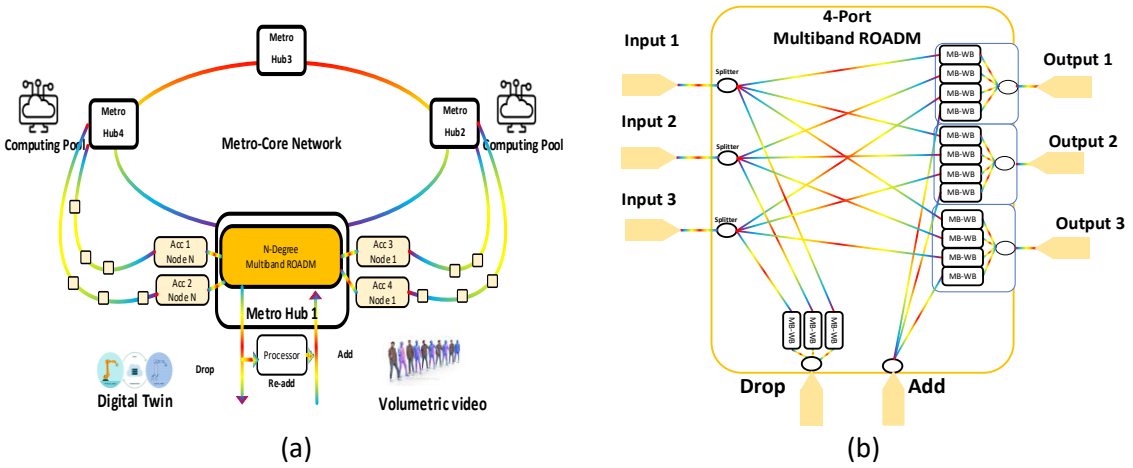

Figure 3-16: (a) Multiple Horseshoe Metro Access Network Topology. (b) Architecture of the 4-Port Multiband ROADM(R).

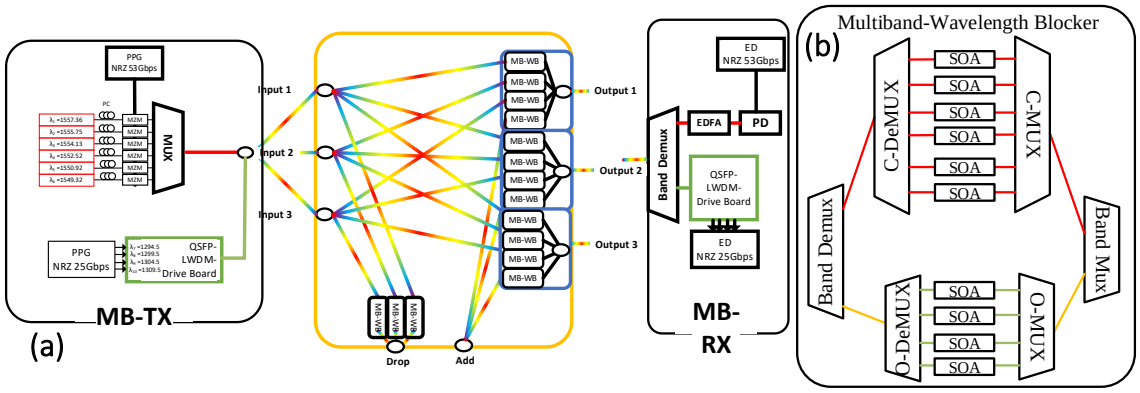

Figure 3-17: (a) Schematic of the experiment setup; (b) Architecture of the Multiband (C- and O-band) Wavelength Blocker.

The design of the MB-WB is shown in Figure 3-17 (b): and consists of a band demultiplexer and multiplexer used to separate and combine the input MB signals. For each band, the WB incorporates a WDM demultiplexer, an array of SOAs operating as gates and amplifiers for

dynamic blocking/passing of each WDM channel, and a WDM multiplexer. Notably, each SOA operates with a single channel to mitigate nonlinearities that could degrade signal quality.

The gain of the SOA compensates for ROADM and can also be used with an external power monitoring system as channel equalizer.

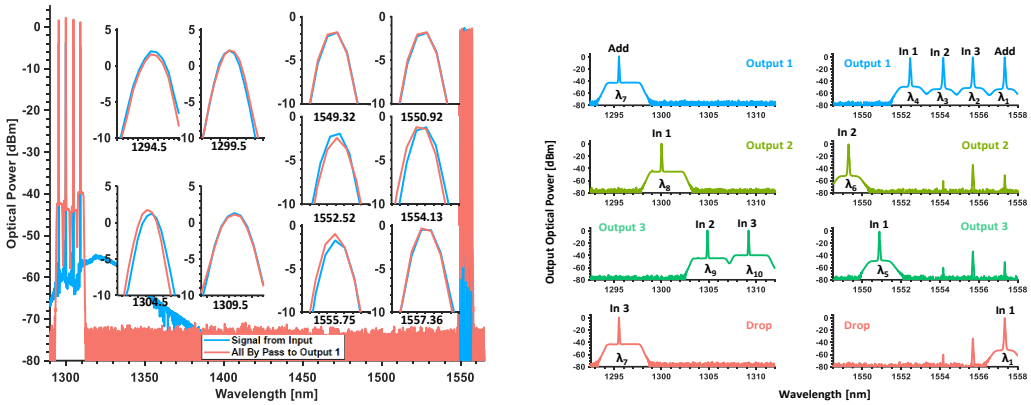

Figure 3-18: (a) Spectra of C-band and O-band channels from Input 1 to Output 1, and other input ports blocked. The subplot is the zoom-in of each channel (b) Spectra of WDM channels from all inputs switched to different Output ports.

The experimental setup for evaluating the multiport ROADM is depicted in Figure 3-17 (a). In the C-band, we utilized six DWDM channels at λ1=1557.36nm, λ2=1555.75nm, λ3=1554.13nm, λ4=1552.52nm, λ5=1550.92nm, and λ6=1549.32nm at 53 Gbit/s OOK-NRZ data streams with a pseudorandom bit sequence (PRBS) length of 2^{13}-1. For the O-band, commercial pluggable O-band LAN WDM (LWDM) transceivers were employed, each supporting four 25Gbit/s OOK-NRZ data streams with 2^13-1 PRBS. The O-band channels were operated at wavelengths of λ7=1294.5nm, λ8=1299.5nm, λ9=1304.5nm, and λ10=1309.5nm.

Figure 3-18 displays the spectral results of different configurations of the ROADM. In Figure 3-18 (a), the ROADM is configured such that all wavelengths from Input 1 pass through Output 1, while all other input ports are blocked. For the C-band, the optical signal-to-noise ratio (OSNR) of the input six wavelengths are 67.5 dB, 66 dB,67 dB, 66 dB, 67 dB, and 68 dB. After passing through the ROADM, the OSNR of each wavelength becomes 42 dB, 37 dB, 38 dB, 39 dB, 38 dB, and 41 dB. Similarly, for the O-band, the OSNR of the four wavelengths is 61.47 dB, 61.5 dB,61.5 dB, and 59.8 dB in B2B. After traversing the ROADM, the OSNR of each wavelength becomes 43 dB, 44 dB, 44 dB, and 40 dB.

The ROADM total loss is 18.5dB (12dB from the two 1x4 couplers, 1.5dB from two band demux/mux, 5dB from the two WDM de-mux/mux). The SOAs operate ~225 mA in C-band to provide ~18.5dB gain with <0.6dB PDG and O-band SOAs provide ~18.5dB gain and <0.2dB PDG at 250 mA. The SOAs compensate for the ROADM losses as can be observed by the zoom-in WDM spectra in Figure 3-18 (a) for both bands.

In a second example, we assess the add and drop operation with full input traffic from all input ports. As a possible routing example, it is assumed that based on instructions from the control plane data at λ1 and λ7 from input 3 and input 1 will be dropped and new traffic will be added at the same wavelength to output 1. Data at λ2, λ3, and λ4 from input 3,2,1 will bypass to output

1. Data at λ6 and λ8 from inputs 2 and 1 will bypass to output 2, and λ5, λ9, and λ10 from inputs 1,2,3 will bypass to output 3. All the other channels will be blocked. Figure 3-18 (b) reports the outputs and drop port spectra according to the desired routing. From the drop port, we can observe an extinction ratio for the O-band larger than 60 dB, while for the C-band larger than 34 dB. This effectively isolates the output channels in the ROADM from the input signal thus enabling wavelength reuse in the metro network. The crosstalk in both C- and O-band of output 1,2,3 is below -60 dB and -34 dB (worst case). Figure 3-19 reports the results of the bit error ratio test conducted for both the C-band (Figure 3-19 (a)) and O-band (Figure 3-19 (b)) channels. At output 1, the power penalties for wavelengths λ2, λ3, and λ4 at a bit error ratio of 10e-9 level are 1.5 dB, 1.6 dB, and 1 dB, respectively. For output 2, the power penalties for wavelengths λ2 in the C-band and λ8 in the O-band are 1.2 dB and 2.8 dB, respectively. At output 3, the power penalties for wavelengths λ3, λ9, and λ10 are 0.75 dB, 1.55 dB, and 1.75 dB, respectively. The power penalties for the add traffic at wavelengths λ1 and λ7 are 1 dB and 1.8 dB, respectively, while for the dropped traffic, they are 1.6 dB and 2.1 dB, respectively.

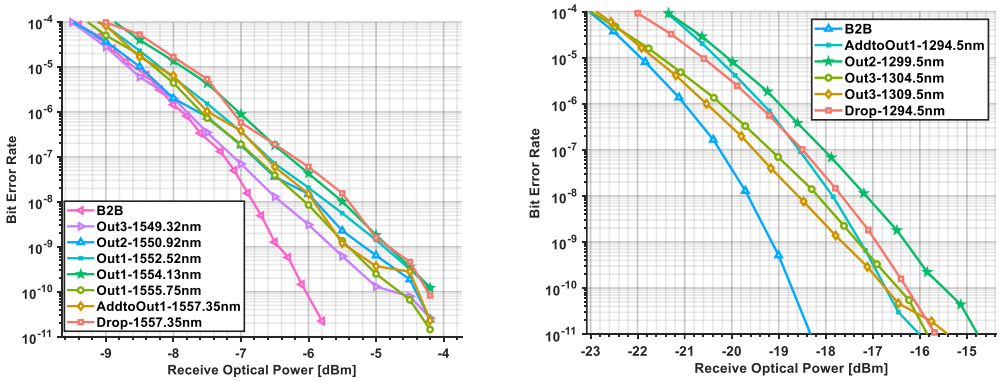

Figure 3-19: (a) Bit Error Rate of C Band with 53Gbps NRZ b) Bit Error Rate of O Band with 25Gbit/s NRZ.

3.1.7 Photonics Integrated C+L Wavelength selective switch

As core component of the WSS with splitters in the ROADM within the Metro-Aggregation Network, we designed and fabricated a C+L band wavelength selective switch. The 1x8 PIC WSS architecture is shown in Figure 3-20. The chip architecture features a single input port that branches into eight WDM modules or WBL, each of which has eight output ports. Each WDM module processes eight channels spaced 400 GHz apart. The module includes an AWG as demultiplexer that separates the WDM channels and an array of SOAs. A second AWG serves as a multiplexer. In total, the module includes three cascaded MMI splitters that split the optical power of the input signal to feed other WBL modules on the chip, and one MMI on the input port and one MMI on the output port for alternative routing. The chip shown in Figure 3-20. uses InP material and all 8 WBL together take up the space of two InP cells, each measuring 4.6×4 mm².

This photonic technology is based on SOAs to provide fast switching and loss-less operation, high contrast ratio and low channel cross-talk. The PIC can select one or multiple wavelength channels and forward the channels to the output ports according to the switching control signals. Turning ON/OFF the SOAs determines which wavelength channel is forwarded to the output or is blocked. The broadband operation of the SOAs enables the operation with any wavelength, whereas the cyclic AWGs allow the PIC to work in dual-band. Moreover, the

amplification provided by the SOA compensates for the loss introduced by the two AWGs and the MMIs.

A testbed has been set up as shown in Figure 3-20 (d) for experimental assessment of the switch. The switch is mounted on a water-cooled heat sink and operated at 20°C to stabilize the chip temperature. Fiber-to-chip coupling was performed using lensed fibers. The alignment was performed via two three-axis stages with two lensed fibers used to couple the light from the laser to the chip or from it to the optical spectrum analyzer. A polarization controller was used before the chip input to tune the polarization. A multichannel current controller is used to switch on/off the SOAs. The characterization was performed using a tuneable laser at wavelengths ranging from C to L band with 0 dBm optical power.

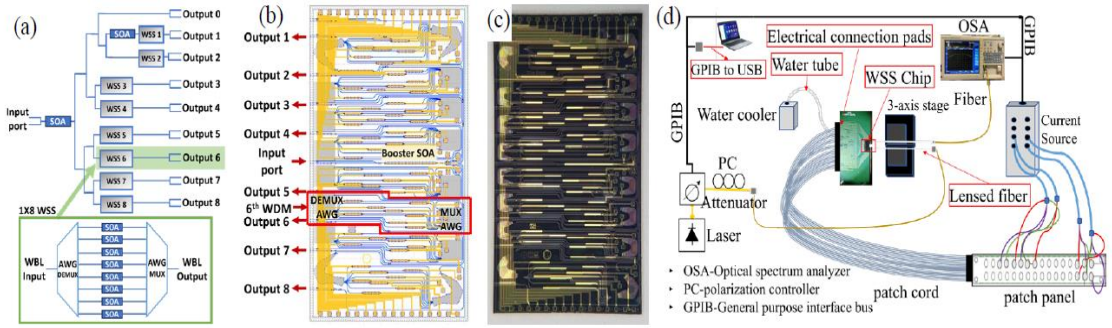

Figure 3-20: (a) WSS chip schematic, (b) layout, (c) fabricated 1x8 WSS chip, (d) experimental setup.

The 8 WDM channels of the AWG at port 6 were characterized. The results show in Figure 3-21, confirm the 3.2 nm channel separation, with crosstalk of -22 dB and -20 dB for the two bands. We also examined the switching performance of WSS output port 6, as shown in Figure 3-21, revealing a consistent 40 dB average extinction ratio in both C and L bands. The C-band maintains an average optical OSNR of 30 dB, while the L-band reaches an average of 35 dB OSNR. Similar performance has been observed in other AWGs across various output ports.

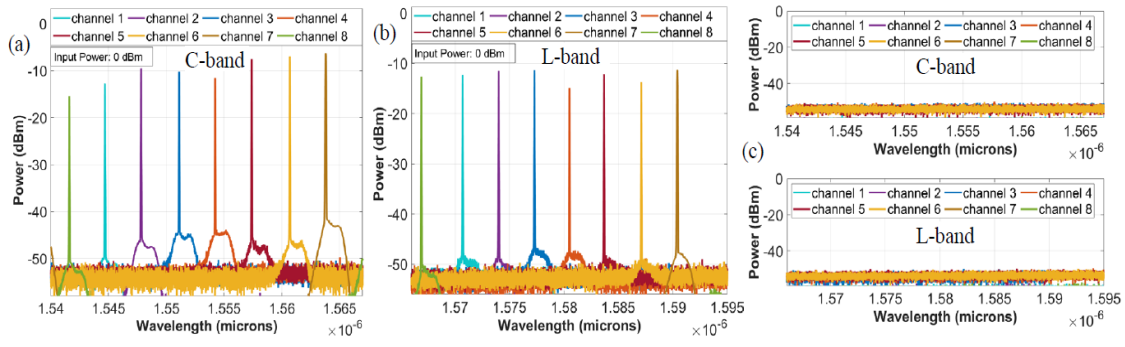

Figure 3-21: Switching operation: (a) C-band channels switched ON, (b) L-band channels switched ON, (c) C- and L-band channels switched ON/OFF.

The WSS channel peak powers in the C-band vary from -15 dBm to -6 dBm. In each optical path, the five 1X2 MMIs introduce a 17.5 dB loss, while 2 AWGs result in a 6 dB loss, and link and bends contribute an additional 1 dB loss, summing up to 24.5 dB on-chip loss. Input and output coupling losses add roughly 12 dB loss. So, the total channel loss due to these factors is

approximately 36.5 dB. The SOAs (booster and gate) offer about 21.5 to 30.5 dB gain, compensating for on-chip losses. In the L-band, peak power ranges from -15 dBm to -11 dBm, and SOAs provide roughly 21.5 to 25.5 dB gain to counteract on-chip losses.

For system level characterization, a measurement setup was built to transmit data through the WSS PIC and analyze the transmission. The experimental setup depicted on Figure 3-22 (a) was aimed to assess the bit-error-ratio (BER) for the C- and L-band channels. In this setup a continuous wave (CW) source was followed by a PC used to control the SOP to the input of the electro-optic-modulator (EOM), which was driven by a pattern generator with a $2^{31} - 1$ pseudo-random binary sequence (PRBS). Figure 3-22 shows the BER measurement results for C- and L-band channels where the power penalties are 1.5 dB and 2.5 dB, respectively. The power penalties are mainly caused by the ASE of cascaded SOAs which degrades the OSNR.

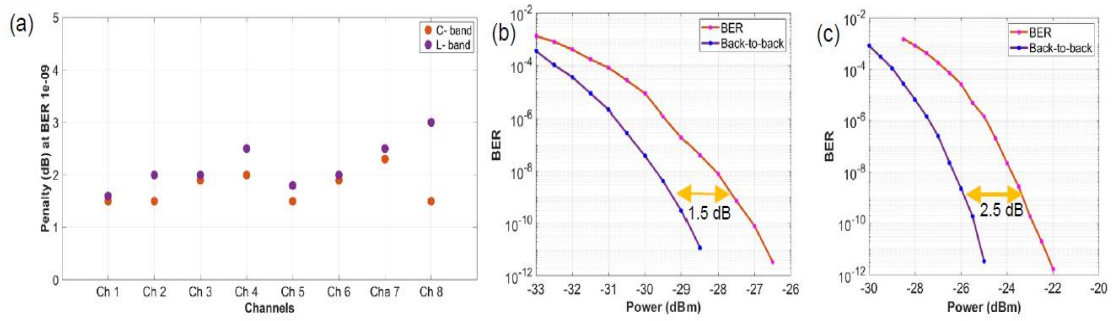

Figure 3-22: Bit-Error-Ratio measurements at 10Gbps NRZ-OOK: (a) power penalty at BER 1e-09 (b) C-Band BER Performance for Representative Channel and (c) L-Band BER Performance for Representative Channel.

3.1.8 Physical Layer design tool

The physical layer (transmission) performance evaluation tool assesses physical layer performance in the context of transmission systems with Multiple Optical Bands. It is tailored to estimate the physical layer performance of terrestrial fibre-optic European national networks.

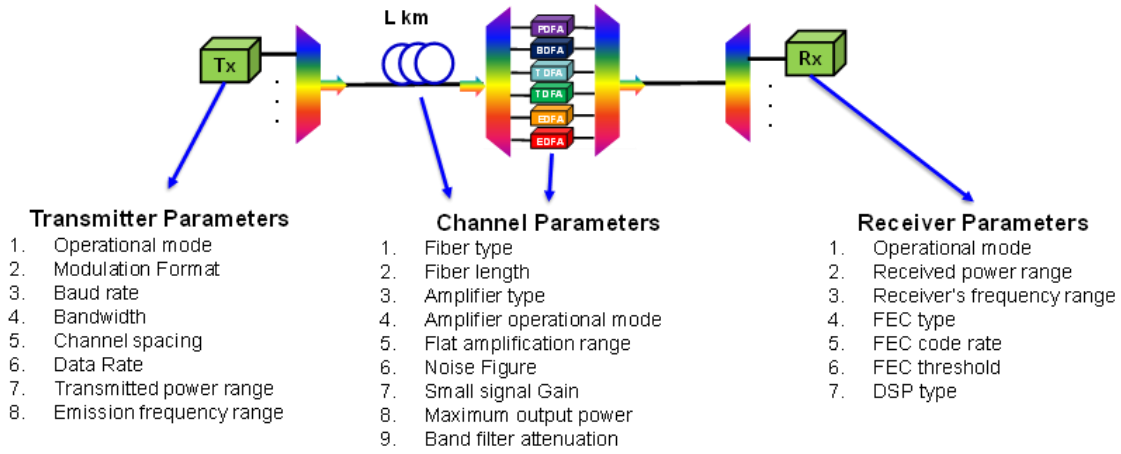

Figure 3-23: The system-level parameters taken as input.

Figure 3-23 illustrates the system level input parameters for the estimation of the physical layer performance of a Metro/Core point-to-point link. The physical layer phenomena taken into account are ASE accumulation, intra-band nonlinearity (FWM) and inter-band nonlinearity (SRS). Because of the latter, there is power transfer from the lowest wavelength channels to the higher wavelength channels in the spectrum leading to an uneven power distribution (tilt) at the output of each span that accumulates with the number of fibre spans as in Figure 3-24.

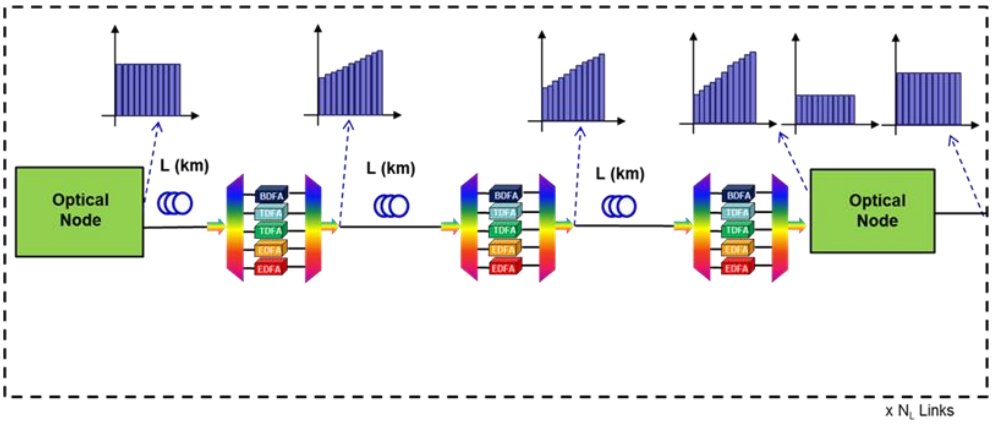

Figure 3-24: Gain/power tilt due to SRS and compensation.

To compensate this effect in the particular tool implementation, WSS-based optical nodes are assumed every third span that compensate for this tilt, so all channels enter the fibre of the next link with the same nominal power level (Figure 3-24).

The details of the physical layer modelling used by the tool have been presented in D3.1 and the validation of the model was presented in D3.2. Here we extend the description of the optimization methodology used presenting new approaches for the design methodology.

3.1.8.1 Multi-Band launch power optimization

As described in D3.2 section 3.1.2.2, the different $P_{ch,\{band\}}$, representing the power all channels in a band are launched, are used as free variables of a co-optimization that tailors the optical to signal noise plus interference ratio (OSNIR) performance per band. This method manifests a very good balance between complexity and accuracy, it applies to an arbitrary number of bands, while not requiring frequent adjustments and tweaks of the corresponding optical amplifiers.

The objective is to support two possible OSNIR tuning schemes, specifically:

- 'flat' (less than 1-dB) variation across the entire E-band to L-band spectrum. This is made possible by trading the OSNIR performance in C and L bands in favor of E and L bands.
- 'step-like' where the OSNIR performance in some bands is maximized at the expense of the performance in the remaining ones. This is interesting in case some bands are used for shorter-length connections only.

Given that the physical layer impairment model internally works with a discrimination of the power levels down to the individual channel, this approach can be further expanded towards a more fine-grained power optimization, partitioning each band in smaller segments. Moreover, this optimization is applicable for an arbitrary number of channels per band.

The optimization algorithm presented is based on simulated annealing [Kir83], and is shown below:

```
Initialize Pch per band values;
Set E  = current system energy;
Set T = start temperature;
while T > end temperature do
  Modify one band's Pch value;
  Set E' = current system energy;
  Set ΔE = E' – E;
  if ΔE < 0 or e^(-ΔE / (K * T)) > some uniform random number
    Set E = E';
  else
    Undo earlier Pch modification;
  end if
  Multiply T by the cooling rate;
end while
```

Algorithm 3-1: global optimization algorithm.

In the methodology presented in D3.2 the system's energy (the cost function in the context of simulated annealing) is given by Eq. 3-9:

$$E = \sum_{band} \frac{C_{band}}{(OSNIR_{band})^2}$$

Eq. 3-9

Where the $OSNIR_{band}$ values are calculated using the physical layer impairment model presented in D3.1, while the constants C_{band} allow us to tune the OSNIR performance per band. Unfortunately, it turns out this approach has a major disadvantage: Adjusting the C_{band} constants is necessary to get a result consistent with either of the two OSNIR tuning schemes presented earlier, and this cannot be done in advance but needs to happen in an iterative process over multiple optimization steps. This can be seen in the following figure showing the result of the same system with constant and adjusted C_{band} values.

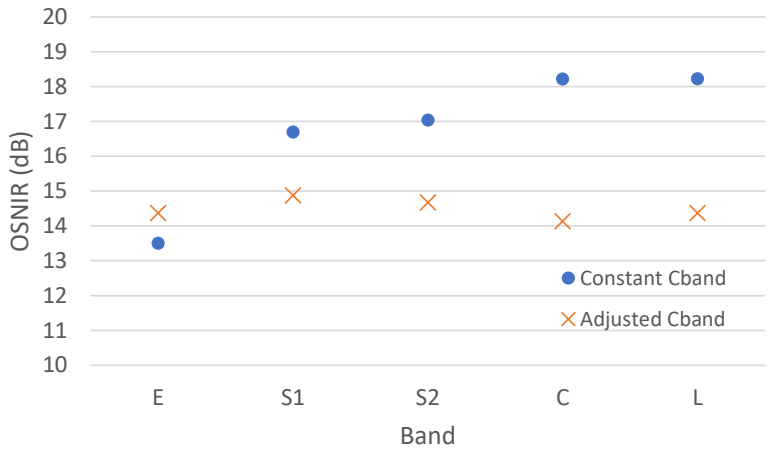

Figure 3-25: Optimized OSNIR result with initial constant C_{band} and final, after individual C_{band} value tuning.

From Figure 3-25 we can see that without adjusting the constants the optimization trades off performance in one band for better performance in multiple bands, while with individually adjusted per band constants the overall OSNIR can be contained in the same 1dB zone, as specified for the 'flat' OSNIR tuning scheme.

An alternative energy function is given in Eq. 3-10:

$$E = \sum_{band} \left(\log \frac{OSNIR_{band}}{C_{band}} \right)^2$$

Eq. 3-10

Here, C_{band} can be decided in advance and is the desired target value for the OSNIR, and can be different per band for the `step-like` OSNIR tuning scheme. Again a few iterations may be required, but fewer than with the previous energy function as we can start with a low target OSNIR and gradually increase it until no further improvement is possible. A variation of this energy function is given in Eq. 3-11:

$$E = \sum_{band} \begin{cases} \left(\log \frac{OSNIR_{band}}{C_{band}} \right)^2, & OSNIR_{band} \geq C_{band} \\ 100 \left(\log \frac{OSNIR_{band}}{C_{band}} \right)^2, & OSNIR_{band} < C_{band} \end{cases}$$

Eq. 3-11

Here bands that are under the OSNIR value specified by the respective C_{band} are weighted more, giving slightly better results when the target OSNIR is lower than what can be achieved. Both variations result in better flatness compared with Eq. 3-9.

Finally, an energy function that doesn't require any iterations to reach the best possible OSNIR is given in Eq. 3-12:

$$E = -\min_{band} C_{band} \times OSNIR_{band}$$

Eq. 3-12

This function takes the minimum OSNIR over all bands, and the minus sign ensures this value is maximized in the optimization. In practice this results in all bands converging to the same OSNIR value, the optimal one. Here the value of C_{band} is used to introduce a relative step for each band's OSNIR compared to the other ones, e.g. for 0.5 dB lower OSNIR a value of 0.8913 will be used. An example is shown in the following figure.

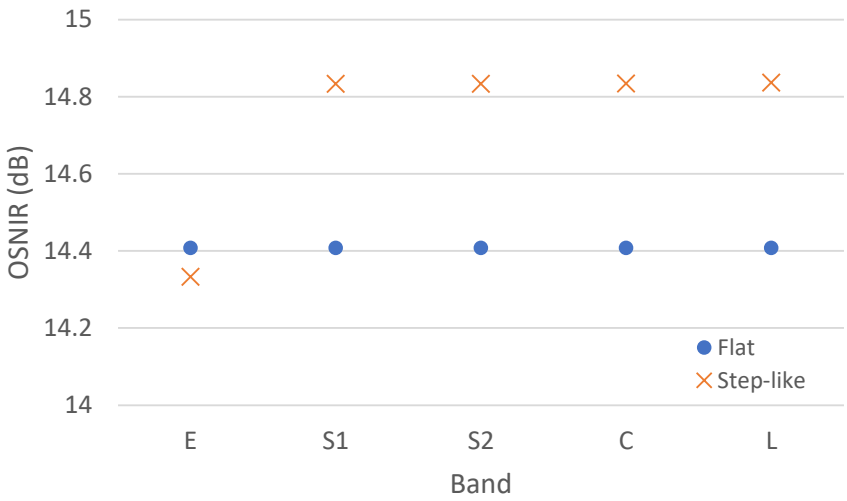

Figure 3-26: Optimized OSNIR result with Eq. 3-12for 'flat' and 'step-like' schemes. For 'step-like' the target value for the E band is 0.5 dB lower than the other bands.

Another aspect worth considering is the optimization algorithm execution time. Algorithm 3-1 is a global optimization algorithm and as such takes some time to run. However, it can be easily modified into a local optimization variation by removing the steps that accept intermediate states that are worse in order to get out of local minima. This is the variation shown in algorithm 3-2.

```
Initialize Pch per band values;
Set E  = current system energy;
for a fixed number of iterations do
  Modify one band's Pch value;
  Set E' = current system energy;
  Set ΔE = E' – E;
  if ΔE < 0
    Set E = E';
  else
    Undo earlier Pch modification;
  end if
end for
```

Algorithm 3-2: local optimization algorithm

The local optimization algorithm runs several orders of magnitude faster than the global optimization one, but we find the end result, at least with Eq. 3-12, is acceptable. An example is shown in Figure 3-27.

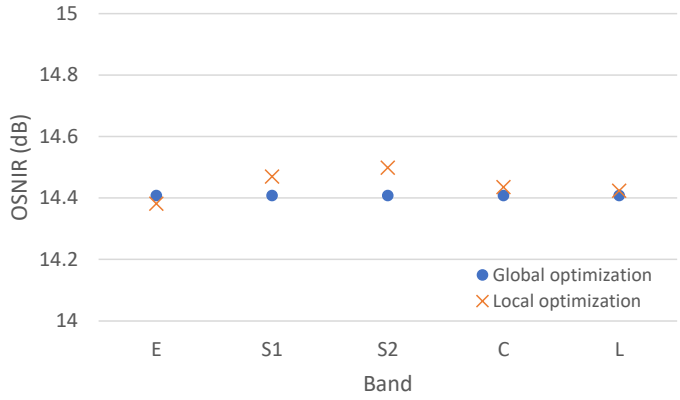

Figure 3-27: Optimized OSNIR result with Eq. 3-12 using either local or global optimization.

The local optimization result is within a small fraction of a dB of the global optimization one, making it an attractive alternative.

3.2 Integrated Access and X-haul options

3.2.1 Programmable Packet-Optical white-box deployment for integrated access and X-haul interconnection towards Edge Continuum

Recent advances fueled by the deployment of beyond 5G technologies clearly identify edge computing as a balancing point between the low latency provided by onboard computations on end-user equipment and the virtually unlimited compute power of the cloud. In the last years, serverless computing has attracted significant research interest in the edge domain. Serverless and its main implementation, Function as a Service (FaaS), offer fast and efficient deployment and scaling for short-lived stateless components, dubbed functions, running in containerized environments. In converged fronthaul and backhaul packet-optical networks SDN concepts have shown up to facilitate more flexible network traffic steering. Here, P4 has emerged as one of the most prominent technologies. Recent works have shown that combining FaaS with P4 programmable networks enables fast service re-deployment in overloaded 5G optical networks [Pel21]. In B5G-OPEN, we deepen the interaction between these two technologies to enhance application performance when deployed on edge resources that approach full utilization. Thus, here we present a three-fold contribution. First, we introduce a novel solution enabling effective interaction between FaaS deployment and application components and a P4 load balancer that can spread computation tasks to multiple edge nodes. Second, we give the details on our P4 implementation supporting two different load balancing methods. One of these takes decisions based on online telemetry of edge node CPU utilization, as it highly affects application performance. Third, we evaluate our implementations using a remote vehicle control application (RVCA) in a programmable packet-optical edge environment. We demonstrate that using our best load balancing method, it is possible to steer traffic dynamically to different edge nodes based on their actual CPU load while the application can successfully operate without observable latency increase even when one of its edge nodes reaches overload.

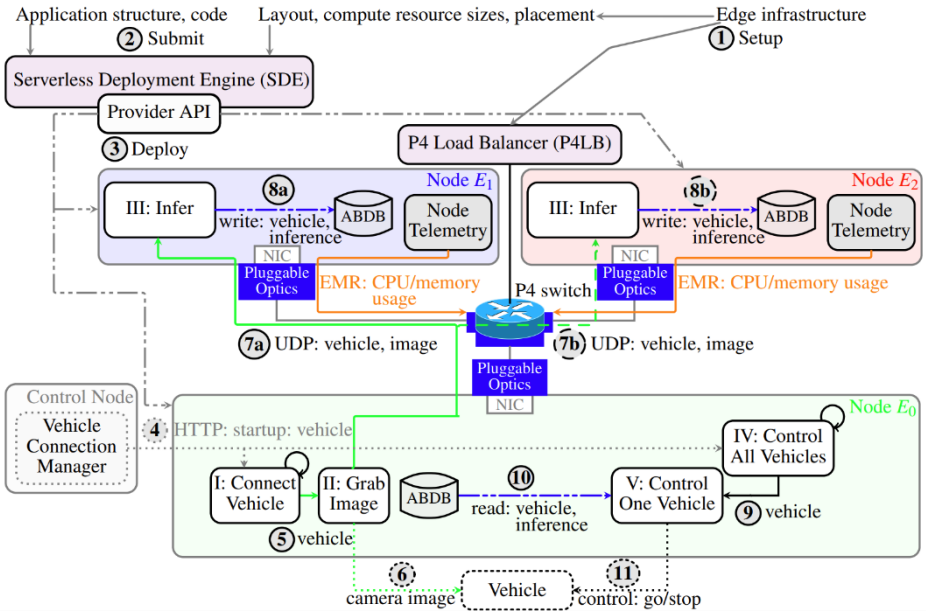

Figure 3-28: Application deployment to testbed infrastructure.

3.2.1.1 *Proposed* Serverless Application Deployment and P4-Driven Load Balancing

To realize load balancing, we tie three crucial concepts together. i) We use stateless on-demand FaaS functions that are instantiated on multiple edge nodes and can serve requests on any of those. ii) We monitor the load on the nodes and iii) feed it to a P4 programmable packet-optical switch that can interpret the metrics and alter its behavior based on them.

The top part of Figure 3-28 shows a more detailed view on how we combine these. In step 1, we use the edge infrastructure description to set up our application layout, resource and placement specifications (LRPS) and our novel P4 Load Balancer (P4LB). We use layouts where specific application components are deployed to multiple edge nodes among which the P4LB distributes the traffic. In step 2 of Figure 3-28, we submit the application's structure and code to our Serverless Deployment Engine (SDE) that transforms the application into deployable serverless artifacts based on the LRPS. The SDE merges the specified *f* application components into $F = W(f)$ FaaS functions (multiple *fs* can be part of a single F) and adds a special *W* wrapper. When deployed, *W* will handle all interactions between *fs*, datastore access and monitor these actions (capturing latency, rate and transferred data sizes). The SDE adds special Node Telemetry functions (NTF) that capture node CPU and memory load and provide those for the P4LB. In step 3, the SDE deploys these artifacts to the given edge (or cloud) infrastructure via a Provider API that gives low-level access to infrastructure components. We use Amazon Web Services (AWS) as a provider and leverage its IoT Greengrass v1 service at the edge. After deployment, *W* works as an extension to the default Greengrass runtime and provides direct connection between edge nodes using UDP. (The default AWS mechanism does not offer direct communication channels between nodes.) The NTFs periodically send load metrics with a rate of 3/s to specific layer 2 and 3 addresses using novel Edge Resource Monitoring (ERM) messages.

As shown in Figure 3-29, the 4 bytes-long ERM extra-header runs over UDP and includes the protocol version, the sender edge node identifier (i.e., Edge ID) and the list of monitored metrics

with their actual values. In this work, we convey the edge CPU load and consumed memory as monitored metrics, both expressed in percentage, however, we consider only the CPU load information for traffic steering operation. The P4LB parses the ERM messages and can alter application traffic steering based on the carried metrics.

As depicted in Figure 3-29, the P4LB includes a parser, two pipelines and two main P4 registers. The Parser includes the custom ERM header detection. ERM messages are processed by the ERM Flow Table with the aim of updating the state of the sending edge node in terms of current CPU load, stored in the Edge Resource State (ERS) register and computing the best destination edge node to be written in the Next Edge (NE) register. Two algorithm actions are implemented in this work. The Round-Robin action reads the NE and switches its value to the value of the alternative edge node. The Least Loaded (LL) action reads the ERS, compares the current CPU loads, computes the least loaded edge node and stores it in the NE. Application traffic is submitted to the Next Hop Flow Table, with the possibility to perform either ERM steering or standard SDN forwarding (forward action using control plane API flow rules). In the former case, the assigned output port is read from the NE register and applied to the packet. Moreover, its MAC and IP destination addresses are updated according to the selected edge node. The P4LB design enables three main balancer options: i) normal forwarding (NF), using the forward action and ignoring ERM; ii) round-robin (RR), using ERM steering and the Round-Robin action, with the result of equally splitting traffic between the two edge nodes; iii) CPU load-based (CB), using ERM steering and the Least Loaded action, with the result to steer the traffic to the currently least loaded edge node.

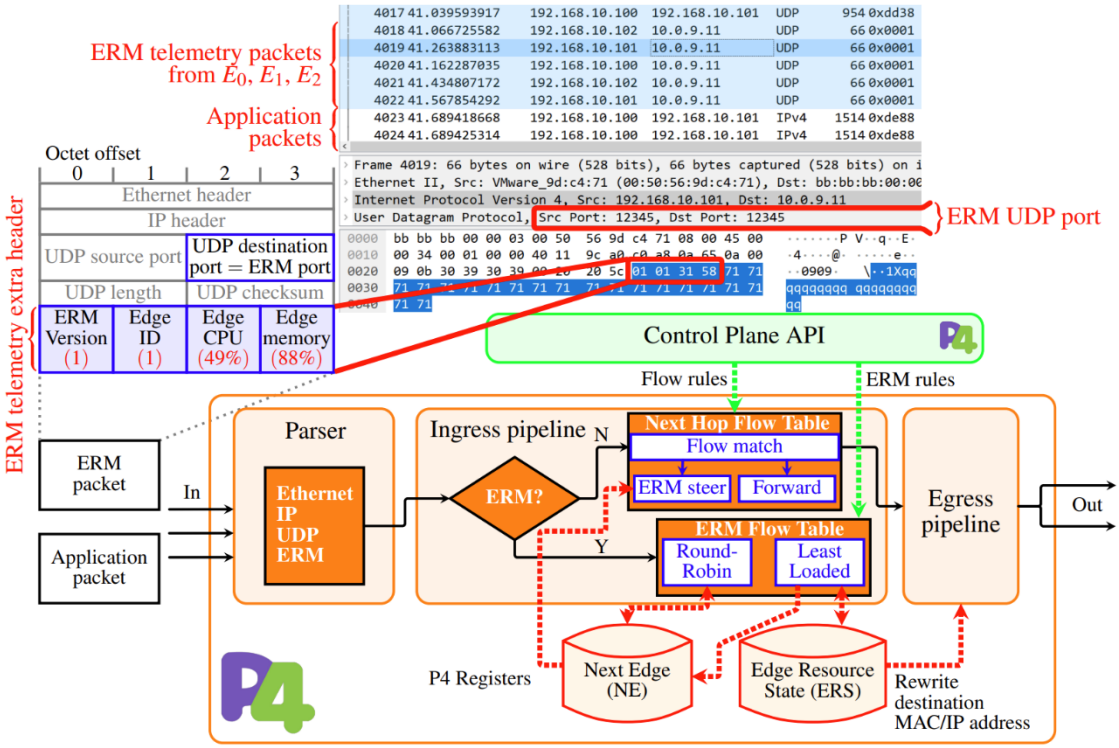

Figure 3-29: ERM and P4LB operation schematics.

3.2.1.2 *Experimental Testbed and Results*

We deploy our RVCA to four edge nodes, as depicted in Figure 3-28. The RVCA is controlled from the Control Node that supplies data of multiple v vehicles (step 4). The deployment contains a detection (DL) and a control loop (CL) using 5 FaaS functions. In the DL (steps 5–8), Connect Vehicle picks a vi from which Grab Image collects a camera image and Infer analyzes it. In the CL (steps 9–11), Control All Vehicles takes a *v_j* and Control One Vehicle (COV) interprets the result of the corresponding inference and sends a control message to *v_j* . The DL is triggered with a rate of 12/s and the CL 10/s. To avoid the cold start phenomenon of the FaaS functions, our *W* wrapper warms up 4 instances of each on-demand function that is sufficient for handling the given trigger rates (based on benchmark function execution delays). Infer, the most compute-intensive function, is deployed to nodes E1 and E2 while the rest of the RVCA and vehicle emulation are deployed to E0. These three nodes also host an AnnaBellaDB (ABDB) cluster used by the Infer and the COV functions to share data. ABDB is an in-memory key-value store that provides access to a key from all nodes but stores it only on the node where it is most frequently used (to reduce mean access delay). The Control Node and E0 are physical machines. E1 and E2 are virtual machines (8 Intel Xeon E5-2650 v3 vCPUs, 6 GB RAM) that run Greengrass v1.11.3 and are initialized with an ~37% CPU load. All nodes are connected via an optical fronthaul through the P4 BMv2 software switch executing the P4LB on a server with 6 Intel Xeon E5-2620 (2.10 GHz) CPU cores, 16 GB of RAM and three Gigabit Ethernet Network Interface Cards. The P4LB determines which node receives the image of a certain vi (steps 7a/b). Each testbed device runs Ubuntu 18.04.

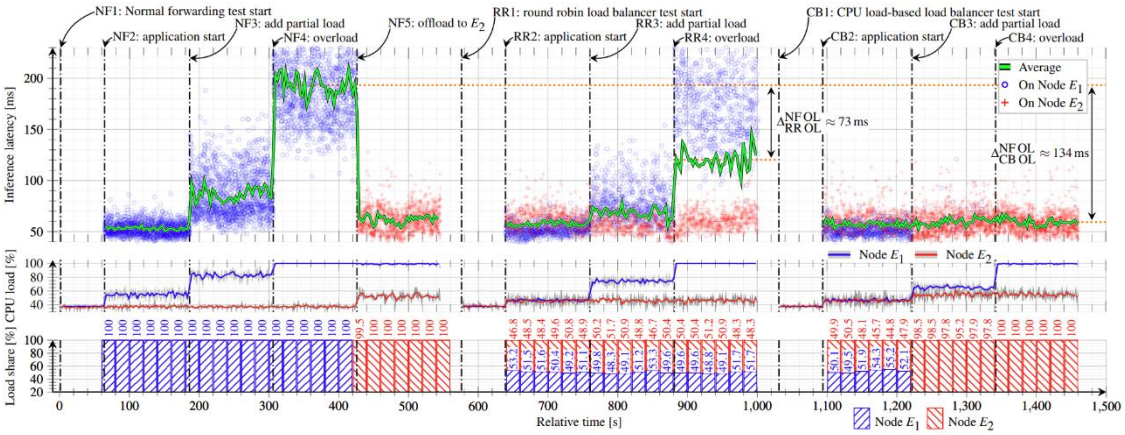

Figure 3-30: Experimental results. Top: latency of the Infer function capped at 230 ms (3 s average: green; individual executions on E1: blue; on E2: red). Middle: CPU load on E1–2 (1 s [gray] and 3 s [colored] averages). Bottom: ratio of Infer functions executed on E1 (blue) and E2 (red) in 20 s windows.

Figure 3-30 shows RVCA DL delay (DLD, latency of producing inference for an image) under varying CPU load and different forwarding behaviors. In the first ~560 s of the test, the P4LB executes the NF balancer option where the application determines which node to use for the Infer function. Under base load (BL) mean DLD is 53 ms. At the NF3 point (see top of Figure 3-30), we add an extra ~30% partial load (PL) on E1 by an external application which increases DLD but does not overwhelm the node. We increase this load to a level that overloads (OL) E1 at NF4 which causes mean DLD to rise to 193 ms. Forcing the application to E2 at NF5 reduces DLD to high-normal level (62 ms) which is caused by a slight difference between E1 and E2. Between 580–1000 s in our test in Figure 3-30, we can observe the RR balancer option. As expected, it

always splits the load between E1 and E2 approximately equally (see Figure 3-30 bottom). Under BL (between the RR2 and RR3 points), CPU load also reaches the same level on both nodes while DLD is 57 ms. In later phases (after RR3), the increase of the mean DLD is around half of what we see in the respective phase of the NF case. Under PL, we see only a 10 ms addition, while we achieve 73 ms lower DLD under OL. The CB balancer option acts similarly to RR under BL halving the load between the used nodes. Adding PL already produces a higher CPU load on E2 than in RR's case. Looking at the mid chart of Fig. 3, we can see that occasionally the CPU load at E1 dips below that of E2 which gives reason for the P4LB to keep 1%–5% of the inference executions at E1. Thanks to the severely reduced number of executions at E1, the node receives a smaller load from the application than in the RR case which enables it to complete executions with a 15 ms lower delay on average (calculated on the individual executions displayed in the top chart of Fig. 3). When overloading E1, all inferences are executed at E2. CB manages to keep a low DLD: under BL it matches RR's 57 ms while it achieves 59 ms throughout the PL and OL phases, without observable increase between them. The Wireshark capture of Figure 3-29 (top) shows an excerpt of the packets processed by the P4LB with the CB option. Application packets (e.g., frame 4017) are first sent by E0 (IP address 192.168.10.100) and steered to E1 (101). Then, ERM telemetry packets are received from all the nodes, triggering ERS and NE register updates. The capture shows the details of the metric fields sent by E1 reporting its current CPU load at 49% (frame 4019). In this case, traffic continues to be steered to E1 due to a higher E2 CPU load (see frames 4023–4024). The latency introduced by the P4LB when application traffic is processed (i.e., intra-switch latency) is around 250 µs with NF and around 300 µs with RR and CB. Thus, the impact of ERM-based stateful steering is an approximately 50 µs increased latency with respect to plain forwarding, corresponding to the additional ESR register read operation performed by both the RR and LL actions.

To summarize, in this work we presented a novel framework jointly exploiting serverless computing and P4 network programmability specifically designed for latency-sensitive 5G applications running in packet-optical access networks supporting edge computing. The framework successfully enables serverless deployments, on a per-packet basis, between two edges for load balancing (or reliability) purposes. Results show effective dynamic distribution of computational load with negligible increase of application latency with respect to static forwarding towards a single edge. This work has been published in [Pel23].

3.2.2 Programmable MB S-BVT for metro/access networks

An Openconfig-based software defined networking (SDN) agent has been developed to suitably reconfigure the proposed MB S-BVT prototype within B5G-OPEN, detailed in a previous section (3.1.2). The SDN paradigm arises as a possible solution for dynamically adapting and configuring the network to meet the changing traffic demand while enhancing overall network performance. Integrating SDN with the proposed MB S-BVT prototype maximizes overall network efficiency and resource utilization to suit network needs. The SDN control plane, by means of SDN agents, can program different parameters of the MB S-BVT based on specific network requirements/conditions. This can include settings such as power levels and central wavelengths of tunable laser sources, as well as configuration of DAC/ADC channels within each BVT. Additionally, SDN can enable end-to-end network visibility and retrieve detailed configuration information of the transceivers and network elements offering a comprehensive view of the network. Centralized SDN control and orchestration can significantly improve the

coordination of network operations, while reducing complexity and associated costs. In a disaggregated scenario, where network elements come from diverse providers, the use of open standards and APIs becomes very important to promote interoperability and avoid vendor lock-in. On this regard, the OpenConfig open data model is gaining special attention for developing vendor-neutral, programmable interfaces for network devices [OpenConfig]. One advantage of the OpenConfig model is its ability to manage transceivers from multiple vendors using a unified, standardized interface, thus simplifying the management of complex optical networks. Additionally, the OpenConfig model's extensibility allows for the seamless integration of new attributes as needed, ensuring adaptability to evolving network requirements. Within this framework, specific abstract modules of the OpenConfig data model, particularly those related to packet and optical SDN operations, are leveraged for implementing the MB S-BVT SDN agent. These modules, such as the Platform and Optical Transport modules, play a crucial role in enabling the SDN controller to conduct optical planning and validate transmission impairments end-to-end. Through the extraction of operational data from the OpenConfig platform model, including supported operational modes by the MB S-BVT, the SDN controller gain insights into device structure, interfaces, configurations, and supported features. This information facilitates the configuration of optical channels and logical channel assignments between different transceivers, ensuring efficient network connectivity. The operational mode field, specific to each vendor, encodes transceiver features, enabling SDN agents to configure optical channels with the desired parameters effectively. The implemented OpenConfig SDN agent will use NETCONF/YANG and perform a subset of the OpenConfig data models with some extensions to include details about the transceiver operational mode. Constraints and capabilities related to MB S-BVT operational mode extensions are identified and summarized in Table 3-5 and Table 3-6 for physical layer characterization. For the proposed MB S-BVT, considerations and operational mode constraints have been tailored for C-band PtP transmission over a 100 km distance.

Table 3-5: Parameters linking total added optical powers from the two Leaf nodes.

Parameter	Value
Modulation format	MODULATION-FORMAT-QPSK
Bit-rate	TRIB-RATE-40G
Baud-rate	20GBd QPSK
Optical-channel-spectrum-width	50 GHz
Min-tx-OSNR	>40 dB
Min-rx-OSNR	33 dB
Min-input-power	0 dBm
Max-input-power	9 dBm
Max-chromatic-dispersion	2000 ps/nm
Max-differential-group-delay	1 ps
Max-polarization-dependent-loss	0.12 dB

Table 3-6: MB S-BVT configuration constraints for physical layer characterization.

Parameter	Value
Min-central-frequency	191675803.99 MHz in C-band
Max-central frequency	205281058.6 MHz in S-band
Grid-type	FLEX

Adjustment-granularity	G-50GHz
Min-channel-spacing	50 GHz
Min-output-power	0 dBm
Max-output-power	25 dBm

The integration of the OpenConfig MB S-BVT agent with the ONOS SDN controller involves the mapping of operational mode information into its North Bound Interface (NBI). This enables the TAPI Network Orchestrator to utilize and query this information, facilitating connectivity between distributed MB S-BVTs in the network. Configuring the MB S-BVT involves three main actions: i) device discovery, ii) optical channel configuration, and iii) extending operational modes for physical layer characterization.

During device discovery, the controller retrieves the list of components from the MB S-BVT using the get NETCONF message following the OpenConfig platform mode. This provides details such as device model, manufacturer, supported bitrate, tuneability range, and operational modes. After discovering the device details, the controller configures an optical channel to establish transmission between source and destination MB S-BVTs. New optical channel requests are received by the ONOS SDN controller via its NBI interfaces, typically including a suggested path and frequency slot. The configuration process includes setting up the central frequency, target output power, operational mode, enabling the interface for logical channel configuration, and assigning client ports to line ports. Regarding the extension of operational modes for physical layer characterization, specific attributes and properties have been defined to enhance operational mode details, previously outlined. Clients can retrieve physical layer information associated with transmission modes, focusing the SDN assessment on this aspect for physical layer characterization and impairment validation. Clients can request details of a given operational mode using standard NETCONF/Yang protocols. The response time to obtain parameters for a specific operational mode (100 operations mode in Figure 3-31) is measured at 323 ms, as depicted in Figure 3-32.

```
<get>
    <filter type="subtree">
        <operational-modes xmlns="http://example.net/yang/openconfig-terminal-device-properties" xmlns:oc-opt-term-prop-
types="http://example.net/yang/openconfig-terminal-device-property-types" xmlns:oc-opt-types="http://opencon-
fig.net/yang/transport-types">
            <mode-descriptor>
                <mode-id>100</mode-id>
            </mode-descriptor>
       </operational-modes>
    </filter>
</get>
```

Figure 3-31: Request of 100 operational mode.

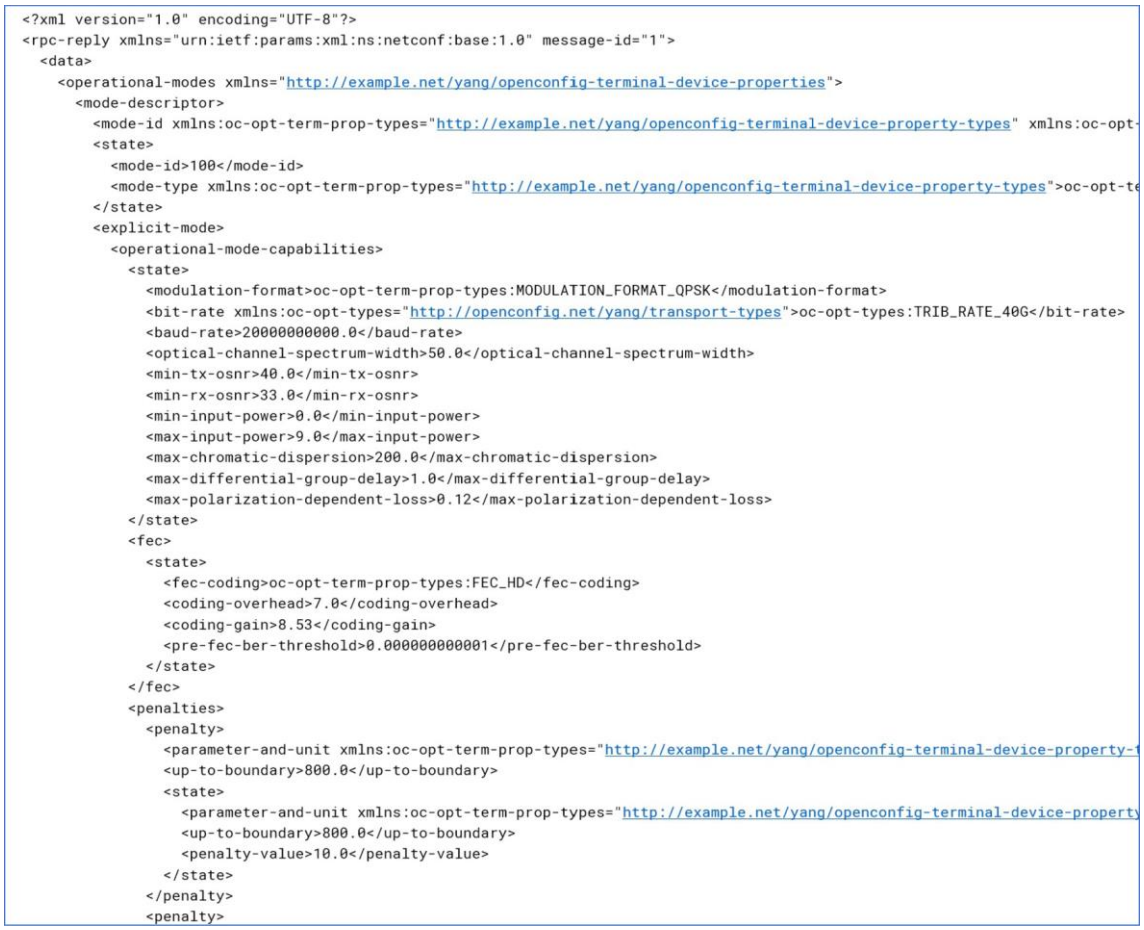

```
<?xml version="1.0" encoding="UTF-8"?>
<rpc-reply xmlns="urn:ietf:params:xml:ns:netconf:base:1.0" message-id="1">
  <data>
    <operational-modes xmlns="http://example.net/yang/openconfig-terminal-device-properties">
      <mode-descriptor>
        <mode-id xmlns:oc-opt-term-prop-types="http://example.net/yang/openconfig-terminal-device-property-types" xmlns:oc-opt-
        <state>
          <mode-id>100</mode-id>
          <mode-type xmlns:oc-opt-term-prop-types="http://example.net/yang/openconfig-terminal-device-property-types">oc-opt-te
        </state>
        <explicit-mode>
          <operational-mode-capabilities>
            <state>
              <modulation-format>oc-opt-term-prop-types:MODULATION_FORMAT_QPSK</modulation-format>
              <bit-rate xmlns:oc-opt-types="http://openconfig.net/yang/transport-types">oc-opt-types:TRIB_RATE_40G</bit-rate>
              <baud-rate>20000000000.0</baud-rate>
              <optical-channel-spectrum-width>50.0</optical-channel-spectrum-width>
              <min-tx-osnr>40.0</min-tx-osnr>
              <min-rx-osnr>33.0</min-rx-osnr>
              <min-input-power>0.0</min-input-power>
              <max-input-power>9.0</max-input-power>
              <max-chromatic-dispersion>200.0</max-chromatic-dispersion>
              <max-differential-group-delay>1.0</max-differential-group-delay>
              <max-polarization-dependent-loss>0.12</max-polarization-dependent-loss>
            </state>
            <fec>
              <state>
                <fec-coding>oc-opt-term-prop-types:FEC_HD</fec-coding>
                <coding-overhead>7.0</coding-overhead>
                <coding-gain>8.53</coding-gain>
                <pre-fec-ber-threshold>0.000000000001</pre-fec-ber-threshold>
              </state>
            </fec>
            <penalties>
              <penalty>
                <parameter-and-unit xmlns:oc-opt-term-prop-types="http://example.net/yang/openconfig-terminal-device-property-t
                <up-to-boundary>800.0</up-to-boundary>
                <state>
                  <parameter-and-unit xmlns:oc-opt-term-prop-types="http://example.net/yang/openconfig-terminal-device-property
                  <up-to-boundary>800.0</up-to-boundary>
                  <penalty-value>10.0</penalty-value>
                </state>
              </penalty>
              <penalty>
```

Figure 3-32: Reply of the OpenConfig terminal device.

3.2.3 Photonics Integrated Multi-cast and select switch in Filterless Horseshoe Network for DSCM

For the filterless architecture within the Metro-Access Network, as depicted in Figure 3-33, the Access architecture employs high-speed coherent transceivers to allocate subcarriers for point to multipoint operation and traffic distribution. Furthermore, upstream and downstream data are transmitted through two separate optical fibers (Figure 3-33 (a)). In the downstream link, we employ SOAs for power compensation to counteract signal attenuation over long-distance transmissions. In the upstream link, ensuring the proper demodulation of each subcarrier requires power balancing. Therefore, prior to transmitting the upstream signal, power compensation is applied to the signal from the preceding node, followed by early compensation for transmission losses through a BOOST-type SOA.

We have introduced a multicast selective switch in both the transmitter and receiver sections to accommodate a broader range of users. This switch plays a crucial role as optical bypass and amplifier of the uploaded and downloaded signals from the access. Therefore, it is important to design multicast and select (MCS) switches that can expand the number of users by controlling different optical paths.

We have designed a low polarization-dependent MCS based on a recently developed bulk SOA that has been co-integrated with passive waveguides.

Figure 3-33 (b) presents the block diagram of our 1x8 WDM MCS switch. This configuration consists of nine active SOAs, with one serving as a booster and the remaining eight acting as optical gates. To connect the booster with the gates, we employ Multi-Mode Interference (MMI) devices, which serve as power splitters/combiners. The connections are made using a combination of passive straight and curved waveguides. Within the booster, the input signal undergoes amplification, and the amplified signal's power is then split and distributed to the eight SOA gates through three stages of cascaded 1x2 MMIs. At each of these eight SOA-based gates, the optical signal can either pass through or be blocked, depending on the applied on/off current.

The mask design and a photograph of the fabricated chip is shown in Figure 3-33 (c) and (d). The SOA gate lengths vary between 300 µm and 900 µm to enable a comparison of output optical

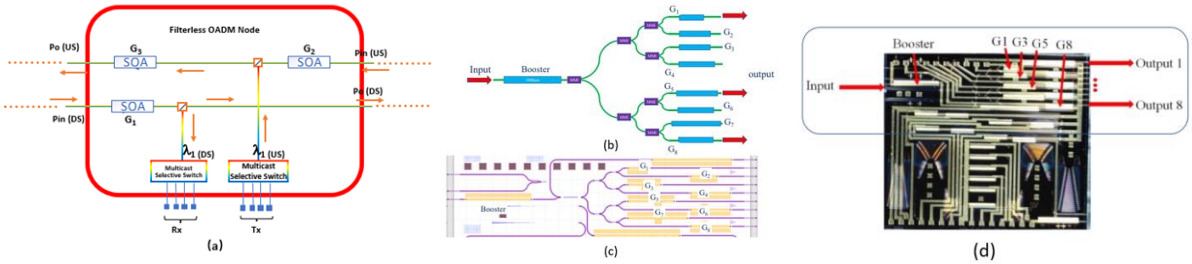

Figure 3-33: (a) Filterless OADM Node architecture (b) Schematic of the low PDG bulk SOA co-integrated with butt-coupled waveguides. (c) The Mask design. (d) the fabricated chip picture under the microscope with two needles to inject current into the SOA.

power, bandwidth, and polarization-insensitive functionality across the MCS switch under varying SOA lengths. To minimize reflections, anti-reflection coating is applied to the chip's facets. To ensure manufacturing reliability, the spacing between the gate SOAs is consistently maintained at 250 µm.

The Extinction Ratio (ER) and Optical Signal-to-Noise Ratio (OSNR) serve as critical metrics for evaluating the switch's performance in terms of signal blocking or passage to the output. Figure 3-34 (a) and (b) depict the ON/OFF switching performance of the MCS switch at two of the MCS ports. In this configuration, the booster SOA remains continuously ON, while the gate SOA is alternately turned ON and OFF to measure the ER. Across all ports, both the OSNR and ER consistently exceed 42 dB and 45 dB, respectively.

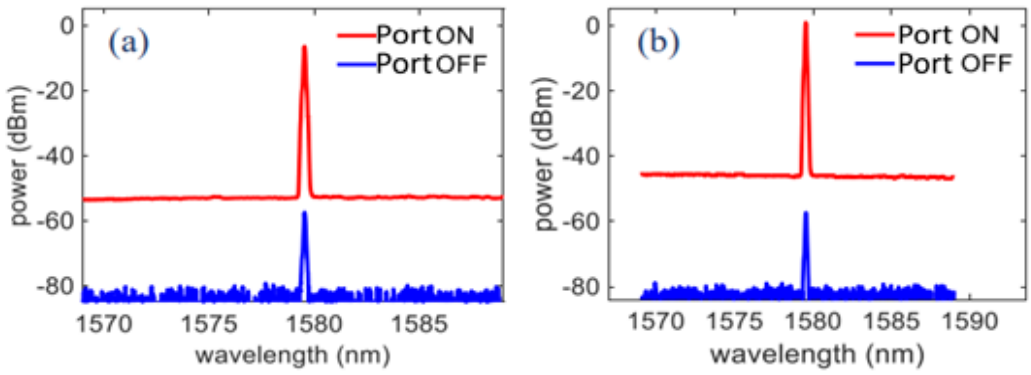

Figure 3-34: Switching characteristics of the MCS switch from (a) port 1, and (b)port 2.

Figure 3-35 (a)-(d) present the results of the BER tests conducted on the 8th output port of the MCS switch at data rates of 10 Gbit/s, 20 Gbit/s, and 30 Gbit/s. Specifically, Figures 16(a) and 16(b) represent the BERT at 10 Gbit/s for wavelengths of 1580 nm and 1570 nm, respectively. Remarkably, the device exhibited a power penalty of less than 0.75 dB consistently across all tested data rates, including 10 Gbit/s, 20 Gbit/s, and 30 Gbit/s.

The study also investigated the dynamic power penalty range of the MCS switch, revealing an input power dynamic range of greater than 20 dB while maintaining a power penalty of less than 3 dB for a 10 Gbit/s NRZ signal.

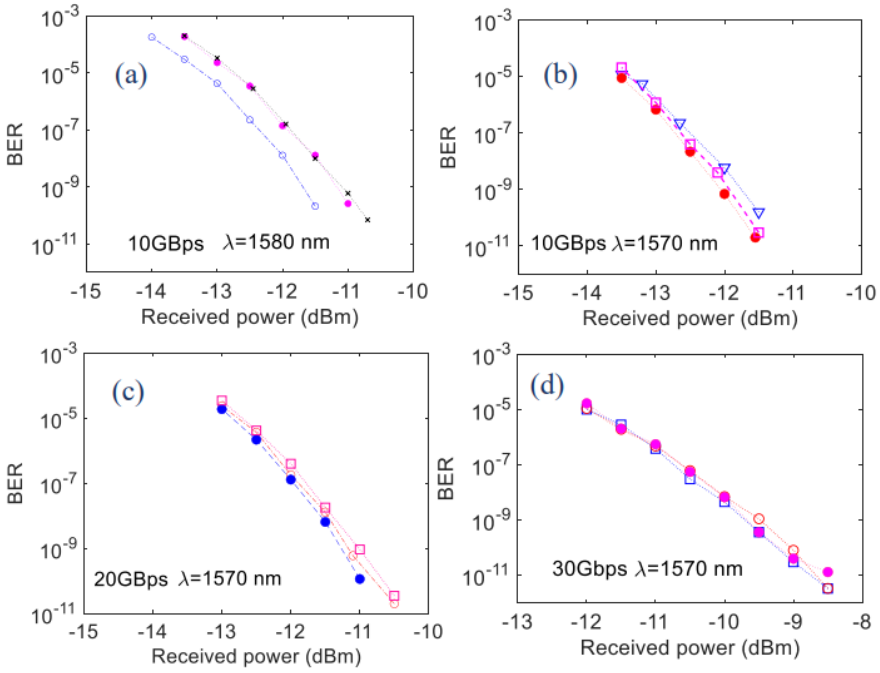

Figure 3-35: 10 Gbit/s BERT for MCS switch for the output power from port 8, at (a) wavelength of 1580 nm and (b) 1570 nm. (c) 20 Gbit/s and (d) 30 Gbit/s BERT for MCS switch from port 8 at the wavelength of 1570 nm.

3.2.4 LiFi Access

The LiFi access prototype has been introduced in last deliverable [D3.2]. Updates since last report and the final implementations are described here.

a) Updated list of devices in the LiFi prototype
- LiFi Access Point (AP):
  - **Physical Layer Implementation**: Utilizes the 802.11 OFDM PHY for modulation and demodulation processes, ensuring efficient data transmission over optical channels.
  - **Conversion Systems**: Equipped with digital-to-analog and analog-to-digital converters. These convert digital signals into analog signals for downlink transmission and vice versa for uplink reception.
  - **MAC Layer Interface**: Acts as a bridge between the PHY layer and upper network layers, following IEEE 802.11 standards. The MAC is enhanced for full-duplex

operation, optimizing protocol efficiency and supporting multiple users simultaneously.

- LiFi Transmitters and Transmitter Drivers:
  - **Functionality**: Serve as both lighting devices and antennas for transmitting optical wireless signals. LED lamps are used, operating in visible spectrum for downlink and infrared spectrum for uplink.
  - **Driver Electronics**: These components ensure that the transmitters function under optimal conditions, maximizing performance and reliability.
- LiFi User Dongle (Station Unit):
  - **Role**: Acts as the user interface for receiving downlink signals and transmitting uplink signals. It connects users to the LiFi network seamlessly.

b) Updated LiFi PHY/OFE (optical front-end component)

- Downlink design:
  - The lamp uses a blue LED with a phosphor coating to produce white light. Due to the low bandwidth of the phosphor, a blue filter is placed in front of the downlink receiver to enhance signal quality and reduce interference.
- Uplink design:
  - The uplink operates at an infrared wavelength, utilizing an IR filter to mitigate ambient light noise and eliminate self-interference from the white LED. This ensures clearer signal reception and improved communication stability.
- Light Concentrator:
  - A light concentrator is employed to gather more light efficiently, enhancing the system's performance by focusing the optical signals onto the receiver for improved sensitivity and range.

c) LiFi Scheduler

Considering the hardware architecture, a uniformly assigned average channel-time scheduling algorithm is used to allocate users. As shown in Figure 3-36, each user is assigned a specific counter, which tracks the CPU ticks accumulated during packet transmission. This ensures fair distribution of resources. Upon a new packet's arrival, the system compares the counter values across all users. The user with the lowest counter value is prioritized for transmission. This method ensures balanced access and minimizes latency, effectively optimizing the network's overall performance.

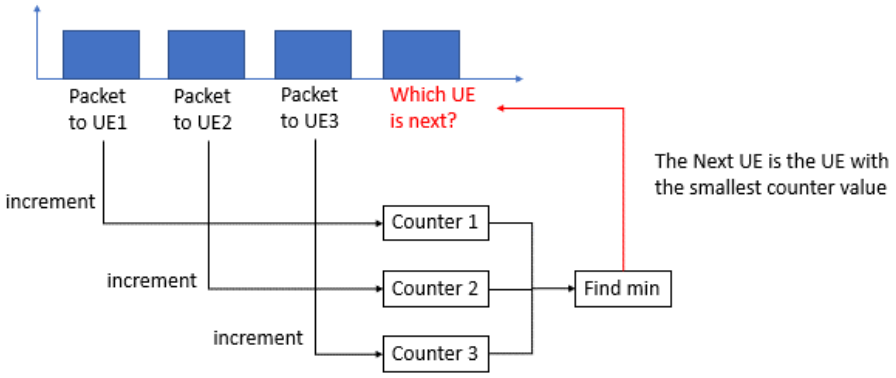

Figure 3-36: LiFi scheduling process.

d) RSSI Against User Location

Measurements have been taken using the same introduced OFEs to evaluate signal strength variations relative to user positioning within the coverage area. Measurements are taken at various distances and angles from the LiFi AP. Data is collected to analyse how physical obstructions and distance impact the received signal strength indicator (RSSI), helping optimize AP placement for improved network performance.

Test set-up and results are shown in Figure 3-37:

(a) With one functional LiFi AP, the user dongle is placed 1.5 m under the AP across the whole lighting area. For each measurement, coordinates, link distance, and RSSI are recorded to assess the distribution and coverage within the AP's range.
(b) Coordinates are recorded for each measurement.
(c) The average RSSI at each location is calculated to provide insights into the coverage area. As shown in the Figure, within a 1-meter diameter directly under the AP, the RSSI remains at its maximum. However, as the distance from the centre increases, the RSSI value decreases.

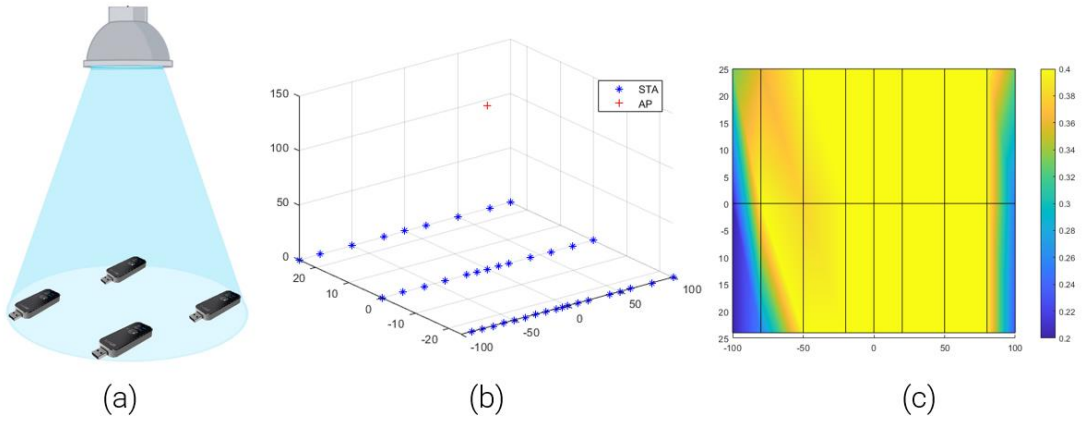

Figure 3-37: LiFi RSSI measurement under one AP: (a) set-up; (b) coordinates; (c) 2D RSSI Plot.

3.3 ADVANCED MONITORING

Optical communications leverage more and more coherent technologies as it is capable of increasing capacity close to the Shannon's fundamental limit. To further optimize capacity, the network dimension has to be considered. In particular, close to zero-margin optical network will allow additional capacity to accommodate the unstoppable traffic growth.

To get one step closer to marginless operation, massive monitoring needs to be deployed to gather as much information as possible about optical transmission and components impairments. It would allow the detection of soft failures as well as their localization, to make better and faster decisions in terms of operational maintenance and outage avoidance.

Recent works on monitoring focused on soft failures detection and identification while localization during operation is often limited to span granularity. Additional hardware may be needed, notably for filter faults identification with the use of optical spectrum analyser (OSA) or for power losses characterization with the use of optical time-domain reflectometers (OTDR). The rise of coherent transmission with powerful DSP at the receiver side opens advanced monitoring capabilities with no extra hardware. This is an appealing area of research. A challenge with receiver-based technique is to have access physical parameters at a given distance of the link beyond cumulative quantities of the entire link, e.g. cumulative chromatic dispersion, PDL. It is applicable to pluggables as well as transponder solutions.

3.3.1 Monitoring in programmable IPoWDM Networks

The recent advancements in coherent transmission technology have led to the shrinking of transmitter and receiver components, transitioning from traditional 8RU-size modules to compact pluggable form factors like QSFP-DD. Apart from saving space and power, these smaller form factors facilitate the integration of coherent modules into cost-effective packet switches designed for data center operations. These switches offer impressive throughput performance and customizable features, leveraging technologies like P4.

In our previous work (reported in D3.1), we introduced an innovative P4-based solution tailored for packet-optical nodes equipped with coherent pluggable modules, enhancing packet switching programmability. This integration offers potential savings in both capital and operational expenditures and could eliminate the need for standalone transponders, thus reducing latency and avoiding unnecessary opto-electro-optical conversions. In D3.1, we also presented a monitoring solution utilizing P4 in-network processing to expedite the exchange and processing of optical telemetry parameters, initially applied to a point-to-point configuration. In subsequent developments (D3.2), we achieved a notable enhancement enabling support for mesh topologies. We introduced a novel framework for in-network P4 processing of distributed multi-layer telemetry data, facilitating efficient soft failure detection and recovery strategies executed in microseconds.

In this section, we first provide an overview of the monitoring architecture proposed in D3.2. Then, we detail the design and evaluation of a new solution for in-network processing of telemetry data. This solution complements the threshold-based approach for failure detection from our previous work by introducing a novel technique for failure classification and prediction. This technique utilizes Deep Neural Networks (DNN) implemented as cascaded Look Up Table (LUT) distillation within P4-based packet-optical nodes.

3.3.1.1 *Monitoring Architecture*

The proposed monitoring scheme operates as follows: each packet-optical node monitors the performance of active lightpaths by gathering relevant optical parameters at the receiver side. These parameters, such as received optical power, signal-to-noise ratio (SNR), and pre-FEC bit error rate (BER), are collected by the driver of the pluggable module. The growing adoption of the C-CMIS standard should ensure good interoperability among pluggables from different manufacturers. For instance, C-CMIS specifies over 20 parameters including transmitter (TX) and receiver (RX) power levels, optical SNR (OSNR) and electrical SNR, and modulator bias values. Two methods can be employed to access the driver data. The first method relies on a lightweight script that directly interfaces with the C-CMIS driver. The second method accesses the internal database of the packet-optical box's operating system (e.g., a Redis database in the case of a SONiC operating system), which already has access to the driver data. The latter method abstracts the complexity of direct driver access and provides a unified solution for collecting all node parameters. However, it may face scalability challenges due to the involvement of the database responsible for controlling the entire node. Once the parameters are extracted, they are stored in local P4 registers. For this purpose, a thrift connection could be established between a client reading the driver (or the Redis database) and a server running within the P4 docker containing the P4 software development kit. P4 registers, leveraging P4's stateful capabilities, implement a floating-window mechanism considering, for example, the last N values. Basic operations such as averaging and identifying minimum and maximum values can be automatically performed in P4 on the stored values. These values are then compared with predefined thresholds or ranges to identify critical deviations, enabling the detection of performance degradations at the receiver due to both hard failures (e.g., fiber cut) and soft failures (e.g., malfunctioning of an intermediate amplifier or narrow filtering induced by laser shift). Extracted data, particularly if above thresholds, are included in P4-generated telemetry reports sent to other packet-optical nodes, specifically to the node containing the lightpath transmitter interface. These reports are newly generated packets designed for telemetry purposes, derived from the telemetry reports sent to telemetry collectors in traditional INT systems. Upon reaching the node managing the transmitter interface, in-network P4 data processing occurs. Collected data, possibly handled through P4 registers for further analysis, are eventually evaluated using flow rule-matching operations that can enforce specific traffic steering rules (e.g., rerouting) on all or selected traffic flows. For example, in the event of a soft failure involving a moderate increase in pre-FEC BER at the receiver interface of a node, a telemetry report is sent to the transmitting node. This report triggers a predefined flow rule that redirects high-priority traffic towards an alternative available route, safeguarding such traffic against potential subsequent hard failures. Additional information can be found in D3.2.

The aforementioned threshold-based scheme is effective for failure detection. In this B5G-OPEN it is complemented with a DNN-based solution enabling in-network failure classification and forecasting.

3.3.1.2 *State of the art and limit with existing in-network Machine Learning solutions*

The programmability of SDN data plane has advanced to a mature level of abstraction, language capabilities (e.g., P4), and data plane acceleration tools (e.g., eBPF, DPDK). This advancement allows developing network functions while abstracting from the complexity of hardware platforms. However, when complex data plane offloading strategies are implemented, such as those involving machine learning algorithms, significant limitations still exist. The primary

limitation is that current programmable hardware platforms are primarily designed for specific network functions. The P4 language facilitates in-network functions programming through pipeline structures and logic workflows. Stateful objects (e.g., registers) enable the processing of any packet content along with flow/session statistics. Additionally, P4 supports high-level language properties, allowing for logic and arithmetic manipulation, which can be used to instruct the arithmetic manipulation of metadata variables to derive neuron compute functions, including the non-linear stage at the end of the linear combination of neuron states and weights. However, this approach has two main drawbacks: i) parallelized operation is either prevented or severely limited; ii) hardware backends do not fully support all the capabilities of the P4 language.

The first drawback results in suboptimal latency performance. For instance, in the P4 DNN implementation in software switches leveraging the full potential of the P4 language, intra-switch latency is approximately one order of magnitude higher for standard pipelines (e.g., forwarding and steering). The second drawback is due to the design policies of hardware vendors' chipsets, which prioritize accelerating typical network functions such as routing, forwarding, and load balancing. Thus, so far, DNNs on telemetry data have been only implemented in external elements encompassing GPUs, introducing extra costs and latency due to the need for two devices operating at wire speed. Deploying neural networks within the data plane pipeline using conventional methods is indeed not feasible. DNNs are distributed architectures of interconnected primitives (artificial neurons) that rely on the repetition of simple mathematical tasks, mainly constituted by multiply-accumulate operations. While the high resolution of floating-point is not mandatory, and the related computational burden can be avoided with integers, the programmable ASIC pipelines of commercially available P4 switches do not currently support floats or fast integer arithmetic. An example of DNN implementation inside a P4 software switch is provided in [Pao21], comprising two main P4 stages: the feature extraction and the DNN function. However, porting such P4 codes inside a programmable ASIC backend is only successful for the feature extraction stage, while the DNN function requires a complete remapping design, mainly avoiding ALU-based operations.

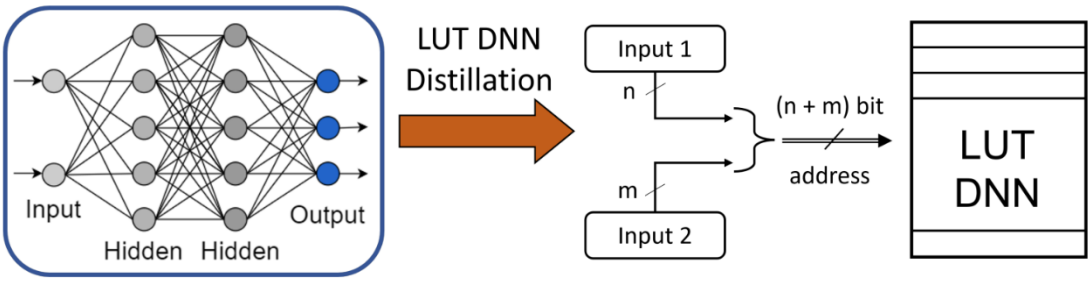

Figure 3-38: Deep neural network distillation in a lookup table for inference acceleration. Integer-encoded inputs are treated as a compound address of the LUT, whose entries encode the corresponding output of the distilled DNN.

3.3.1.3 *Proposed cascaded LUT as DNN*

To deploy machine learning (ML) models within hardware pipelines with limited arithmetic capabilities, we've developed a strategy to distill the knowledge of a trained DNN into a Look-Up Table (LUT), leveraging the advantage of integer-encoded variables. The core idea of our knowledge distillation technique is illustrated in Figure 3-38. Consider a scenario with a 2-input

network, where the inputs are integers with *n* and *m* bits, respectively. After training the DNN, the inputs are paired and treated as a compound address of the final LUT, with a bitwidth of *n + m*. The table is generated by collecting the DNN outputs for all possible input pair combinations, which are *2^(n+m)*. This approach ensures lossless inference, considering exhaustively all possible DNN outcomes. Unlike other table-based quantization strategies, we utilize LUTs not to accelerate quantization or multiplication but to distill the knowledge of the entire DNN.

However, the LUT distillation method has limitations: (1) Memory consumption grows exponentially with the number of bits composing the input features. (2) Features should use the integer format, not floating-point. (3) The number of output variables linearly affects the LUT size. Nevertheless, the LUT distillation method offers significant advantages, primarily enabling the deployment of DNNs in hardware P4 switches without constraints on complexity or type. This method applies to large DNNs and other ML algorithms if input and output requirements are met. Training more complex DNNs yields a more accurate model, albeit with increased training and LUT distillation times.

For use cases requiring periodic retraining, the neural model can be retrained on a co-processor and applied by replacing the LUT. However, memory requirements for ML tasks with multiple input features could be prohibitive. For instance, a DNN with one 8-bit output and four 8-bit input features would require 0.537 gigabytes of memory, exceeding the capabilities of current P4 switches. To address this challenge, a hierarchical structure composed of simple and cascaded DNNs can be designed instead of a single DNN. Input features are paired and sent to a first layer of DNNs, with outputs paired and sent to subsequent layers recursively until the final output is computed. This hierarchical architecture of simple 2-input neural networks allows for the application of the LUT distillation method to each neural model, resulting in a cascaded structure of tables with reduced memory usage. For example, with four 8-bit inputs, the final model would have three tables with *2^16* entries each, totaling *24.6* kilobytes of memory usage. The cascaded method enables the distillation of DNNs into LUTs even with multiple inputs, forming a deeper hierarchy of tables with a depth determined by the logarithm of the number of inputs per small DNN and the total number of inputs.

3.3.1.4 *Performance assessment*

To demonstrate the capabilities and potentiality of the LUT distillation method, we carried out experiments considering in-network telemetry processing. The considered DNN-based soft-failure identification relies on the end-to-end optical signal-to-noise ratio (OSNR) and pre-forward-error-correction bit error rate (pre-FEC BER) monitored at coherent receivers. A possible compression of OSNR and pre-BER values is reported in the table below. Assuming OSNR in [dB] expressed as a decimal number and assuming to saturate its value to 30 dB, if OSNR is expressed with 8 bits, a resolution of 0.11 dB can be achieved. Assuming pre-FEC BER expressed as $x*10^{-y}$, with x a decimal comprised between 0 and 10 and y an integer, if x is expressed with 6 bits a resolution of 0.156 is achieved, while if y is expressed with 3 bits up to 10^{-8} can be achieved.

Thus, 8 bits are considered for OSNR and 9 for pre-FEC BER, implying 131072 entries in the flow table. It is important to highlight that modern chipsets (e.g., Broadcom Tomahawk) support even 1 million of entries.

Metric	bits	Resolution
OSNR [dB]	8	0.11 dB
Pre-FEC BER = x * 10^{-7}	6 for x, 3 for y	0.156 for x, 1 for y

3.3.2 Longitudinal link power profile monitoring

The research on longitudinal power profile monitoring has emerged as a very promising tool to monitor many transmission parameters and there are now dedicated sessions in the major optical conferences (e.g. OFC, ECOC) devoted to this topic. In D3.1, we reported how we can leverage a networking scenario with the diversity of lightpaths and link tomography for C+L bands. In D3.2 we reported advances regarding transmission distances and the possibility to use XPM nonlinear effect.

3.3.2.1 On the accuracy of different techniques

In this deliverable, we first compare the accuracy of the two main methods enabling the longitudinal power profile. This has been published at OFC24. Receiver-side digital signal processing technique is receiving a lot of attention as it is not intrusive and does not need extra hardware devices. Regarding more specifically longitudinal power profile, it is also agnostic to waveforms. However, a different accuracy may be obtained. Two main methods have emerged: i) correlation-based method (CM) [Tan19] and ii) minimum mean square error (MMSE) methods [Sas23]. To increase the spatial resolution, the CM can be deconvoluted with a spatial response function [Hah22]. It provides accurate and robust results and can now be compared with the MMSE method.

A reminder of the exact implementation details is available in [May24]. We use the numerical setup described in Figure 3-39. Default parameters are directly written while those varying are identified with a star *.

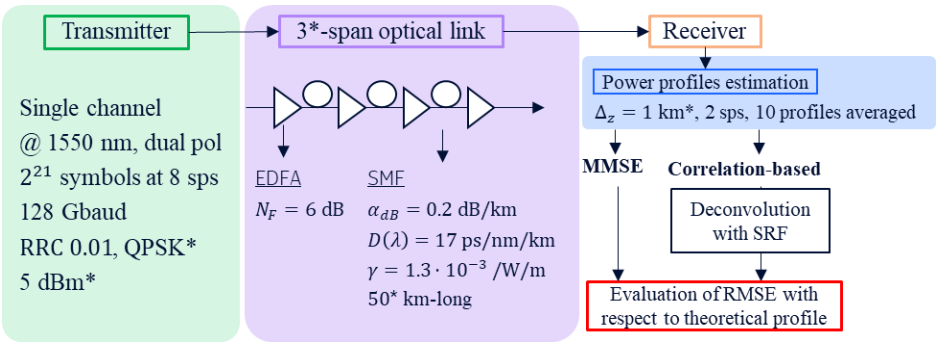

*Figure 3-39: Numerical set-up with default parameters. SMF: single-mode fiber. SRF: spatial response function. RRC: root-raised cosine. RMSE: root-mean square error. Parameters with * will be varied.*

First, we evaluate the impact of the span input power. To this end, the power is varied from -5 to 12 dBm. We show in Figure 3-40 a) the RMSE as a function of powers for 50 km or 80km -long spans. For 5 dBm and 50 km -long spans, we obtain a RMSE of 0.15 dB for deconvoluted and MMSE profiles. For all powers, we see that the RMSE are close for both methods. The RMSE continuously decreases when the power increases, due to the higher nonlinear effects, needed for power profile estimation. At -5 dBm, the RMSE is maximum and equals 0.43 dB (0.58 dB

resp.) for the deconvoluted (MMSE, resp.) profile. An asymptote is reached when the power is larger than 1 dBm. Regarding the 80-km spans, the obtained RMSE are quite similar for MMSE and deconvoluted profiles, the difference with the 50-km span case being that the asymptote value is higher (~0.4 dB) due to the lower SNR and is reached for ~2 dBm. This study confirms the relevance and the robustness of the deconvolution to many input powers, including powers slightly lower than the nonlinear threshold (see Figure 3-40 b) showing the Bell curve.

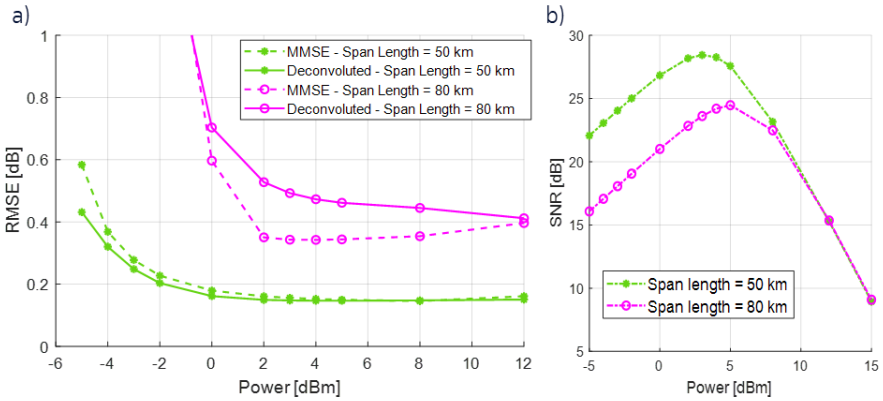

Figure 3-40: Results for QPSK 128 Gbaud 3-span transmission. a) RMSE as a function of span input powers for MMSE and deconvoluted profiles for 50 and 80 km-long spans. b) Bell curve – SNR as a function of powers – for 50 and 80 km-long spans.

Finally, we investigate the impact of the modulation format, knowing the CM is sensitive to it. We plot in Figure 3-41 a) the RMSE for QPSK, 16-QAM and 64-QAM as a function of the number of spans. For all formats the RMSE increase when the number of spans increases. Note that the 'deconvoluted – QPSK' clearly stands out since the RMSE value equals 0.48 dB for 24 spans, while it is between 0.18 and 0.27 dB for all others. This is partly due to the poorer accuracy for the first spans at the end of them for QPSK compared to 16 and 64 QAM. We can see this effect in Figure 3-41 b) and c) where we focus on two subsets 0-100 and 750-850 km of the obtained deconvoluted profiles for the 24-span transmission for $\Delta_z = 1\ \mathrm{km}$. Compared to QPSK, with a higher modulation format, the accuracy of the deconvoluted profiles is improved and closer to the one of the MMSE for $\Delta_z = 1\ \mathrm{km}$ for longer links.

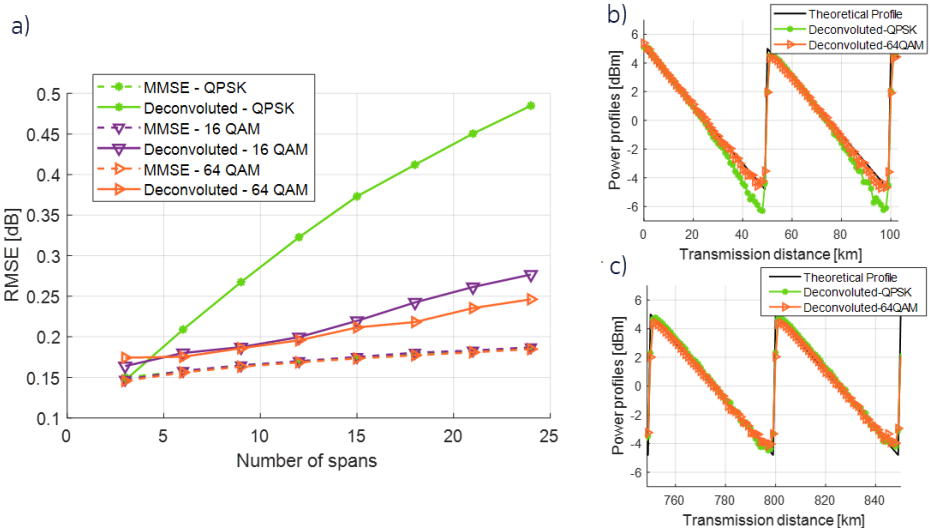

Figure 3-41: Results for 128 Gbaud 5 dBm. a) QPSK, 16 QAM and 64 QAM. Theoretical and deconvoluted profiles for 24 spans for QPSK and 64 QAM between b) 0 and 100 km and c) 750 and 850 km.

To conclude, we determined the accuracy of two power profile estimation methods: the deconvolution of CM and the MMSE method. We demonstrated that both methods show a similar accuracy for various powers and higher order modulation formats for Δ_z=1 km with a slight advantage for the MMSE method. We also showed the possibility to use both power profile estimation methods for longer links at the expense of a reasonable increase of the RMSE. For larger Δ_z, the deconvoluted profile can exhibit a better accuracy than MMSE profile.

3.3.2.2 Cost and power consumption of longitudinal power profile

We also studied a relative cost and power consumption of such a monitoring technique compared to an already commercially deployed solution of OTDR. OTDR and power profile monitoring are complementary: despite many similarities there are also applications only available with either power profile (e.g. amplifiers, filter detuning, PDL monitoring, etc.) or OTDR (e.g. link failure localization). In particular, we propose a monitoring placement algorithm that take into account single and multiple monitors per link (defined as NPL: number of monitored LPs that traverse the link).

The problem of optimized monitoring placement (OMP) of PPM can be stated as follows: Given a network topology and a set of LPs, Decide the placement of PPM modules, Constrained by placing PPMs over the existing LPs, with the Objective of minimizing the unsatisfied NPL (defined as the additional number of monitors required to achieve the required NPL) in all links as the first objective and minimizing the number of PPM modules as the second objective. Note that this problem is different from the failure localization problem, as the OMP problem aims to deploy monitoring modules, while the failure localization problem aims to localize the soft/hard failure in the network based on the monitoring data. The details of the proposed OMP algorithm are described in Algorithm 1 in [Zha24].

In the following, we provide illustrative numerical results. We first evaluate the number of monitors under different loads, and then compare the cost and power consumption of PPM and OTDR. We consider PPM deployment in two network architectures, i.e., opaque (the cases with and without OMP are named as Op-O and Op, respectively) and transparent (the cases with and

without OMP are named as Tr-O, Tr, respectively) architectures, which are compared to the OTDR deployment. When comparing the cost and power consumption under 1% rejection rate, all the links are traversed by at least one LP due to higher traffic, leading to the same number of OTDRs deployed for both opaque and transparent architectures.

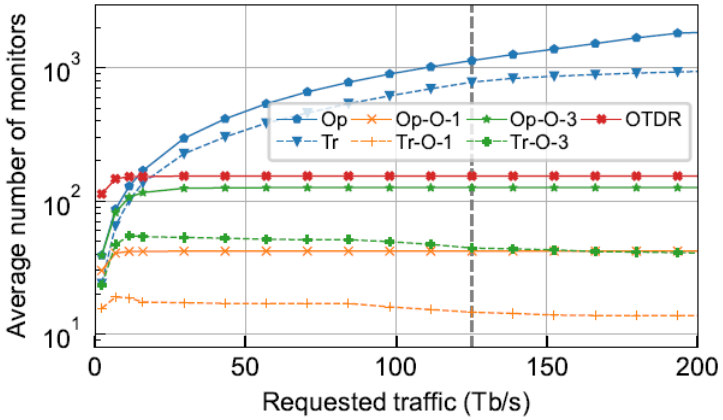

Figure 3-42: Average number of monitors vs. load in N14.

In Figure 3-42, the number of PPMs for Op and Tr always increases with the growing traffic due to the higher number of established LPs, and all LPs are equipped with PPMs. Note that OTDR modules are only placed to monitor the links that are monitored with PPM to have a fair comparison of OTDR and PPM. Therefore, as the traffic approaches 30 Tbit/s, the number of OTDRs increases to 154 and then remains constant, given that all links are already monitored by at least one PPM. With OMP, for Tr-O-1, the number of monitors increases up to 19 when the traffic grows to 7 Tbit/s because more links are monitored. Then, the number of monitors decreases from 19 to 15 when the traffic grows because more LPs with a larger number of hops can be used. Instead, for Op-O-1, the number of monitors never decreases since all LPs have only one hop. When NPL equals 3, the number of monitors of Op-O-3 and Tr-O-3 follows the consistent trend as in Op-O-1 and Tr-O-1. After all the links satisfy the required NPL, the number of required OTDRs is greater than all the tested cases that place PPM with OMP. For instance, the number of OTDRs required is around 7x to 11x the number of PPMs in Tr-O-1 when increasing the network traffic.

We now evaluate the cost of PPM compared to OTDR in N14, shown in Figure 3-43 a). The cases with OMP have much smaller crossing values than the cases without OMP, showing that OMP is fundamental to lower PPM monitoring costs. Without OMP, the cost of one PPM must be less than 0.7% and 1.0% of one transponder for Op and Tr, respectively, to compete with OTDR. However, with OMP, the cost of PPM should be below 18.3% and 52.7% of the cost of transponder for Op-O-1 and Tr-O-1, respectively, to compete with OTDR. Note that the cost difference between Op-O-1 and Tr-O-1 is due to the bypassing of nodes in the transparent architecture. Moreover, when the required NPL is 3, the crossing value of cost is reduced to around 1/3 of that of the cases with the required NPL equal to 1. Specifically, the crossing value of Op-O-3 and Tr-O-3 is 6.1% and 17.4%, respectively.

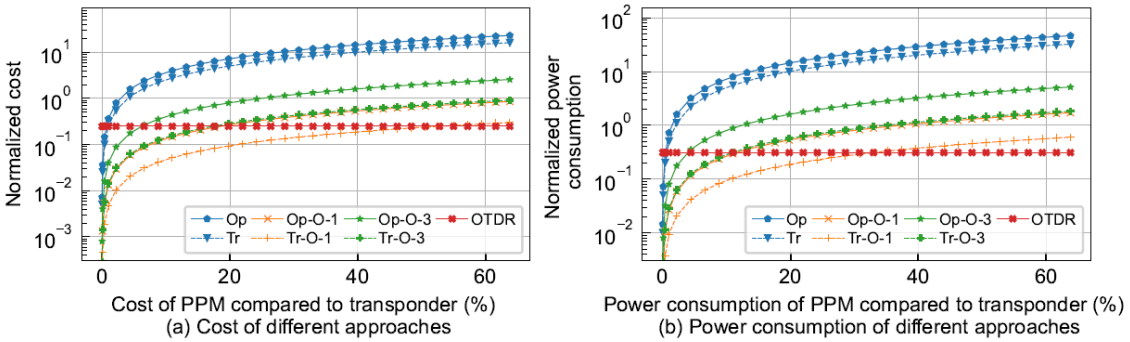

Figure 3-43: cost and power consumption of different approaches in N14.

Figure 3-43 b) plots the power consumption of PPM compared to OTDR. Without OMP, the power consumption of PPM relative to one transponder must be less than 0.4% and 0.6% of the transponder's power consumption. With OMP, the power consumption of PPM can be up to 11.5% and 33.0% of the transponder's power consumption for Op-O-1 and Tr-O-1, respectively. When the required NPL is 3, the crossing value of power consumption is reduced to around 1/3 that of the cases when the required NPL is 1.

To conclude, we investigated the problem of optimized monitoring placement for PPM and we quantified the cost and power consumption of PPM compared to OTDR to provide guidelines for deployment of PPM modules. Results show that in a large continental-wide topology as N14, PPM's cost (power consumption) should be below 10.2 times that of OTDR, which corresponds to 53% (33%) of that of a transponder. This means that the cost and power consumption of PPM are not limiting factors for PPM deployments, as PPM is not expected to have such a high cost and power consumption.

3.3.3 Monitoring of chromatic dispersion in multiband networks

In the framework of B5G-OPEN, an experiment has been performed to demonstrate a wide band technique to monitor the chromatic dispersion (CD) using MB optical OFDM bandwidth/bit rate variable transceivers (BVTs).

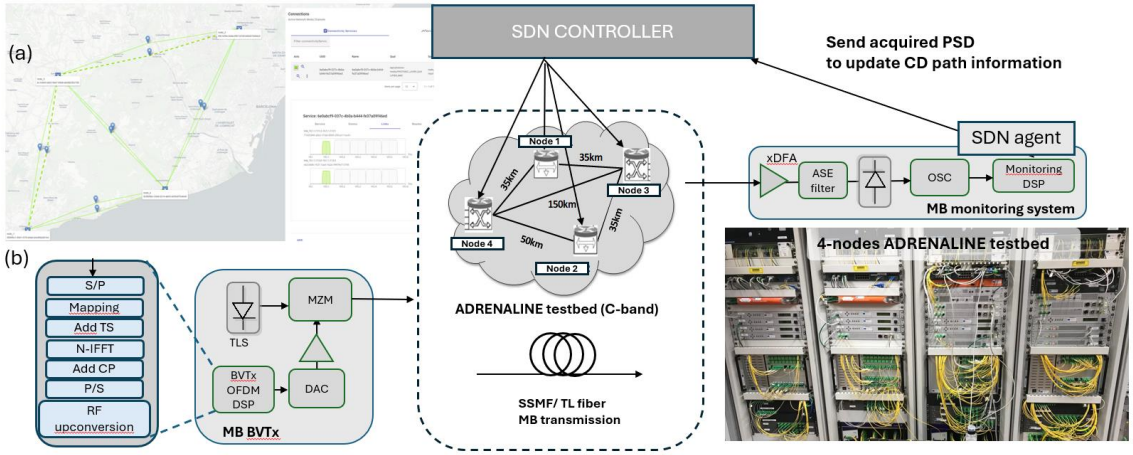

Figure 3-44: Experimental setup for CD monitoring. (a) GUI of the SDN controller to stablish the optical path. (b) Setup used to perform the experiment with the MB-BVT: The OFDM data are generated, sent through the optical testbed or Fiber spool, amplified, filtered, and then sampled by an oscilloscope. The monitored data are sent to the controller via the SDN agent.

Specifically, the MB BVTs, depicted in Figure 3-44, can be seen as a building block of the MB S-BVT B5G-OPEN prototype, described in section 3.1.2 of this document. The transmitter's DSP block encompasses various functions including data parallelization and mapping (such as employing 4 QAM modulation for each subcarrier), insertion of training symbols (TS), implementation of a 512-point inverse fast Fourier transform, insertion of cyclic prefix (CP), serialization, and radio frequency (RF) up-conversion. The signals transmitted have a bandwidth of 20 GHz and operate across different spectral bands (S+C+L-bands). To generate double side band (DSB) OFDM signals, a high-speed DAC operating at 64 GSa/s is employed. External modulation is achieved through Mach-Zehnder modulators (MZMs) and a tuneable laser sources (TLSes). Subsequently, the different signals are transmitted through different types of optical fibers, and at each direct detection (DD) receiver they are amplified, using doped fiber amplifiers (xDFA), filtered, and photodetected, with PIN photodiodes. In particular, erbium DFAs (EDFAs) are utilized for the L band and C band, while a thulium DFA (TDFA) is employed for the S-band. A 50 GSa/s digital oscilloscope (OSC) with a bandwidth of 20 GHz is used to digital-to-analog convert the received data. The received spectra at the OSC are sent to the SDN controller by means of implemented SDN agents to process and extract CD information of a particular fiber link. The proposed method is here described in detail. The linear OFDM channel has a transfer function given analytically as [Bar10]:

$$\mathrm{H_{eq}} = \cos\left((\pi \cdot \ (\mathrm{f} \cdot \lambda)^2 \cdot \mathrm{D}(\lambda) \cdot \mathrm{L})/\mathrm{c}\right)$$

Eq. 3-13

where f is the frequency, λ the channel central wavelength and D(λ) is the dispersion parameter. Eq. 3-13 characterizes a sinusoidal variation, that can be seen in Figure 3-45 (left), where notches (zeros) are determined by the accumulated dispersion $D(\lambda) \cdot L$

$$(\ (f \cdot \lambda)^2 \cdot D(\lambda) \cdot L)/c = \kappa + 1/2$$

Eq. 3-14

where κ is an integer. In our OFDM system, we monitor the power spectrum density (PSD) of the received signal in the positive frequency domain of the received samples, acquired from the OSC. This PSD is expected to conform to the square of the transfer function described in Eq. 3-13. Consequently, estimating CD properties of a fiber link involves several steps: i) for each lightpath with a central wavelength λ_j, we record a 2048-points PSD against frequency, ii) we employ a moving average filter with a block size of 15 to smooth the monitored PSD, iii), we determine the notches (zeros), in a least mean square fashion, in the PSD versus frequency, starting from the accumulated CD based on the datasheet fiber type and the measured fiber length, iv) through Eq. 3-13, we compute the accumulated $\mathrm{CD_j}$ corresponding to the wavelength λ_j, v) we estimate each link's dispersion by correlating the accumulated dispersions of lightpaths [Sev24], vi) leveraging the measured accumulated link CD versus frequency curve, we compute the dispersion parameter D versus frequency curve, assuming precise knowledge of the fiber length L and vii) lastly, we fit the curve of D versus λ using a derived three-term Sellmeier formula for the relative group delay [Coh85]:

$$D(\lambda) = \frac{S_0}{4}\left(\lambda - \frac{{\lambda_0}^4}{\lambda^3}\right)$$

Eq. 3-15

where λ_0 is the zero-dispersion wavelength and S_0 is the dispersion slope at λ_0.

To establish the validity of the method, we have studied the accuracy of the proposed solution considering different fiber types, i.e. standard single mode fiber (SSMF) and Teralight (TL) with different fiber lengths (50 and 75 km) and dispersion values in three optical bands S, C and L. The S and C-band transceivers have been developed in B5G-OPEN within the MB S-BVT prototype. However, the L-band transceiver is not developed in B5G-OPEN but has been here used to also evaluate/investigate the proposed CD monitoring method within this particular band. Evaluation of transceiver performance is detailed in [Nad23, Nad24], focusing here on CD evaluation/assessment by incorporating at the bandwidth/bit rate variable receivers (BVRxs) monitoring capabilities, without necessarily activating the receiver OFDM-based DSP. Specifically, to assess CD across different bands, the central wavelength of TLS within each band is adjusted before data capture for various fiber types and lengths. For each acquisition, within the receiver DSP block depicted in Figure 3-44, a 2048-points PSD analysis is conducted and adjusted through fitting with a function accounting for the linear OFDM channel (Eq. 3-13) and the scope bandwidth.

$$\mathrm{PSD(f)} = \mathrm{P_0}\,|\cos\left((\mathrm{f}\lambda)^2\ \ (\mathrm{D\_}\lambda * \mathrm{L})/c\right)|^2\ 10^{(\alpha * \mathrm{f})} + \mathrm{N_0}\ ,$$

Eq. 3-16

where α is an attenuation coefficient related to the scope bandwidth, N_0 is accounting for multiple electrical and optical noise and is a background level, D_λ is the dispersion coefficient at the wavelength λ, L the fiber length. α is fixed for all the experiment 0.2 dB.GHz^{-1}. Figure 3-45 (left) shows a typical PSD (cross markers) with fitted curve from Eq. 3-16 in dashed line.

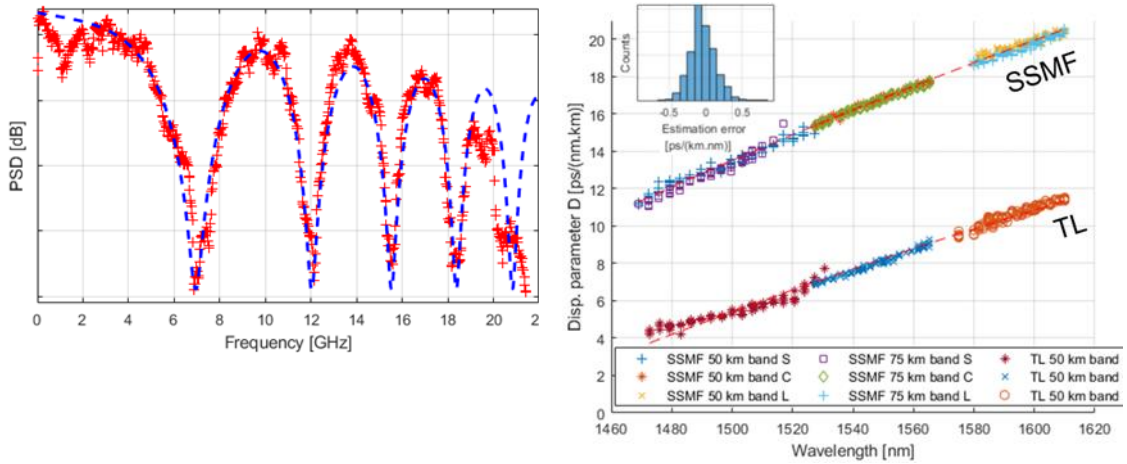

Figure 3-45: (left) Power spectral density of detected signal after 75 km of propagation in standard single mode fiber. Crosses are experimental points; dashed line is the fit based on Eq. 4. (right) Dispersion parameter D as a function of the wavelength obtained from the fitting with Eq. (4) for different fiber types and fiber lengths. Red dashed lines are the results of the fit with Eq. (3) for each fiber type. Inset: histogram of the estimation error.

The results of this fitting process for various fiber types, lengths, and channel wavelengths are visually represented in Figure 3-45 (right). For each fiber type, we conduct a fitting procedure using Equation (3), aiming to minimize the root mean square error between the data and the model to determine the fiber parameters λ_0 and S_0. The resulting fit is depicted as a dashed red

line in Figure 3-45 (right). The parameters obtained for each fiber type and length are tabulated in Table 3-7.

Table 3-7: Tested fiber type, length and fitted parameters.

Fiber	Length [km]	λ_0 [nm]	S_0 [ps/(km.nm^2)]
SSMF	50	1335	0.0968
	75	1337	0.0966
TL	50	1416	0.0703

The curve aligns well with the data for SSMF yet exhibits deviations at lower wavelengths for TL fiber. This discrepancy arises due to the limited accuracy in the region of low accumulated dispersion, where the notch frequency nears the signal bandwidth. Lastly, the inset of Figure 3-45 (left) displays a histogram illustrating the distribution of errors, indicating an overall good performance of the methods. The standard deviation of the errors is calculated as 0.19 ps/(km.nm), with a mean value of -0.03 ps/(km.nm).

Finally, the proposed monitoring solution is integrated to a SDN controller, within the ADRENALINE testbed available at CTTC, as joint WP3-WP4-WP5 project activity. The related work/activity will be reported in D5.2.

4 DELIVERED PROTOTYPES

This chapter gives the complete list of "prototypes" developed by the partners in collaboration with other WPs during the entire duration of the Project. It is reported in the form of a table updated of the one included in D3.2 [D3.2].

Table 4-1: List of delivered prototypes.

Prototypes	Description	Software Control Parameters	Software Control Mode	Delivery Time
MB S-BVT (PtMP transceiver)	Optimized programmable MB S-BVT based on multicarrier modulation and direct detection. PtP and PtMP C+S transmission enabled.	Laser central wavelength (TLS); Laser output power and DAC channels (enable/disable)	SDN OpenConfig agent	April 2024
(Semi-) Filterless Node Prototype		Input and Output port routing.	Matlab-based Instrument Control	N/A
2-degree C ROADM		Explicit/operational mode: drop channels (C- band, add channels (C-bands), drop and continue channels (C- bands), channel power (C-bands)	Config by FPGA	First of Oct, 2023
2-degree O,C,L ROADM		Explicit/operational mode: drop channels (O-, C-, L- band） add channels (O-, C-, L-bands), drop and continue channels (O-, C-, L- bands), channel power (O-, C-, L-bands)	Config by FPGA	First of Feb, 2024
MCS switch PIC		Explicit/operational mode: Select the path from the access. Not packaged PIC, test will be done in TUE labora-tory.	Config by FPGA	Chip delivery end of Nov, 2023. Characterization by end of February 2024.

				System transmission assessment by end of June 2024.
C and L band WSS PIC		Explicit/operational mode: Select the channel in C and L-bands. Not packaged PIC, test will be done in TUE laboratory.	Config by FPGA	Chip delivery end of Nov, 2023. Characterization by end of February 2024. System transmission assessment by end of June 2024
Power Profile Monitoring DSP Software		Received Coherent Waveform	HHI's Matlab DSP Toolbox	N/A
MB Offline Transceiver Prototype		Yet to be decided	Matlab-based Instrument Control	Jan/2024
Impairment validation tool	Network analysis tool focusing on OSNR performance, implementation cost, and power consumption for filterless DSCM-powered metro-aggregation networks	Tx/Rx parameters, network topology (i.e., design) and parameters (i.e., link and devices properties)	Matlab-based numerical tool	July 2024
7-node mesh network		Transmitter, receiver, Path, …	SDN OpenConfig agent	Feb 2023
Packet-optical white box with SONiC Operating System, OpenZR(+) transceivers		Transceiver parameters (frequency, power, application code) packet forwarding rules	OpenConfig SDN Agent with telemetry support	Jan 2024

P4 switch		Fow rules, optical transmission parameters embedded within in-band telemetry	P4runtime	Oct 2023
Multiband Amplifier	Amplifier setup comprises multiple wavelength bands that are combined by means of an optical band splitter and band combined	Tilt and gain of the amplifiers can be adjusted	Controlled via network element management software and local computer	January 2024
S-band		N/A	N/A	March 2024
LiFi Access	Optimized LiFi access prototype includes: LiFi AP, LiFi lamp with driver, user device, with configured data/control management tools.	LiFi enable, parameters for monitoring purpose	SDN agent, telemetry exporter	May 2024

5 CONCLUSIONS

This deliverable is the last one of WP3 and describes the project's final proposed solution for the data plane.

Many technical aspects of the solution are described only in broad terms as most of them have already been extensively covered in previous documents. The solution concept is defined in B5G-OPEN as a series of recommendations and detailed studies of technical proposals and transmission, architectural, control and monitoring issues.

The document also includes the most recent results obtained in the various data plan contexts in the last period of the project. This new information integrates what has already been discussed previously and adds technical details to the proposed solution.

What has been reported allows us to state that substantially the objectives set for the data plan in the context of WP3 have been achieved and that a significant general and innovative contribution to the problems of increasing network capacity while maintaining reasonable costs and performance has been well analyzed in the context of B5G-OPEN.

6 REFERENCES

[Agr13] G. P. Agrawal, Nonlinear Fiber Optics. 2013, Academic Press.

[Anc22] A. Anchal and E. Lichtman, “Few Milliseconds-Fast SRS-Induced Loss and Tilt Compensation Algorithm for Dynamic C+L-band Networks”. European Conference on Optical Communication (ECOC). Basel, Switzerland, 2022.

[Bar10] D. J. F. Barros and J. M. Kahn, “Comparison of Orthogonal Frequency-Division Multiplexing and On-Off Keying in Amplified Direct-Detection Single-Mode Fiber Systems,” Journal of Lightwave Technology, vol. 28, no. 12, pp. 1811–1820, 2010. 10.1109/jlt.2010.2048999.

[Chr92] A. R. Chraplyvy, J. A. Nagel and R. W. Tkach, “Equalization in amplified WDM lightwave transmission systems”. IEEE Photonics Technology Letters, 4(8), 920-922, 1992.

[Coh85] L. Cohen, “Comparison of Single-Mode Fiber Dispersion Measurement Techniques,” Journal of Lightwave Technology, vol. LT-3, no. 5, pp. 958–966, 1985. 10.1109/jlt.1985.1074327

[100ZR] https://www.adtran.com/en/products-and-services/open-optical-networking/pluggables-and-subsystems/coherent-zr-series/coherent-100zr-series

[HER20] J. A. Hernández, M. Quagliotti, E. Riccardi, V. López, O. González de Dios, R. Casellas, “A techno-economic study of optical network disaggregation employing Open-Source Software business models for Metropolitan Area Networks”, in IEEE Communications Magazine 58(5), 40-46, 2020.

[Kon24] N. Koneva, A. Sánchez-Macián, J. A. Hernández, F. Arpanaei and Ó. González de Dios, “A Queuing Envelope Model for Estimating Latency Guarantees in Deterministic Networking Scenarios”, 2024, article under review in IEEE Comm. Letters, online available in https://arxiv.org/pdf/2406.16452

[Cug21] F. Cugini, D. Scano, A. Giorgetti, A. Sgambelluri, L. De Marinis, P. Castoldi, and F. Paolucci, “Telemetry and AI-based security P4 applications for optical networks [Invited]”, Journal of Optical Communications and Networking, vol. 15, no. 1, pp. A1–A10, 2023.

[D2.1] B5G-OPEN deliverable D2.1 “Definition of use cases, requirements, and reference Network architecture”.

[D3.1] B5G-OPEN deliverable D3.1, “First year results on data plane infrastructure”.

[D3.2] B5G-OPEN deliverable D3.2, “Second year results on data plane infrastructure”.

[Hah22] C. Hahn, J. Chang and Z. Jiang, "Localization of Reflection Induced Multi-Path-Interference Over Multi-Span Transmission Link by Receiver-side Digital Signal Processing" in Optical Fiber Communications Conference and Exhibition (OFC), 2022.

[Kir83] S. Kirkpatrick, C.D. Gelatt Jr and M.P. Vecchi, “Optimization by simulated annealing”. Science, vol. 220, no. 4598, pp. 671-680, May 13, 1983.

[Man03] I. Mandelbaum and M. Bolshtyansky, “Raman amplifier model in single–mode optical fiber”. Photonics Technology Letters, 15(12), 1704-1706, 2003

.

[May24] A. May, F. Boitier, A. Ore Remigio, P. Layec, “On the Accuracy of Power Profile Estimation using MMSE or Deconvoluted Correlation-Based Profiles,” in Optical Fiber Communications Conference and Exhibition (OFC), 2024.

[Nad23] L. Nadal, R. Casellas, J. M. Fàbrega, F. J. Vílchez, and M. Svaluto Moreolo, "Capacity scaling in metro-regional aggregation networks: the multiband S-BVT", J. Opt. Commun. Netw. 15, F13-F21, 2023.

[Nad24] L. Nadal, M. Svaluto Moreolo, J. M. Fàbrega, F. J. Vílchez, and R. Casellas, "Enabling Capacity Scaling in Metro Networks with Multi Band Sliceable Transceiver Architectures", SPIE Photonics West, Paper 12894, Sant Francisco, US, January 2024.

[Cas24] C. Castro, S. Xia, A. Napoli, J. Pedro, Y. Rumaldo, N. Costa, N. Calabretta, B. Spinnler and A. Rafel ,"A low-cost network architecture enabled by SOA-based filter-less OADMs and digital subcarrier multiplexing", OFC Conference 2024, Paper W2A.14, 2024.

[OpenConfig] OpenConfig, Mar. 2018, OpenConfig web site. [Online] Available: http://www.openconfig.net/

[Pao21] F. Paolucci, L. De Marinis, P. Castoldi, and F. Cugini, "Demonstration of P4 neural network switch," in 2021 Optical Fiber Communications Conference and Exhibition (OFC), 2021.

[Pel21] I. Pelle, F. Paolucci, B. Sonkoly, F. Cugini, "Latency-sensitive edge/cloud serverless dynamic deployment over telemetry-based packet-optical network", IEEE Journal on Selected Areas in Communications 39 (9), 2849-2863, 2021.

[Pel23] I. Pelle, F. Paolucci, B. Sonkoly, F. Cugini "P4-based Hitless FaaS Load Balancer for Packet-Optical Network Edge Continuum", Optical Fiber Communication Conference (OFC), Th1D. 5, 2023.

[Pog14] P. Poggiolini, G. Bosco, A. Carena and V. Curri, "The GN-Model of Fiber Non-Linear Propagation and its Applications". *Journal of Lightwave Technology, 32*(4), 694-721, 2014.

[Ren17] J. Renaudier et al., "First 100-nm continuous-band WDM transmission system with 115 Tb/s transport over 100 km using novel ultra-wideband semiconductor optical amplifiers," in Proc. Eur. Conf. Opt. Commun., Gothenburg, Sweden, pp. 1–3, Paper PDP.A.3, 2017.

[Ren19] J. Renaudier et al., "107 Tb/s transmission of 103-nm bandwidth over 3 × 100km SSMF using ultra-wideband hybrid Raman/SOA repeaters," in Proc. Opt. Fiber Commun. Conf., San Diego, CA, USA, pp. 1–3, Paper Tu3F.2, 2019.

[Rap07] L. Rapp and D. Setti, "Comparison of Tilt Control Techniques for Erbium–doped Fiber Amplifiers". Journal of Optical Communications, 28, 162-167, 2007.

[Rap21-1] L. Rapp and M. Eiselt, "Ultra-wideband amplification strategies," in Proc. Summer Topicals Meeting Ser., Virtual Conf., pp. 1–2, PaperWE1.1, 2021.

[Rap21-2] L. Rapp and M. Eiselt, "Optical amplifiers for multi–band optical transmission systems," Journ. Lightwave Technol., vol. 40, pp. 1579–1589, 2021.

[Rap22] L. Rapp, "Design and performance characteristics of extended C–band amplifiers," in ITG–Symposium Photonics Networks. Berlin, Germany: VDE Verlag, pp. 31–37, 2022.

[Rap23-1] L. Rapp, "Energy efficiency of amplification technologies for ultra–wideband transmission," in Summer Top. Meeting Series. Giardini Naxos, Italy: IEEE, 2023.

[Rap23-2] L. Rapp, "Compensation of Phase Noise induced by Higher–Order Codirectional Raman Amplifiers," IEEE Photonics Technology Letters, 2023.

[Rap24-1] L. Rapp, “Challenges for Multiband Optical Amplification and Solutions Therefore”, Journal of Lightwave Technology Vol. 42, Issue 12, pp. 4202-4212, 2024.

[Rap24-2] L. Rapp, “Amplifiers in Multi–Band Scenarios—Output Power Requirements, Control and Performance Characteristics”. *Journal of Lightwave Technology, 42*(6), 1991-1999, 2024.

[Sas23] T. Sasai et al., “Performance Limit of Fiber-Longitudinal Power Profile Estimation Methods,” in Journal of Lightwave Technology, vol. 41, no. 11, pp. 3278-3289, June 2023.

[Sen22] M. Sena, R. Emmerich, B. Shariati, J.K. Fischer, R. Freund, “Link tomography for amplifier gain profile estimation and failure detection in C+L ban open line systems,” in Optical Fiber Communications Conference (OFC), 2022.

[Sev24] E. Seve, S. Bigo and P. Layec, “Identification of Optical Links with Heterogenous Fiber Types in a Production Network” in Optical Fiber Communications Conference (OFC), W3C.4, 2024.

[Sim24] G. Simon, et al. "200 Gb/s Coherent Point-to-Multipoint Coexistence with 50G-PON for Next-Generation Optical Access." IEEE Photonics Technology Letters, pp. 665-668, 2024.

[Sou24] Andrè Souza et al., “Node Architectures for High-Capacity Multi-band Over Space Division Multiplexed (MBoSDM) Optical Networks”, invited paper at ICTON 2024, Bari (Italy), July 12-14 2024.

[Sun97] Y. Sun, J. W. Sulhoff, A. K. Srivastava, J. L. Zyskind, C. Wolf, T. A. Strasser, J. R. Pedrazzani, J. B. Judkins, R. P. Espindola, A. M. Vengsarkar, and J. Zhou, “An 80 nm ultra–wide band EDFA with low noise figure and high output power,” in Europ. Conf. Opt. Comm. Edinburgh, UK: IEE, pp. 69–72, 1997.

[Tan19] T. Tanimura, K. Tajima, S. Yoshida, S. Oda and T. Hoshida, “Experimental demonstration of a coherent receiver that visualizes longitudinal signal power profile over multiple spans out of its incoming signal,” presented at the European Conference on Optical Communications (ECOC), pp. 1-4, 2019.

[Tan20] T. Tanimura, S. Yoshida, K. Tajima, S. Oda, and T. Hoshida, “Fiber Longitudinal Anomaly Position Identification Over Multi-Span Transmission Link Out of Receiver-end Signals,” in IEEE/OPTICA Journal of Lightwave Technology, vol. 38, no, 9, pp. 2726-2733, 2020

[Zir98] M. Zirngibl, “Analytical model of Raman gain effects in massive wavelength division multiplexed transmission systems”. Electronics Letters, 34(8), 789-790, 1998.

[Zha24] Q. Zhang, P. Layec, A. May, A. Morea, A. Attarpour and M. Tornatore, “Cost and Power-Consumption Analysis for Power Profile Monitoring with Multiple Monitors per Link in Optical Networks,” submitted to Journal of Lightwave Technology, 2024.

[Xia23] S. Xia, M. Rombouts, H. Santana and N. Calabretta,”Performance Assessment of Multiband OADM in Metro-Access Network for Converged Xhaul Traffic”. In 49th European Conference on Optical Communications, 2023

[Sch22] R. Schmogrow, ”Solving for scalability from multi-band to multi-rail core networks”. Journal of Lightwave Technology, 40(11), 3406-3414, 2022.